UNIVERSITY OF CALIFORNIA, SAN DIEGO

Astrocyte activity modulated by S1P-signaling in a multiple sclerosis model

A dissertation submitted in partial satisfaction of the requirements for the degree
Doctor of Philosophy

in

Neurosciences

by

Aran Groves

Committee in charge:

Professor Jerold Chun, Chair
Professor JoAnn Trejo, Co-Chair
Professor Jody Corey-Bloom
Professor Mark Mayford
Professor William Mobley

2015

The Dissertation of Aran Groves is approved, and it is acceptable in quality and form for publication on microfilm and electronically:

_____

_____

_____

_____

Co-Chair

_____

Chair

University of California, San Diego

2015

TABLE OF CONTENTS

LIST OF FIGURES

Chapter 1: Introduction

Chapter 2: Assessing the capabilities of c-Fos reporter mice to indicate EAE activity

Chapter 3: Spatial and temporal properties of astrocyte activation in EAE and correlation to clinical severity with modulation of S1P receptors

Chapter 4: Functional properties of astrocyte activity during acute EAE with modulation of S1P receptors

LIST OF TABLES

Chapter 4: Functional properties of astrocyte activity during acute EAE with modulation of S1P receptors

ACKNOWLEDGEMENTS

I thank Dr. Jerold Chun for the challenge and opportunity to conduct this rewarding research in his laboratory. The talent and atmosphere he has imparted into his lab have provided the tools and motivation for taking on this challenging project and for not giving up when problems seemed insurmountable. I was reluctant to leave my comfort zone and Jerold aptly realized and instructed me that it is outside of this zone that the most progress can be made.

I would also like to thank the members of my dissertation committee. Dr JoAnn Trejo I met while mentoring for a summer undergraduate research program. Dr. Trejo taught me the value of not only being a mentor, but also finding mentors throughout all stages of my professional development. I have greatly appreciated her mentorship during these last few years. I have had several opportunities to interact Dr. William Mobley, the Chair of the Department of Neurosciences, and a teacher my favorite graduate school class. The incredible wealth of knowledge he has in seemingly all areas of science and his clarity in communicating this knowledge is something I will forever strive to emulate. I asked Dr. Jody Corey-Bloom to be on my committee because of her expertise in multiple sclerosis care and research. I admire the harmonious balance that she has been able to achieve in balancing a career in research and patient care. I hope to continue to get her guidance as I forge a similar career of my own. Last but not least, I wish to thank Dr. Mark Mayford. His ingenuity in

leveraging transgenic mice to examine some of the most complex interworking of the brain in learning and memory have given me the tools to repurpose and learn about a complex disease. I truly appreciate the guidance that Dr. Mayford and those in his lab have given me in working with his impressively useful mice.

The Chun lab has been a wonderful source of knowledge, camaraderie, and friendship. I wish to thank Dr. Hope Mirendil for getting me started on my thesis project, giving me technical guidance, teaching me about solid experimental design, and helping me to navigate effectively within the labs structure. I wish to thank Grace Kennedy for her vast technical knowledge that was instrumental in the many immunohistochemistry experiments and tissue clearance techniques we tried. I also must thank her for the endless supply of candy and some of the best Bluefin tuna I have ever tasted, and I implore her to keep me in mind if the catch is plentiful enough to share again. I wish to thank Dr. Richard Rivera for his tremendously kind and generous spirit that pairs incredibly well with his scientific mind to the benefit of everyone in the Chun lab. I could not imagine the lab functioning without Rich as a cornerstone. Thank you to Danielle Jones who keeps everything in the lab in order, all the while bringing calm and joy. I especially wish to thank the EAE Team. Dr. Yasuyuki Kihara joined our lab as a post-doc during my second year. In my mind he invented EAE as his name was on the induction protocol labeled the “Kihara Method”, in my lab book years before I met him. I owe much of my productive training as a graduate student to Yasu. He has been my research “Guiding Light”. Dr. Deepa Jonnalagadda is the

newest member of our EAE Team and quickly became the most vital to me. I have learned more training her, pushing the boundaries of my own knowledge, and troubleshooting problems with her during the last 1.5 years than I had in my entire scientific career prior. I have also learned to love Indian cuisine, not only when she brings in some for me to try, but also through the shared recipes. There has been many other Chun lab members who have helped me with technical issues, commiserated failed experiments with me, and have been good friends. To all of you, thank you!

I wish to thank my family, as they are the inspiration for all that I wish to achieve in my scientific career and they are the meaning in my life. My mother has proven throughout my entire life that she would stop at nothing to help me. My father, who at an early age instilled in me a curiosity of science and helped foster all the interests I had. My brother, sisters, and cousins who are my best friends and challenge me in every way, but do so in a way that is always backed by the most genuine of love. My aunt Lynda and late uncle Michael, for providing a structured, exciting, and loving home when I may have needed it most, and giving me a second set of parents, sisters, and a brother. To my mother-in-law and father-in-law, my third set of parents, for giving me their beautiful and sweet daughter, and for being some of the best people on the face of this earth. Most importantly, I wish to thank my wife Raquel. We have grown together from teenagers to now, tackling all that life has thrown at us. Tackling this PhD was something that I thought I would do alone, but it was quickly evident that there

were many shared sacrifices. These sacrifices we powered through together and I must credit Raquel for some of the work done in this project, as she would lend a hand to do a PCR or accompany me while I imagined on the microscope late into the nights. This PhD truly belongs to us both.

The introduction in Chapter 1 contains, in part, material as it appears in a review article of the Journal of Neurological Sciences, 2013, Groves, Aran; Kihara, Yasuyuki; Chun, Jerold. The dissertation author was a co-primary author of this review article.

VITA

2015 Doctor of Philosophy in Neurosciences
University of California, San Diego

2008 Bachelor of Science in Chemistry, Northern Arizona University

PUBLICATIONS

"Fingolimod: Direct CNS effects of sphingosine 1-phosphate (S1P) receptor modulation and implications in multiple sclerosis therapy" Groves A, Kihara Y, Chun J (2013). *Journal of the Neurological Sciences* vol. 328 (1) p. 9-18

"Dimethyl fumarate inhibits integrin a4 expression on activated lymphocytes in multiple sclerosis models" Kihara Y, Groves A, Chun J (2015). *Annals of Clinical and Translational Neurology*. doi: 10.1002/acn3.251

POSTERS AND PRESENTATIONS

A new reporter mouse for CNS cellular activity selectively identifies astrocyte activation produced by experiemental autoimmune encephalomyelitis (EAE) and inhibited by fingolimod. Groves A, Kihara Y, Rivera R, Mayford M, Chun J. 29th congress of the European Committee for Treatment and Research in Multiple Sclerosis (2013).

Neuroanatomical organization and global transcriptome analyses of c-Fos activated astrocytes in EAE lesions, altered by administration of fingolimod. Groves A, Kihara Y, Rohrback S, Mayford M, Chun J. 2014 Joint ACTRIMS-ECTRIMS Meeting (2014).

c-Fos reporter reveals temporal, spatial and transcriptional astrocytic activity in experimental autoimmune encephalomyelitis (EAE), correlated with disease severity and modulated by S1P-signaling. Groves A, Kihara Y, Jonnalagadda D, Chun J. 31st congress of the European Committee for Treatment and Research in Multiple Sclerosis (2015).

ABSTRACT OF THE DISSERTATION

Astrocyte activity modulated by S1P-signaling in a multiple sclerosis model

by

Aran Groves

Doctor of Philosophy in Neurosciences

University of California, San Diego, 2015

Professor Jerold Chun, Chair
Professor JoAnne Trejo, Co-Chair

Fingolimod is the first oral disease-modifying therapy approved for relapsing forms of multiple sclerosis (MS). Following phosphorylation *in vivo,* the active agent, fingolimod phosphate (fingolimod-P), acts as a sphingosine 1-phosphate (S1P) receptor modulator, binding with high affinity to four of the five known S1P receptors ($S1P_1$, $S1P_3$, $S1P_4$ and $S1P_5$). The mechanism of action of fingolimod in MS has primarily been considered as immunomodulatory, whereby

fingolimod-P modulates $S1P_1$ on lymphocytes, selectively retaining autoreactive lymphocytes in lymph nodes to reduce damaging infiltration into the central nervous system (CNS). However, emerging evidence indicates that fingolimod has direct effects in the CNS on MS relevant neural cell types including astrocytes, oligodendrocytes, neurons, and microglia. To study the roles of fingolimod and S1P signaling in MS, a transgenic activity reporter mouse was used in experimental autoimmune encephalomyelitis (EAE) to identify and characterize active cells during the disease process that may be altered by relevant S1P signaling. A subset of astrocytes is robustly activated at EAE sign onset in clusters that progressively expand along white matter tracts. The extent of astrocyte activation is highly correlated with disease severity and is limited by the loss of astrocytic $S1P_1$. Transcriptome analyses of these EAE-activated astrocytes reveal several pathways that are both independently changed by astrocyte $S1P_1$ knockouts and by fingolimod administration and concurrently changed by these S1P modulations. Among the pathways that have shared transcript differences in EAE-activated astrocytes from astrocyte $S1P_1$ knockouts and by fingolimod administration, and control EAE-activated astrocytes, direct CNS effects of fingolimod may be uncovered.

Chapter 1:

Introduction

1.A. Fingolimod: direct CNS effects of sphingosine 1-phosphate receptor modulation and implications in multiple sclerosis therapy

Multiple Sclerosis

Multiple Sclerosis (MS) is among the world's most common autoimmune and neurodegenerative diseases, with at least 2.3 million patients affected worldwide [1, 2]. The onset of disease typically occurs between ages 20 and 40 and often becomes debilitating with up to 50% of patients requiring ambulatory assistance within 15 years of diagnosis [3]. While most prevalent in North America and Europe, MS is found in all regions with prevalence trending upwards, highlighting this disease as a significant global burden [2].

The signs and symptoms of MS are primarily the result of autoimmune lesions in the white matter tracts of the central nervous system (CNS). Lesions occur anywhere in the CNS; throughout the brain, spinal cord, and optic nerve. Locations of these lesions determine the clinical presentation, which is extremely varied and diverse. The most common symptoms include weakness and/or numbness of limbs, monocular visual loss from optic neuritis, tremors and ataxic gait due to cerebellar dysfunction, double vision, dysarthria, or dizziness from brainstem dysfunction, and fatigue. In 10% of MS diagnoses known as primary-progressive MS (PPMS), the course of disease advances steadily without intermediate remissions and decline into disability is generally more rapid. Approximately 85 percent of patients experience early disease in a pattern known as relapsing-remitting MS (RRMS) in which there are episodic increases in disease activity and symptoms, often lasting days to months. Remission is often complete

initially, with a return to a normal apparent neurological state or with few and mild symptoms. Relapses strike approximately every 12 to 18 months and, with effective therapy, some remain in a relapsing-remitting status, with few deficits decades after diagnosis. However, many more begin to experience persistent, chronic attacks with diminished remissions after about 5 to 15 years of disease. This stage steady deterioration is known as secondary progressive MS (SPMS).

The pathogenesis and pathophysiology of MS are not fully understood and likely vary in the different forms of MS and stages of disease. A central initiating event is generally considered to be the peripheral activation, proliferation, and maturation of lymphocytes autoreactive to myelin, the lipid sheath around axons made by oligodendrocytes. These autoreactive lymphocytes can then egress out of lymphoid tissues and into circulating blood, cross the blood-brain barrier (BBB), and enter the CNS. In RRMS, it is these recurrent inflammatory attacks, which cause demyelination, gliosis, and axonal damage thus impairing nerve conduction that are generally regarded to lead to the many neurological symptoms during relapses. In both PPMS and SPMS it seems that neurodegeneration is responsible for the progression of neurological deficits, as evidence of inflammation is often absent by pathological and by MRI examination [4]. Additionally, all tested current therapies, which are described as immunosuppressive agents that reduce inflammatory relapses, are not efficacious during progressive forms of MS.

Treatments for MS are used to alleviate symptoms, manage relapses, and modify the course of the disease. As a vast set of symptoms may present in MS patients, medications to treat these symptoms are abundant. There are over 25 medications used to treat autonomic problems affecting the bladder and bowels, and several more that can effectively treat each depression, dizziness, gait problems,

emotional changes, sexual dysfunction, spasticity, tremors, pain, and fatigue. Symptomatic medications have different mechanisms of action (MOA), mostly relevant to the physiology of the symptoms and not directly to MS pathophysiology. Most relapses resolve gradually without treatment. Corticosteroids may be indicated during severe relapses in which there are deficits in vision, strength, and/or balance that may affect mobility, safety, and general function. Administered in three- to five-day courses, intravenous corticosteroids reduce inflammation and end relapses more rapidly, though this treatment exhibits no long-term benefits to a patient's MS progression. Long-term benefits of treatment have been achieved in the last couple decades with disease-modifying therapies (DMTs). Currently, there are twelve U.S. Food and Drug Administration (FDA)-approved DMTs, which reduce relapse frequency and progression to disability in patients with relapsing forms of MS. All available DMTs reduce relapse frequency in part via some variation of limiting the access of autoreactive lymphocyte to the CNS. For example, one of the most widely used first line therapies, interferon beta 1a, reduces inflammatory cells that cross the BBB [5] and reduces production of Th17 cells *in vitro* [6], a subset of T lymphocytes that are believed to play a key role in the pathophysiology of MS. DMTs were first available as either infusions or injections. In 2010 the FDA approved fingolimod as the first oral DMT for RRMS, offering patients a more convenient and comfortable option compared to self-injections or infusions in medical facilities. Fingolimod modulates through sphingosine 1-phosphate receptors, which had previously not been appreciated in the pathophysiology of MS and may unveil new, direct therapeutic MOA in the CNS.

Sphingosine 1-phosphate

Sphingosine 1-phosphate (S1P), a naturally occurring lipid mediator and part of the larger family of lysophospholipids, can act as a regulator of diverse physiological and pathophysiological processes, including those involved in the pathogenesis of multiple sclerosis (MS) [7-9]. S1P is produced from sphingolipids present in the cell membrane, which are in part defined by the constituent presence of the amino alcohol sphingosine. A prominent sphingolipid is sphingomyelin, from which sphingosine is formed through a series of reactions catalyzed by metabolic enzymes, including sphingomyelinase and ceramidase [10, 11]. Sphingosine can then be phosphorylated to produce S1P by sphingosine kinase 1 (SphK1) or 2 (SphK2). Both of these enzymes have fairly broad tissue distribution, with SphK1 predominating in the lungs and spleen, and SphK2 predominating in the heart, brain, and liver [12, 13]. Extracellular S1P acts in both autocrine and paracrine fashions by binding to five cell-surface, S1P receptor subtypes named $S1P_1$, $S1P_2$, $S1P_3$, $S1P_4$ and $S1P_5$ [14], which belong to the G protein-coupled receptor (GPCR) super family [7, 15]. $S1P_1$, $S1P_2$ and $S1P_3$ show broad tissue gene expression, while $S1P_4$ shows gene expression primarily in immune system cells, and $S1P_5$ primarily in the spleen (on natural killer cells and other lymphocytes) and cells of the central nervous system (CNS; mainly on oligodendrocytes) [7]. These receptors can, therefore, function in multiple organ systems, including the CNS, the immune system, the cardiovascular system, and the respiratory systems. In particular, CNS effects have been well characterized for lysophospholipids (both S1P and lysophosphatidic acid [LPA], whose GPCRs share homology), including effects on a vast range of neurobiological processes [16-35]. **Figure 1.1** provides a composite picture of S1P receptor gene expression reported in the literature for neurons and glia [14, 36, 37]. Binding of S1P to each of the S1P receptor subtypes triggers a range of different

intracellular signaling pathways mediated by distinct, heterotrimeric G proteins [7, 38-42].

S1P Signaling in MS

In the CNS, S1P receptors are expressed on oligodendrocytes, astrocytes, neurons, and microglia. Some findings suggests that S1P signaling is disrupted in MS. Compared with control individuals, patients with MS have been reported to have a lower content of sphingomyelin (from which endogenous sphingosine and S1P are derived) in their white matter [43] but an increased level of S1P in the cerebrospinal fluid [44]. S1P levels have been found to be lower and sphingosine levels higher in the white matter and lesions of patients with MS compared with white matter from control individuals [45]. In active and chronic inactive MS lesions, reactive astrocytes show high expressions of $S1P_1$ and $S1P_3$ [46]. In addition, astrocytes in pro-inflammatory conditions up regulate $S1P_3$ and SphK1 [47]. These combined reports suggest that S1P signaling in the CNS is altered in patients with MS.

Fingolimod

Fingolimod (FTY720; GILENYA™, Novartis Pharma AG, Basel, Switzerland) is a modulator of S1P receptors and is the first oral, disease-modifying therapy to be approved for relapsing forms of MS. Fingolimod is phosphorylated *in vivo* by sphingosine kinase, particularly SphK2, to produce the active metabolite fingolimod phosphate (fingolimod-P). Fingolimod and fingolimod-P are structural analogues of sphingosine and S1P, respectively. Being a structural analogue of S1P enables fingolimod-P to bind to and activate four of the five S1P receptor subtypes. Receptor studies have shown that fingolimod-P binds $S1P_1$, $S1P_4$, $S1P_5$ (half maximal effective concentration [EC_{50}] values

of ~0.3–0.6 nM) and $S1P_3$ (EC_{50} values of ~3 nM), but has shown essentially no binding activity with $S1P_2$ (EC_{50} values of > 10 uM) [48, 49].

Lymphocyte trafficking effects of fingolimod

Modulation of $S1P_1$ on lymphocytes by fingolimod is thought to retain circulating pathogenic lymphocytes in the lymph nodes, thereby preventing their infiltration into the CNS where they would promote pathological damage [50-52]. Fingolimod-P initially acts as an $S1P_1$ agonist [48, 49]; however, chronic exposure to fingolimod-P leads to irreversible receptor internalization resulting in 'functional antagonism' of $S1P_1$-mediated S1P signaling [53-55]. Circulating T cells express $S1P_1$ and lower levels of $S1P_4$ and $S1P_3$ [54, 56], and the interaction of extracellular S1P with $S1P_1$ is thought to initiate lymphocyte egress from lymph nodes by overcoming retention signals mediated by chemokine (C-C motif) receptor 7 (CCR7) expressed on B cells and naïve and central memory T cells. In the presence of fingolimod-P, functional antagonism of $S1P_1$ prevents the egress of CCR7-positive naïve and central memory T cells from lymph nodes [52, 57], consistent with experimental evidence generated using hematopoietic $S1P_1$ receptor knockout mice to study lymphocyte circulation [53, 58]. Importantly, fingolimod does not significantly affect activation and proliferation of redistributed naïve and central memory T cells, and does not block the egress from lymph nodes of effector memory T cells that are CCR7-negative, a distinct subpopulation of T cells that are important for immunosurveillance [57]. Thus, fingolimod has a targeted mechanism of action, selectively affecting lymphocyte subsets.

Direct CNS effects of fingolimod

In addition to these immunological actions, and in view of the general actions of lysophospholipid receptors in the CNS and a growing literature that has identified S1P signaling effects on neural cells, fingolimod would be expected to have direct effects on CNS cells that express S1P receptors. Indeed, fingolimod, which is lipophilic, is able to cross the blood–brain barrier (BBB) into the CNS and, following oral administration of fingolimod, fingolimod-P has been detected at sub-nanomolar levels in the cerebrospinal fluid [59], which are sufficient for modulating human CNS cell properties *in vitro* [60, 61]. In addition, recent data utilizing conditional knockout of $S1P_1$ from neural lineages have identified key roles for astrocytes in reducing the severity of pathological changes in an animal model of MS, experimental autoimmune encephalomyelitis (EAE). Moreover, the astrocytic loss of $S1P_1$ also prevents the efficacy of fingolimod in this model [62]. This emerging evidence for direct CNS effects of fingolimod through alteration of S1P signaling will be further explored in cell types and functional process related to MS here.

Direct CNS effects of fingolimod: *Astrocytes*

Astrocytes are the most abundant cells in the human CNS and have an extremely diverse and important range of roles that are relevant to normal brain activity and its alteration in disease states [63-71]. In MS, evidence suggests that astrocytes have a dual, paradoxical role. At sites of demyelination in MS lesions, reactive astrocytes form a glial scar that impairs remyelination [72, 73]. However, astrocytes have also been shown to act as cellular mediators of CNS myelination by promoting oligodendrocyte progenitor migration, proliferation and differentiation [73]. Indeed, astrogliosis appears to be an early CNS response to MS-related insults [74]. Astrocytes preferentially express $S1P_3$ and $S1P_1$, and can express $S1P_2$ at a low level; $S1P_5$ expression is not detectable under basal conditions, but can be up regulated by

astrocytes grown in culture [17, 18, 75, 76]. Injection of S1P into the striatum of mice induced astrogliosis [77]. A mouse model of Sandhoff disease, another neurodegenerative disease associated with astrogliosis, was attenuated by genetic deletion of either SphK1 or $S1P_3$ [78]. Critically, selective removal of $S1P_1$ from astrocytes attenuated EAE severity and reduced histological sequelae of EAE challenge in the CNS [62].

Fingolimod-P treatment of cultured human astrocytes has been shown to inhibit production of inflammatory cytokines [46]. In cultured rat astrocytes, fingolimod-P stimulated extracellular signal-regulated kinase (ERK) phosphorylation and cell migration; these effects were also seen with selective $S1P_1$ agonists, suggesting that fingolimod-P acted as a functional agonist of $S1P_1$ in these *in vitro* experiments [79, 80]. In contrast, results from an *in vivo* study performed using a mouse EAE model supported functional antagonism of astrocyte $S1P_1$ rather than forms of agonism as the predominant receptor mechanism (with regard to CNS cells) for fingolimod efficacy [62]. In this study, inflammatory cytokine levels, as well as disease-associated increases in S1P levels, were reduced in animals lacking $S1P_1$ on astrocytes. All conditional null mutants lacking $S1P_1$ in CNS cell lineages displayed wild-type lymphocyte trafficking that responded normally to fingolimod treatment. EAE severity was attenuated in mutants lacking $S1P_1$ on glial fibrillary acidic protein-expressing (GFAP) astrocytes, compared with un-recombined littermate controls [62]. Reductions in EAE severity were accompanied by reductions in demyelination, axonal loss and astrogliosis. If lymphocyte depletion was solely responsible for fingolimod efficacy, then EAE severity in $S1P_1$ null mutants should have been further reduced with fingolimod treatment; however, this was not observed and clinical scores were refractory to fingolimod treatment, despite the maintained immunological effects on peripheral blood lymphocyte depletion. Mutants

lacking $S1P_1$ on neurons but not on astrocytes showed the same response to fingolimod treatment as littermate controls. These *in vivo* results were supported by experiments in astrocyte cultures, in which fingolimod treatment was found to induce rapid internalization of $S1P_1$ that was not followed by recycling of $S1P_1$ to the cell surface [62]. Overall, these findings identified functional antagonism of $S1P_1$ on astrocytes as a non-immunological, direct CNS effect of fingolimod necessary for its efficacy [62].

Direct CNS effects of fingolimod: *Oligodendrocytes*

Oligodendrocytes are myelinating cells of the CNS. Demyelination and failure of remyelination by oligodendrocytes contribute to the progression of disease in MS; therefore, targeting the oligodendrocyte is a potentially important therapeutic strategy [81]. Remyelination requires oligodendrocyte precursor cell (OPC) proliferation, migration to sites of demyelination, and differentiation into mature myelin-forming oligodendrocytes. Mature oligodendrocytes preferentially express $S1P_5$ and may express $S1P_1$, $S1P_2$ and $S1P_3$ at lower levels, while OPCs show high levels of $S1P_1$ gene expression and lower levels of $S1P_5$ and $S1P_3$ expression [39, 60, 82-87]. The effects of S1P on oligodendrocyte lineages include differentiation, migration and survival, depending on the developmental stage [84, 87]. However, mice deficient in $S1P_5$ do not show impaired myelination [84, 87], suggesting at least some functional redundancy among S1P receptor subtypes in OPCs and oligodendrocytes.

Results from *in vitro* studies show that the effects of fingolimod-P on cultured oligodendrocyte lineage cells are diverse and are affected by developmental stage, treatment dose and duration [39, 60, 84-88]. Fingolimod protected cultured rodent OPCs from apoptosis induced by inflammatory cytokines and microglial activation (both of which have been implicated in the pathogenesis of MS), via apparent activation of ERK

1/2 and Akt signaling [88]. Additionally, activation of $S1P_5$ by fingolimod impeded spontaneous migration of cultured neonatal rat OPCs [39], but fingolimod did not inhibit OPC migration when platelet-derived growth factor was used as a chemoattractant [84]. The differentiation of OPCs was stimulated by fingolimod at low nanomolar doses [84], but was inhibited at higher concentrations [84, 86, 88]. Similarly, the effects of fingolimod on process dynamics in mature oligodendrocytes depended on both dose and treatment duration [60].

Direct CNS effects of fingolimod: *Neurons*

Neural progenitor cells can express $S1P_1$, $S1P_2$, $S1P_3$ and $S1P_5$ [16, 89], while neurons predominantly express $S1P_3$ and $S1P_1$ [89, 90]. Genetic deletion of $S1P_1$ or deletion of both SphK1 and SphK2 in mice caused severe defects of neurogenesis [91]. $S1P_2$ knockout mice showed defects in the inner ear that are associated with neurodegeneration and can result in loss of hearing and balance [29, 92, 93]. In addition, while phenotypes of $S1P_2$ deletion mutants appeared relatively normal [93, 94], some background strains promoted increased excitability [93] and seizure activity [95].

In primary cultures of neural progenitor cells, S1P produced many similar effects to those reported for LPA, including induced proliferation, morphological changes and enhanced survival [89, 96, 97]. S1P modulated neurite extension in cultured PC12 cells and dorsal root ganglion neurons [97], and enhanced nerve growth factor-induced excitability of adult sensory neurons [98]. In primary hippocampal neurons, S1P acted both as a secretagogue, triggering glutamate secretion, and as an enhancer, potentiating depolarization-evoked glutamate secretion [90]. These cell culture phenomena require further examination *in vivo*.

As described above, in the study by Choi *et al.* [62], neuronal $S1P_1$ mutants responded to fingolimod treatment in the same way as did littermate controls, indicating that $S1P_1$ on astrocytes but not on neurons is a major locus for direct CNS effects of fingolimod [62]. In a rat model of optic neuritis, fingolimod treatment reduced inflammation, demyelination and axonal damage, but did not prevent apoptosis of retinal ganglion cells, the neurons that form the axons of the optic nerve [99]. Rossi *et al.* used electrophysiological recordings to investigate whether fingolimod could ameliorate synaptic defects in EAE mice and found that oral fingolimod prevented and reversed the presynaptic and postsynaptic alterations of glutamate transmission [100]. These effects were associated with reduced clinical deterioration. In addition, prophylactic fingolimod treatment significantly reduced the dendritic spine loss observed during the acute phase of EAE. Fingolimod did not alter the spontaneous excitatory postsynaptic currents in neurons from healthy control mice, indicating that fingolimod does not interfere with physiological synaptic transmission [100].

Direct CNS effects of fingolimod: *Microglia and dendritic cells*

Microglia are involved in both innate and adaptive immunity in the CNS. Microglial activation seems to be critical for MS pathogenesis [101] and inhibition of activation suppressed relapsing paralysis in EAE [102]. Activated microglia have been shown to differentiate into M1 and M2 microglia that contribute to both protective and detrimental aspects of the inflammatory process through antigen presentation, cytokine release and phagocytosis [101]. S1P receptor expression on microglia varies according to the activation state of these cells [37]. Microglia in an inactive state isolated acutely from rat brain showed gene expression for $S1P_1$ and $S1P_3$ that was higher than $S1P_2$, and much higher than $S1P_5$ [37]. *In vitro*, S1P increased the release of pro-inflammatory

cytokines from activated microglia [103]. Fingolimod-P has been reported to have no effect on cytokine production by cultured human microglia [104]. Non-phosphorylated fingolimod, but not fingolimod-P, induced apoptosis of a human microglia cell line by activating sterol regulatory element-binding protein-2 [105]. In rats, fingolimod treatment attenuated infiltration of reactive macrophages/microglia into lesions produced by traumatic brain injury [106]. Fingolimod also reduced microglial activation in cerebral ischemic lesions in mice [107].

Jackson *et al.* examined the effects of fingolimod on remyelination in rat telencephalic neurospheres[108]. The absence of blood-borne immune cells in this model allowed the direct CNS effects of fingolimod to be assessed. Following lysophosphotidyl choline-induced demyelination, fingolimod treatment significantly augmented expression of myelin basic protein, a marker of remyelination. In addition, fingolimod down regulated ferritin, a marker of microglial activation. Fingolimod also down regulated tumor necrosis factor-α and interleukin (IL)-1b; these cytokines are produced by activated microglia and astrocytes [108]. The $S1P_1$/$S1P_5$-selective receptor modulator BAF312 (siponimod), but not the $S1P_1$-selective receptor modulator AUY954, also increased levels of myelin basic protein in this model, indicating that $S1P_5$ is, in some way, involved in promoting remyelination *in vitro*. Overall, these results indicate that fingolimod can modulate microglial activation and actively promote remyelination via direct interaction with microglia, oligodendrocytes and/or astrocytes [108].

Other immune cells found in MS lesions include dendritic cells. However, the role of dendritic cells in MS pathology is not well understood [109]. Fingolimod has been reported to inhibit induced IL-12 production in human dendritic cells *in vitro* [104].

Direct CNS effects of fingolimod: Blood–brain barrier

Penetration of lymphocytes into the CNS across endothelial cells of the BBB is a critical event in the pathogenesis of MS [110]. Vascular endothelial cells can express $S1P_1$ and $S1P_3$ [111]; hence, the S1P signaling pathway might influence BBB function [112]. Fingolimod can induce adherens junction assembly in human umbilical vein endothelial cells *in vitro* and can reduce vascular leakage induced by vascular endothelial cell growth factor or LPS-mediated acute lung injury in mice *in vivo* [113, 114]. Fingolimod also enhanced human pulmonary endothelial cell barrier function *in vitro* [115]. Enhancement of barrier function in this model appeared to be independent of $S1P_1$ signaling and did not require phosphorylation of fingolimod, indicating a non-$S1P_1$ mechanism of action [115]. Importantly, heterogeneity of vascular beds leaves open the question of whether S1P signaling and prolonged fingolimod exposure actually alters the BBB. This issue is relevant to fingolimod acting as a functional antagonist of $S1P_1$ on astrocytes [62]. Some models implicate astrocyte end-feet as an integral component of the BBB [116]; therefore, it is possible that astrocyte-mediated effects of fingolimod might also influence some aspects of normal BBB function.

Lymphocyte penetration of the BBB is dependent on vascular cell adhesion molecules and matrix metalloproteinases (MMPs), which degrade the endothelial basement membrane [117, 118]. In a rat EAE model, both prophylactic and therapeutic treatment with fingolimod suppressed/reversed neurological deficits and normalized up regulated gene expression of vascular cell adhesion molecules and MMP-9 in the spinal cord [119]. These effects may in part be caused by direct actions of fingolimod on microvascular and/or glial cells in the CNS [119].

Direct CNS effects of fingolimod: Maintenance of myelination

Overall, the *in vitro* and *in vivo* studies described above suggest that fingolimod could affect CNS resident cells in ways that could prevent demyelination or promote myelin repair in MS lesions (**Figure 1.2**). In a relapsing–progressive EAE model in mice, early fingolimod treatment during relapsing EAE inhibited subsequent relapses, inhibited axonal loss in the spinal cord and facilitated motor recovery, although this was not observed when fingolimod was initiated very late (4 months) in the disease course [120]. Administration of fingolimod was also found to reduce the area of demyelination in the spinal cord in other EAE studies [121, 122]. Fingolimod did not promote remyelination [123, 124] but attenuated injury to oligodendrocytes, myelin and axons in the corpus callosum during cuprizone-induced demyelination in mice [124], suggesting a protective effect of fingolimod that is independent of the effect on peripheral lymphocytes. The protective effect of fingolimod was also associated with decreased IL-1β and chemokine (C-C motif) ligand 2 levels in the corpus callosum and altered $S1P_1$ expression [124].

Anthony *et al.* investigated fingolimod in a focal delayed-type hypersensitivity (DTH) model of MS in rats [125]. DTH lesions are initially characterized by breakdown of the blood–brain barrier, macrophage and lymphocyte infiltration, and tissue damage, including myelin loss. Fingolimod treatment during the active phase (when the blood–brain barrier is disrupted) reduced blood–brain barrier breakdown, inflammatory cell infiltration and tissue damage. During the chronic phase, when the blood–brain barrier was functionally intact, fingolimod treatment reduced demyelination and microglial activation without a corresponding reduction in lymphocytes. These results also provide evidence of direct effects of fingolimod in the CNS that are independent of the effects on lymphocyte infiltration. One possible mechanism of CNS direct protective effects was demonstrated using fingolimod in a mouse model of Rett syndrome. Fingolimod increased BDNF levels in the cortex, hippocampus and striatum and also improved

motor functioning [126]; these changes suggest that fingolimod may promote neuronal repair and improve CNS function via BDNF.

Fingolimod promoted remyelination in rat telencephalic neurospheres (see Microglia and dendritic cells section above) [108]. In rat organotypic cerebellar slice cultures, both fingolimod-P and the $S1P_1$-selective agonist, SEW2871, inhibited lysolecithin-induced demyelination, up regulated $S1P_1$ expression on astrocytes and inhibited the release of several chemokines, including lipopolysaccharide-induced CXC chemokine (CXCL5), macrophage inflammatory protein (MIP)-1α and MIP-3α [127]. Fingolimod may therefore attenuate demyelination not only by preventing S1P-receptor-mediated T-cell migration into the CNS but also via a mechanism that includes an S1P-receptor-mediated reduction of cytokine/chemokine release in the CNS [127]. Fingolimod also enhanced remyelination and process extension by OPCs and mature oligodendrocytes in neonatal mouse organotypic cerebellar slice cultures following lysolecithin-induced demyelination [61]. Increased numbers of microglia and astrocytes were also observed with fingolimod treatment. In addition, selective removal of $S1P_1$ from astrocytes also preserved myelin *in vivo* [62]. Taken together, these data suggest that S1P receptor modulation in the CNS can potentially enhance remyelination or limit demyelination.

Direct CNS effects of fingolimod: Summary and challenges ahead

As well as being the first oral MS disease-modifying therapy, fingolimod is the first drug to be approved that targets S1P receptors, and thus has a fundamentally different and validated molecular target compared with all previously approved MS therapies. Emerging evidence from preclinical studies demonstrates that mechanisms independent of peripheral immune effects contribute substantially to the efficacy of

fingolimod in models of MS. Fingolimod readily crosses the BBB into the CNS where it is phosphorylated to its active metabolite, fingolimod-P. Fingolimod-P then potentially interacts with S1P receptors that are expressed on oligodendrocytes, astrocytes, neurons and microglia, as well as on vascular endothelial cells of the BBB. Several animal models and organotypic studies have provided evidence that fingolimod treatment can reduce demyelination and promote remyelination via direct effects in the CNS. Most notably, deletion of $S1P_1$ on astrocytes reduces EAE severity and prevents fingolimod efficacy indicating direct CNS effects [62].

Studying the direct CNS effects of fingolimod during EAE is challenging as the disease is a complex interaction between many cell types, playing vastly different and equally complex roles, and virtually all possessing the capability for disease altering modulation via S1P receptor effects. Despite identifying a cell-type and receptor-specific locus of efficacy for fingolimod in EAE (astrocytic $S1P_1$) [62], teasing apart cell autonomous effects to identify a functional MOA in the ever-complex CNS has proved elusive. An approach that has yielded great discoveries into the foundations of neuronal circuits and behavioral processes has been to examine the expression of immediate early genes as a proxy for neuron activity. This approach to survey complex neuronal circuits for activity may be extended to survey other CNS cell-types during EAE-related activity and with S1P receptor modulation. In this manner, functionally distinct populations denoted by their expression of an immediate early gene may be identifiable for comprehensive characterization.

1.B. Surveying for activity with immediate early genes

Immediate early genes

Immediate early genes (IEGs) are genes induced rapidly and transiently following a wide variety of extracellular stimuli. They represent the mobilization of a cellular response to its outside stimulus, before *de novo* protein synthesis, and may initiate the distinct transcriptional activation and subsequent protein-synthesis dependent responses that follows a given stimulus [128-132]. Thus, IEGs have been called the "gateway to the genomic response". Nearly 50 IEGs have been identified and many are transcription factors or DNA binding proteins [133]. Some of the earliest discovered IEGs were identified upon cell exposure to mitogens and found to be homologous to retroviral oncogenes, therefore their role in the regulation of the cell cycle was implicated [128]. Since then IEGs have been appreciated in virtually every cellular process and are differentially regulated in different cells via different stimuli [132].

Immediate early genes as indicators of neuronal activity

Neuroscientists have long and extensively utilized the increased neuronal IEG expression in response to elevated neuronal firing to observe "active" neurons or neuronal circuits [134]. Following experimental stimulations, IEG expression is induced by action potential firing in active neurons. Examination of the brain by immunohistochemistry for IEG product expression provides a recent record of neuronal activity for several hours prior to sacrifice. One of the most common IEGs used as an indicator of neuronal activity is c-Fos. In the following studies, c-Fos will be explored as indicator of activity during EAE and thus will be the focus of further discussion.

c-Fos as a potential indicator of activity in EAE

c-Fos regulates many physiological and pathophysiological processes and may be leveraged to examine the activity in many cell types relevant to EAE. Proliferation,

differentiation, and cell death are each regulated by c-Fos expression [135]. These processes and more occur to varying levels in all major cell types found in the CNS during EAE (neurons, oligodendrocytes, astrocytes, microglia, and T cells). Specifically, in neurons during EAE, demyelination and damage to axons causes impairment of action potential transduction, which may cause changes in c-Fos expression [136]. Subsequent neurodegeneration may also cause c-Fos expression changes [137, 138]. In oligodendrocytes, several stimuli, including GPCR signaling, signals producing proliferation of progenitors, and insults damaging myelin, can induce c-Fos [139-143]. c-Fos expression in astrocytes has been observed in numerous conditions which may be relevant to EAE, including during astrocytosis, after various insults, in inflammatory conditions, and during S1P signaling [144-165]. While c-Fos is induced in T-cells upon activation and may regulate transcription of several cytokines, it is not required for the activity of peripheral T-cells [166]. Microglia also have the capacity to express c-Fos in response to GPCR signaling and inflammatory signals [167, 168]. This widespread capacity for c-Fos expression during EAE related stimulation could be leveraged in mice with novel methods of labeling such active cells during long and discrete time periods.

TetTag c-Fos reporter mice

A significant limitation to using IEG expression as reporters of activity has been the temporal nature of its expression. The half-life of c-Fos is approximately 1 h and therefore the direct detection of it would only provide a single, brief glimpse into the most recent few hours of activity prior to sacrifice [169]. Genetic manipulations in mice have overcome this problem by using c-Fos promoter regulatory elements to drive c-Fos activity dependent expression of a linked transgene [170]. These linked transgenes can have the abilities to both report activity over longer durations and exclusively during

experimentally defined periods as is accomplished in the TetTag mouse line developed by Dr. Mark Mayford [171].

In the TetTag mice, the tetracycline-transactivator (tTA) system is combined with the c-Fos promoter to tag c-Fos active cells (**Figure 1.3**). In the presence of doxycycline (DOX), tTA is inhibited from driving tetO promoter. When DOX is removed, tTA may bind the tetO promoter and drives the expression of a stable form of green fluorescent protein (GFP), the human histone H2B-GFP fusion protein, which localizes to the nucleus and is stable for several weeks [172-175]. In this manner, c-Fos activity over discrete time periods lasting days to weeks can be examined [176].

Prelude to the dissertation

Understanding S1P signaling in the CNS during MS is of great clinical importance, especially as the most widely used model of MS, EAE, has revealed the functional loss of $S1P_1$ on astrocytes as a primary mechanism of action of fingolimod [62]. This dissertation investigates the functional activities of cells within the CNS using a c-Fos reporter mouse system. Relevant genetic and pharmacological manipulations of S1P receptors are combined with these activity reporter mice to provide comprehensive characterization of a c-Fos active cell type during EAE and with fingolimod treatment. This approach may not only provide important implications to processes occurring in MS and during fingolimod therapy, but also provide framework to studying single, functionally distinct cell types in MS tissues.

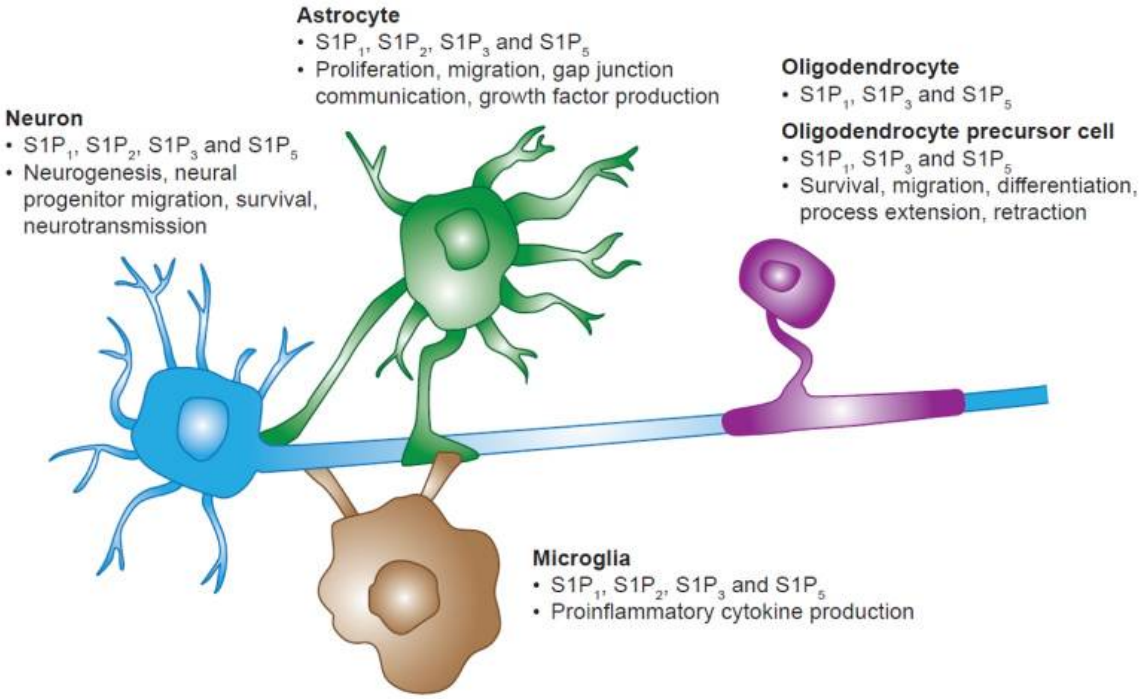

Figure 1.1. Distribution and functions of S1P receptor subtypes in central nervous system cells. Expression and functions come from a composite review of the literature covering many different growth conditions in culture, developmental stages, disease states, models and/or species. For example, S1P receptor expression on microglia varies according to their activation state. Expressions for inactive microglia isolated acutely from the rat brain are represented in the figure [38].

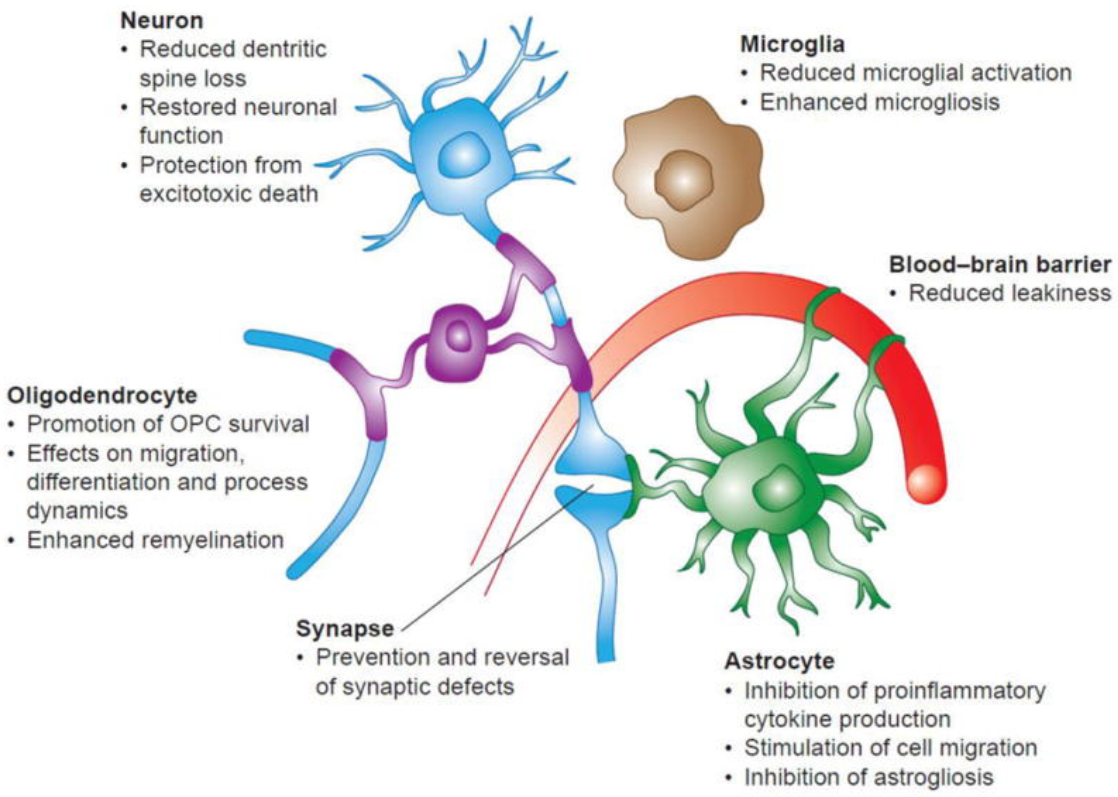

Figure 1.2. Summary of the effects of fingolimod treatment on different cells in the central nervous system.

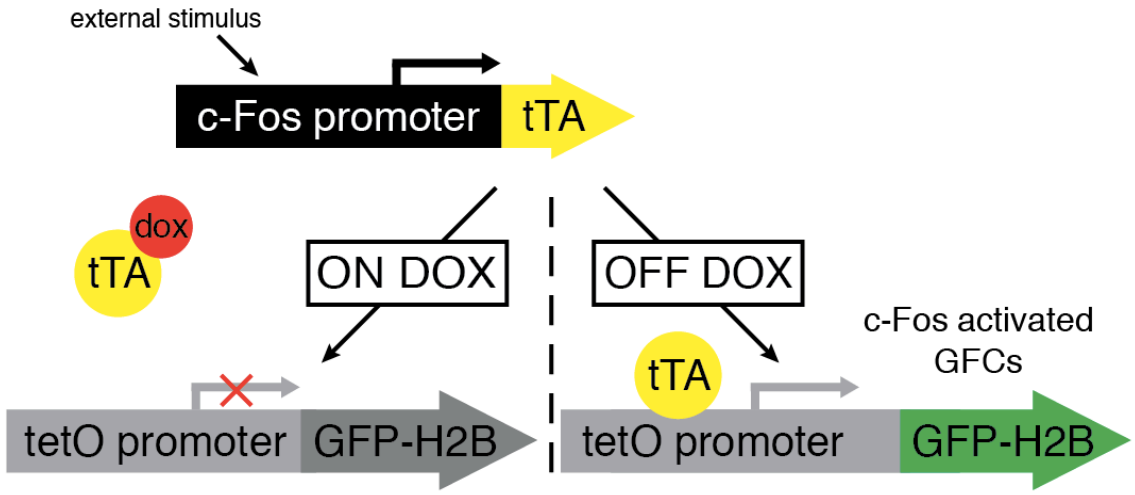

Figure 1.3. The tetracycline transactivator system (tTA) under control of the c-Fos promoter allows persistent identification of active cells over extended and selected durations. Any external stimulus producing c-Fos drives production of tTA, which in turn leads to expression of a nuclear GFP-H2B fusion protein that is stable for weeks. Doxycycline (DOX) prevents extra-experimental expression of activity dependent GFP-H2B.

Chapter 1 References

1. Berer, K. and G. Krishnamoorthy, *Microbial view of central nervous system autoimmunity.* FEBS Lett, 2014. **588**(22): p. 4207-13.

2. *Atlas of MS 2013.* 2013.

3. *The natural history of multiple sclerosis: a geographically based study. I. Clinical course and disability.* Brain, 1989.

4. Confavreux, C. and S. Vukusic, *Accumulation of irreversible disability in multiple sclerosis: from epidemiology to treatment.* Clin Neurol Neurosurg, 2006. **108**(3): p. 327-32.

5. Kieseier, B.C., *The mechanism of action of interferon-beta in relapsing multiple sclerosis.* CNS Drugs, 2011. **25**(6): p. 491-502.

6. Mitsdoerffer, M. and V. Kuchroo, *New pieces in the puzzle: how does interferon-beta really work in multiple sclerosis?* Ann Neurol, 2009. **65**(5): p. 487-8.

7. Mutoh, T., R. Rivera, and J. Chun, *Insights into the pharmacological relevance of lysophospholipid receptors.* Br J Pharmacol, 2012. **165**(4): p. 829-44.

8. Maceyka, M., K.B. Harikumar, S. Milstien, and S. Spiegel, *Sphingosine-1-phosphate signaling and its role in disease.* Trends Cell Biol, 2012. **22**(1): p. 50-60.

9. Strub, G.M., M. Maceyka, N.C. Hait, S. Milstien, and S. Spiegel, *Extracellular and intracellular actions of sphingosine-1-phosphate.* Adv Exp Med Biol, 2010. **688**: p. 141-55.

10. Kanfer, J.N., O.M. Young, D. Shapiro, and R.O. Brady, *The metabolism of sphingomyelin. I. Purification and properties of a sphingomyelin-cleaving enzyme from rat liver tissue.* J Biol Chem, 1966. **241**(5): p. 1081-4.

11. Tani, M., M. Ito, and Y. Igarashi, *Ceramide/sphingosine/sphingosine 1-phosphate metabolism on the cell surface and in the extracellular space.* Cell Signal, 2007. **19**(2): p. 229-37.

12. Kohama, T., A. Olivera, L. Edsall, M.M. Nagiec, R. Dickson, and S. Spiegel, *Molecular cloning and functional characterization of murine sphingosine kinase.* J Biol Chem, 1998. **273**(37): p. 23722-8.

13. Liu, H., M. Sugiura, V.E. Nava, L.C. Edsall, K. Kono, S. Poulton, S. Milstien, T. Kohama, and S. Spiegel, *Molecular cloning and functional characterization of a novel mammalian sphingosine kinase type 2 isoform.* J Biol Chem, 2000. **275**(26): p. 19513-20.

14. Chun, J. and H.P. Hartung, *Mechanism of action of oral fingolimod (FTY720) in multiple sclerosis.* Clin Neuropharmacol, 2010. **33**(2): p. 91-101.

15. Noguchi, K. and J. Chun, *Roles for lysophospholipid S1P receptors in multiple sclerosis.* Crit Rev Biochem Mol Biol, 2011. **46**(1): p. 2-10.

16. McGiffert, C., J.J. Contos, B. Friedman, and J. Chun, *Embryonic brain expression analysis of lysophospholipid receptor genes suggests roles for s1p(1) in neurogenesis and s1p(1-3) in angiogenesis.* FEBS Lett, 2002. **531**(1): p. 103-8.

17. Rao, T.S., K.D. Lariosa-Willingham, F.F. Lin, E.L. Palfreyman, N. Yu, J. Chun, and M. Webb, *Pharmacological characterization of lysophospholipid receptor signal transduction pathways in rat cerebrocortical astrocytes.* Brain Res, 2003. **990**(1-2): p. 182-94.

18. Rao, T.S., K.D. Lariosa-Willingham, F.F. Lin, N. Yu, C.S. Tham, J. Chun, and M. Webb, *Growth factor pre-treatment differentially regulates phosphoinositide turnover downstream of lysophospholipid receptor and metabotropic glutamate receptors in cultured rat cerebrocortical astrocytes.* Int J Dev Neurosci, 2004. **22**(3): p. 131-5.

19. Webb, M., C.S. Tham, F.F. Lin, K. Lariosa-Willingham, N. Yu, J. Hale, S. Mandala, J. Chun, and T.S. Rao, *Sphingosine 1-phosphate receptor agonists attenuate relapsing-remitting experimental autoimmune encephalitis in SJL mice.* J Neuroimmunol, 2004. **153**(1-2): p. 108-21.

20. Weiner, J.A., J.H. Hecht, and J. Chun, *Lysophosphatidic acid receptor gene vzg-1/lpA1/edg-2 is expressed by mature oligodendrocytes during myelination in the postnatal murine brain.* J Comp Neurol, 1998. **398**(4): p. 587-98.

21. Contos, J.J., N. Fukushima, J.A. Weiner, D. Kaushal, and J. Chun, *Requirement for the lpA1 lysophosphatidic acid receptor gene in normal suckling behavior.* Proc Natl Acad Sci U S A, 2000. **97**(24): p. 13384-9.

22. Contos, J.J., I. Ishii, N. Fukushima, M.A. Kingsbury, X. Ye, S. Kawamura, J.H. Brown, and J. Chun, *Characterization of lpa(2) (Edg4) and lpa(1)/lpa(2) (Edg2/Edg4) lysophosphatidic acid receptor knockout mice: signaling deficits without obvious phenotypic abnormality attributable to lpa(2).* Mol Cell Biol, 2002. **22**(19): p. 6921-9.

23. Dubin, A.E., T. Bahnson, J.A. Weiner, N. Fukushima, and J. Chun, *Lysophosphatidic acid stimulates neurotransmitter-like conductance changes that precede GABA and L-glutamate in early, presumptive cortical neuroblasts.* J Neurosci, 1999. **19**(4): p. 1371-81.

24. Estivill-Torrus, G., P. Llebrez-Zayas, E. Matas-Rico, L. Santin, C. Pedraza, I. De Diego, I. Del Arco, P. Fernandez-Llebrez, J. Chun, and F.R. De Fonseca, *Absence of LPA1 signaling results in defective cortical development.* Cereb Cortex, 2008. **18**(4): p. 938-50.

25. Fukushima, N., J.A. Weiner, and J. Chun, *Lysophosphatidic acid (LPA) is a novel extracellular regulator of cortical neuroblast morphology.* Dev Biol, 2000. **228**(1): p. 6-18.

26. Fukushima, N., I. Ishii, Y. Habara, C.B. Allen, and J. Chun, *Dual regulation of actin rearrangement through lysophosphatidic acid receptor in neuroblast cell lines: actin depolymerization by Ca(2+)-alpha-actinin and polymerization by rho.* Mol Biol Cell, 2002. **13**(8): p. 2692-705.

27. Fukushima, N., S. Shano, R. Moriyama, and J. Chun, *Lysophosphatidic acid stimulates neuronal differentiation of cortical neuroblasts through the LPA1-G(i/o) pathway.* Neurochem Int, 2007. **50**(2): p. 302-7.

28. Hecht, J.H., J.A. Weiner, S.R. Post, and J. Chun, *Ventricular zone gene-1 (vzg-1) encodes a lysophosphatidic acid receptor expressed in neurogenic regions of the developing cerebral cortex.* J Cell Biol, 1996. **135**(4): p. 1071-83.

29. Herr, D.R., N. Grillet, M. Schwander, R. Rivera, U. Muller, and J. Chun, *Sphingosine 1-phosphate (S1P) signaling is required for maintenance of hair cells mainly via activation of S1P2.* J Neurosci, 2007. **27**(6): p. 1474-8.

30. Inoue, M., M.H. Rashid, R. Fujita, J.J. Contos, J. Chun, and H. Ueda, *Initiation of neuropathic pain requires lysophosphatidic acid receptor signaling.* Nat Med, 2004. **10**(7): p. 712-8.

31. Ishii, I., J.J. Contos, N. Fukushima, and J. Chun, *Functional comparisons of the lysophosphatidic acid receptors, LP(A1)/VZG-1/EDG-2, LP(A2)/EDG-4, and LP(A3)/EDG-7 in neuronal cell lines using a retrovirus expression system.* Mol Pharmacol, 2000. **58**(5): p. 895-902.

32. Ishii, I., B. Friedman, X. Ye, S. Kawamura, C. McGiffert, J.J. Contos, M.A. Kingsbury, G. Zhang, J.H. Brown, and J. Chun, *Selective loss of sphingosine 1-phosphate signaling with no obvious phenotypic abnormality in mice lacking its G protein-coupled receptor, LP(B3)/EDG-3.* J Biol Chem, 2001. **276**(36): p. 33697-704.

33. Kingsbury, M.A., S.K. Rehen, J.J. Contos, C.M. Higgins, and J. Chun, *Non-proliferative effects of lysophosphatidic acid enhance cortical growth and folding.* Nat Neurosci, 2003. **6**(12): p. 1292-9.

34. Weiner, J.A., N. Fukushima, J.J. Contos, S.S. Scherer, and J. Chun, *Regulation of Schwann cell morphology and adhesion by receptor-mediated lysophosphatidic acid signaling.* J Neurosci, 2001. **21**(18): p. 7069-78.

35. Weiner, J.A. and J. Chun, *Schwann cell survival mediated by the signaling phospholipid lysophosphatidic acid.* Proc Natl Acad Sci U S A, 1999. **96**(9): p. 5233-8.

36. Soliven, B., V. Miron, and J. Chun, *The neurobiology of sphingosine 1-phosphate signaling and sphingosine 1-phosphate receptor modulators.* Neurology, 2011. **76**(8 Suppl 3): p. S9-14.

37. Tham, C.S., F.F. Lin, T.S. Rao, N. Yu, and M. Webb, *Microglial activation state and lysophospholipid acid receptor expression.* Int J Dev Neurosci, 2003. **21**(8): p. 431-43.

38. Siehler, S. and D.R. Manning, *Pathways of transduction engaged by sphingosine 1-phosphate through G protein-coupled receptors.* Biochim Biophys Acta, 2002. **1582**(1-3): p. 94-9.

39. Novgorodov, A.S., M. El-Alwani, J. Bielawski, L.M. Obeid, and T.I. Gudz, *Activation of sphingosine-1-phosphate receptor S1P5 inhibits oligodendrocyte progenitor migration.* FASEB J, 2007. **21**(7): p. 1503-14.

40. Ishii, I., N. Fukushima, X. Ye, and J. Chun, *Lysophospholipid receptors: signaling and biology.* Annu Rev Biochem, 2004. **73**: p. 321-54.

41. Anliker, B. and J. Chun, *Lysophospholipid G protein-coupled receptors.* J Biol Chem, 2004. **279**(20): p. 20555-8.

42. Fukushima, N., I. Ishii, J.J. Contos, J.A. Weiner, and J. Chun, *Lysophospholipid receptors.* Annu Rev Pharmacol Toxicol, 2001. **41**: p. 507-34.

43. Wheeler, D., V.V. Bandaru, P.A. Calabresi, A. Nath, and N.J. Haughey, *A defect of sphingolipid metabolism modifies the properties of normal appearing white matter in multiple sclerosis.* Brain, 2008. **131**(Pt 11): p. 3092-102.

44. Kulakowska, A., M. Zendzian-Piotrowska, M. Baranowski, T. Kononczuk, W. Drozdowski, J. Gorski, and R. Bucki, *Intrathecal increase of sphingosine 1-phosphate at early stage multiple sclerosis.* Neurosci Lett, 2010. **477**(3): p. 149-52.

45. Qin, J., E. Berdyshev, J. Goya, V. Natarajan, and G. Dawson, *Neurons and oligodendrocytes recycle sphingosine 1-phosphate to ceramide: significance for apoptosis and multiple sclerosis.* J Biol Chem, 2010. **285**(19): p. 14134-43.

46. Van Doorn, R., J. Van Horssen, D. Verzijl, M. Witte, E. Ronken, B. Van Het Hof, K. Lakeman, C.D. Dijkstra, P. Van Der Valk, A. Reijerkerk, A.E. Alewijnse, S.L. Peters, and H.E. De Vries, *Sphingosine 1-phosphate receptor 1 and 3 are upregulated in multiple sclerosis lesions.* Glia, 2010. **58**(12): p. 1465-76.

47. Fischer, I., C. Alliod, N. Martinier, J. Newcombe, C. Brana, and S. Pouly, *Sphingosine kinase 1 and sphingosine 1-phosphate receptor 3 are functionally upregulated on astrocytes under pro-inflammatory conditions.* PLoS One, 2011. **6**(8): p. e23905.

48. Mandala, S., R. Hajdu, J. Bergstrom, E. Quackenbush, J. Xie, J. Milligan, R. Thornton, G.J. Shei, D. Card, C. Keohane, M. Rosenbach, J. Hale, C.L. Lynch, K. Rupprecht, W. Parsons, and H. Rosen, *Alteration of lymphocyte trafficking by sphingosine-1-phosphate receptor agonists.* Science, 2002. **296**(5566): p. 346-9.

49. Brinkmann, V., M.D. Davis, C.E. Heise, R. Albert, S. Cottens, R. Hof, C. Bruns, E. Prieschl, T. Baumruker, P. Hiestand, C.A. Foster, M. Zollinger, and K.R. Lynch, *The immune modulator FTY720 targets sphingosine 1-phosphate receptors.* J Biol Chem, 2002. **277**(24): p. 21453-7.

50. Chun, J. and V. Brinkmann, *A mechanistically novel, first oral therapy for multiple sclerosis: the development of fingolimod (FTY720, Gilenya).* Discov Med, 2011. **12**(64): p. 213-28.

51. Cohen, J.A. and J. Chun, *Mechanisms of fingolimod's efficacy and adverse effects in multiple sclerosis.* Ann Neurol, 2011. **69**(5): p. 759-77.

52. Brinkmann, V., A. Billich, T. Baumruker, P. Heining, R. Schmouder, G. Francis, S. Aradhye, and P. Burtin, *Fingolimod (FTY720): discovery and development of an oral drug to treat multiple sclerosis.* Nat Rev Drug Discov, 2010. **9**(11): p. 883-97.

53. Matloubian, M., C.G. Lo, G. Cinamon, M.J. Lesneski, Y. Xu, V. Brinkmann, M.L. Allende, R.L. Proia, and J.G. Cyster, *Lymphocyte egress from thymus and peripheral lymphoid organs is dependent on S1P receptor 1.* Nature, 2004. **427**(6972): p. 355-60.

54. Graler, M.H. and E.J. Goetzl, *The immunosuppressant FTY720 down-regulates sphingosine 1-phosphate G-protein-coupled receptors.* FASEB J, 2004. **18**(3): p. 551-3.

55. Oo, M.L., S. Thangada, M.T. Wu, C.H. Liu, T.L. Macdonald, K.R. Lynch, C.Y. Lin, and T. Hla, *Immunosuppressive and anti-angiogenic sphingosine 1-phosphate receptor-1 agonists induce ubiquitinylation and proteasomal degradation of the receptor.* J Biol Chem, 2007. **282**(12): p. 9082-9.

56. Graeler, M. and E.J. Goetzl, *Activation-regulated expression and chemotactic function of sphingosine 1-phosphate receptors in mouse splenic T cells.* FASEB J, 2002. **16**(14): p. 1874-8.

57. Mehling, M., V. Brinkmann, J. Antel, A. Bar-Or, N. Goebels, C. Vedrine, C. Kristofic, J. Kuhle, R.L. Lindberg, and L. Kappos, *FTY720 therapy exerts differential effects on T cell subsets in multiple sclerosis.* Neurology, 2008. **71**(16): p. 1261-7.

58. Pappu, R., S.R. Schwab, I. Cornelissen, J.P. Pereira, J.B. Regard, Y. Xu, E. Camerer, Y.W. Zheng, Y. Huang, J.G. Cyster, and S.R. Coughlin, *Promotion of lymphocyte egress into blood and lymph by distinct sources of sphingosine-1-phosphate.* Science, 2007. **316**(5822): p. 295-8.

59. Foster, C.A., L.M. Howard, A. Schweitzer, E. Persohn, P.C. Hiestand, B. Balatoni, R. Reuschel, C. Beerli, M. Schwartz, and A. Billich, *Brain penetration of the oral immunomodulatory drug FTY720 and its phosphorylation in the central nervous system during experimental autoimmune encephalomyelitis: consequences for mode of action in multiple sclerosis.* J Pharmacol Exp Ther, 2007. **323**(2): p. 469-75.

60. Miron, V.E., A. Schubart, and J.P. Antel, *Central nervous system-directed effects of FTY720 (fingolimod).* J Neurol Sci, 2008. **274**(1-2): p. 13-7.

61. Miron, V.E., S.K. Ludwin, P.J. Darlington, A.A. Jarjour, B. Soliven, T.E. Kennedy, and J.P. Antel, *Fingolimod (FTY720) enhances remyelination following demyelination of organotypic cerebellar slices.* Am J Pathol, 2010. **176**(6): p. 2682-94.

62. Choi, J.W., S.E. Gardell, D.R. Herr, R. Rivera, C.W. Lee, K. Noguchi, S.T. Teo, Y.C. Yung, M. Lu, G. Kennedy, and J. Chun, *FTY720 (fingolimod) efficacy in an animal model of multiple sclerosis requires astrocyte sphingosine 1-phosphate receptor 1 (S1P1) modulation.* Proc Natl Acad Sci U S A, 2011. **108**(2): p. 751-6.

63. Molofsky, A.V., R. Krencik, E.M. Ullian, H.H. Tsai, B. Deneen, W.D. Richardson, B.A. Barres, and D.H. Rowitch, *Astrocytes and disease: a neurodevelopmental perspective.* Genes Dev, 2012. **26**(9): p. 891-907.

64. Stahl, N. and G.D. Yancopoulos, *The tripartite CNTF receptor complex: activation and signaling involves components shared with other cytokines.* J Neurobiol, 1994. **25**(11): p. 1454-66.

65. Bonni, A., Y. Sun, M. Nadal-Vicens, A. Bhatt, D.A. Frank, I. Rozovsky, N. Stahl, G.D. Yancopoulos, and M.E. Greenberg, *Regulation of gliogenesis in the central nervous system by the JAK-STAT signaling pathway.* Science, 1997. **278**(5337): p. 477-83.

66. Wang, D.D. and A. Bordey, *The astrocyte odyssey.* Prog Neurobiol, 2008. **86**(4): p. 342-67.

67. Pfrieger, F.W., *Roles of glial cells in synapse development.* Cell Mol Life Sci, 2009. **66**(13): p. 2037-47.

68. Murphy, M., R. Dutton, S. Koblar, S. Cheema, and P. Bartlett, *Cytokines which signal through the LIF receptor and their actions in the nervous system.* Prog Neurobiol, 1997. **52**(5): p. 355-78.

69. Sofroniew, M.V. and H.V. Vinters, *Astrocytes: biology and pathology.* Acta Neuropathol, 2010. **119**(1): p. 7-35.

70. Barnabe-Heider, F., J.A. Wasylnka, K.J. Fernandes, C. Porsche, M. Sendtner, D.R. Kaplan, and F.D. Miller, *Evidence that embryonic neurons regulate the onset of cortical gliogenesis via cardiotrophin-1.* Neuron, 2005. **48**(2): p. 253-65.

71. Allaman, I., M. Belanger, and P.J. Magistretti, *Astrocyte-neuron metabolic relationships: for better and for worse.* Trends Neurosci, 2011. **34**(2): p. 76-87.

72. Miljkovic, D., G. Timotijevic, and M. Mostarica Stojkovic, *Astrocytes in the tempest of multiple sclerosis.* FEBS Lett, 2011. **585**(23): p. 3781-8.

73. Moore, C.S., S.L. Abdullah, A. Brown, A. Arulpragasam, and S.J. Crocker, *How factors secreted from astrocytes impact myelin repair.* J Neurosci Res, 2011. **89**(1): p. 13-21.

74. Luo, J., P. Ho, L. Steinman, and T. Wyss-Coray, *Bioluminescence in vivo imaging of autoimmune encephalomyelitis predicts disease.* J Neuroinflammation, 2008. **5**: p. 6.

75. Pebay, A., M. Toutant, J. Premont, C.F. Calvo, L. Venance, J. Cordier, J. Glowinski, and M. Tence, *Sphingosine-1-phosphate induces proliferation of astrocytes: regulation by intracellular signalling cascades.* Eur J Neurosci, 2001. **13**(12): p. 2067-76.

76. Anelli, V., R. Bassi, G. Tettamanti, P. Viani, and L. Riboni, *Extracellular release of newly synthesized sphingosine-1-phosphate by cerebellar granule cells and astrocytes.* J Neurochem, 2005. **92**(5): p. 1204-15.

77. Sorensen, S.D., O. Nicole, R.D. Peavy, L.M. Montoya, C.J. Lee, T.J. Murphy, S.F. Traynelis, and J.R. Hepler, *Common signaling pathways link activation of*

murine PAR-1, LPA, and S1P receptors to proliferation of astrocytes. Mol Pharmacol, 2003. **64**(5): p. 1199-209.

78. Wu, Y.P., K. Mizugishi, M. Bektas, R. Sandhoff, and R.L. Proia, *Sphingosine kinase 1/S1P receptor signaling axis controls glial proliferation in mice with Sandhoff disease.* Hum Mol Genet, 2008. **17**(15): p. 2257-64.

79. Mullershausen, F., L.M. Craveiro, Y. Shin, M. Cortes-Cros, F. Bassilana, M. Osinde, W.L. Wishart, D. Guerini, M. Thallmair, M.E. Schwab, R. Sivasankaran, K. Seuwen, and K.K. Dev, *Phosphorylated FTY720 promotes astrocyte migration through sphingosine-1-phosphate receptors.* J Neurochem, 2007. **102**(4): p. 1151-61.

80. Osinde, M., F. Mullershausen, and K.K. Dev, *Phosphorylated FTY720 stimulates ERK phosphorylation in astrocytes via S1P receptors.* Neuropharmacology, 2007. **52**(5): p. 1210-8.

81. Miller, R.H. and S. Mi, *Dissecting demyelination.* Nat Neurosci, 2007. **10**(11): p. 1351-4.

82. Terai, K., T. Soga, M. Takahashi, M. Kamohara, K. Ohno, S. Yatsugi, M. Okada, and T. Yamaguchi, *Edg-8 receptors are preferentially expressed in oligodendrocyte lineage cells of the rat CNS.* Neuroscience, 2003. **116**(4): p. 1053-62.

83. Yu, N., K.D. Lariosa-Willingham, F.F. Lin, M. Webb, and T.S. Rao, *Characterization of lysophosphatidic acid and sphingosine-1-phosphate-mediated signal transduction in rat cortical oligodendrocytes.* Glia, 2004. **45**(1): p. 17-27.

84. Jung, C.G., H.J. Kim, V.E. Miron, S. Cook, T.E. Kennedy, C.A. Foster, J.P. Antel, and B. Soliven, *Functional consequences of S1P receptor modulation in rat oligodendroglial lineage cells.* Glia, 2007. **55**(16): p. 1656-67.

85. Miron, V.E., J.A. Hall, T.E. Kennedy, B. Soliven, and J.P. Antel, *Cyclical and dose-dependent responses of adult human mature oligodendrocytes to fingolimod.* Am J Pathol, 2008. **173**(4): p. 1143-52.

86. Miron, V.E., C.G. Jung, H.J. Kim, T.E. Kennedy, B. Soliven, and J.P. Antel, *FTY720 modulates human oligodendrocyte progenitor process extension and survival.* Ann Neurol, 2008. **63**(1): p. 61-71.

87. Jaillard, C., S. Harrison, B. Stankoff, M.S. Aigrot, A.R. Calver, G. Duddy, F.S. Walsh, M.N. Pangalos, N. Arimura, K. Kaibuchi, B. Zalc, and C. Lubetzki, *Edg8/S1P5: an oligodendroglial receptor with dual function on process retraction and cell survival.* J Neurosci, 2005. **25**(6): p. 1459-69.

88. Coelho, R.P., S.G. Payne, R. Bittman, S. Spiegel, and C. Sato-Bigbee, *The immunomodulator FTY720 has a direct cytoprotective effect in oligodendrocyte progenitors.* J Pharmacol Exp Ther, 2007. **323**(2): p. 626-35.

89. Harada, J., M. Foley, M.A. Moskowitz, and C. Waeber, *Sphingosine-1-phosphate induces proliferation and morphological changes of neural progenitor cells.* J Neurochem, 2004. **88**(4): p. 1026-39.

90. Kajimoto, T., T. Okada, H. Yu, S.K. Goparaju, S. Jahangeer, and S. Nakamura, *Involvement of sphingosine-1-phosphate in glutamate secretion in hippocampal neurons.* Mol Cell Biol, 2007. **27**(9): p. 3429-40.

91. Mizugishi, K., T. Yamashita, A. Olivera, G.F. Miller, S. Spiegel, and R.L. Proia, *Essential role for sphingosine kinases in neural and vascular development.* Mol Cell Biol, 2005. **25**(24): p. 11113-21.

92. Kono, M., I.A. Belyantseva, A. Skoura, G.I. Frolenkov, M.F. Starost, J.L. Dreier, D. Lidington, S.S. Bolz, T.B. Friedman, T. Hla, and R.L. Proia, *Deafness and stria vascularis defects in S1P2 receptor-null mice.* J Biol Chem, 2007. **282**(14): p. 10690-6.

93. MacLennan, A.J., P.R. Carney, W.J. Zhu, A.H. Chaves, J. Garcia, J.R. Grimes, K.J. Anderson, S.N. Roper, and N. Lee, *An essential role for the H218/AGR16/Edg-5/LP(B2) sphingosine 1-phosphate receptor in neuronal excitability.* Eur J Neurosci, 2001. **14**(2): p. 203-9.

94. Ishii, I., X. Ye, B. Friedman, S. Kawamura, J.J. Contos, M.A. Kingsbury, A.H. Yang, G. Zhang, J.H. Brown, and J. Chun, *Marked perinatal lethality and cellular signaling deficits in mice null for the two sphingosine 1-phosphate (S1P) receptors, S1P(2)/LP(B2)/EDG-5 and S1P(3)/LP(B3)/EDG-3.* J Biol Chem, 2002. **277**(28): p. 25152-9.

95. Akahoshi, N., Y. Ishizaki, H. Yasuda, Y.L. Murashima, T. Shinba, K. Goto, T. Himi, J. Chun, and I. Ishii, *Frequent spontaneous seizures followed by spatial working memory/anxiety deficits in mice lacking sphingosine 1-phosphate receptor 2.* Epilepsy Behav, 2011. **22**(4): p. 659-65.

96. Edsall, L.C., G.G. Pirianov, and S. Spiegel, *Involvement of sphingosine 1-phosphate in nerve growth factor-mediated neuronal survival and differentiation.* J Neurosci, 1997. **17**(18): p. 6952-60.

97. Toman, R.E., S.G. Payne, K.R. Watterson, M. Maceyka, N.H. Lee, S. Milstien, J.W. Bigbee, and S. Spiegel, *Differential transactivation of sphingosine-1-phosphate receptors modulates NGF-induced neurite extension.* J Cell Biol, 2004. **166**(3): p. 381-392.

98. Zhang, Y.H., M.R. Vasko, and G.D. Nicol, *Intracellular sphingosine 1-phosphate mediates the increased excitability produced by nerve growth factor in rat sensory neurons.* J Physiol, 2006. **575**(Pt 1): p. 101-13.

99. Rau, C.R., K. Hein, M.B. Sattler, B. Kretzschmar, C. Hillgruber, B.L. McRae, R. Diem, and M. Bahr, *Anti-inflammatory effects of FTY720 do not prevent neuronal cell loss in a rat model of optic neuritis.* Am J Pathol, 2011. **178**(4): p. 1770-81.

100. Rossi, S., T. Lo Giudice, V. De Chiara, A. Musella, V. Studer, C. Motta, G. Bernardi, G. Martino, R. Furlan, A. Martorana, and D. Centonze, *Oral fingolimod rescues the functional deficits of synapses in experimental autoimmune encephalomyelitis.* Br J Pharmacol, 2012. **165**(4): p. 861-9.

101. Gao, Z. and S.E. Tsirka, *Animal models of MS reveal multiple roles of microglia in disease pathogenesis.* Neurol Res Int, 2011. **2011**: p. 383087.

102. Adams, R.A., J. Bauer, M.J. Flick, S.L. Sikorski, T. Nuriel, H. Lassmann, J.L. Degen, and K. Akassoglou, *The fibrin-derived gamma377-395 peptide inhibits microglia activation and suppresses relapsing paralysis in central nervous system autoimmune disease.* J Exp Med, 2007. **204**(3): p. 571-82.

103. Nayak, D., Y. Huo, W.X. Kwang, P.N. Pushparaj, S.D. Kumar, E.A. Ling, and S.T. Dheen, *Sphingosine kinase 1 regulates the expression of proinflammatory cytokines and nitric oxide in activated microglia.* Neuroscience, 2010. **166**(1): p. 132-44.

104. Durafourt, B.A., C. Lambert, T.A. Johnson, M. Blain, A. Bar-Or, and J.P. Antel, *Differential responses of human microglia and blood-derived myeloid cells to FTY720.* J Neuroimmunol, 2011. **230**(1-2): p. 10-6.

105. Yoshino, T., H. Tabunoki, S. Sugiyama, K. Ishii, S.U. Kim, and J. Satoh, *Non-phosphorylated FTY720 induces apoptosis of human microglia by activating SREBP2.* Cell Mol Neurobiol, 2011. **31**(7): p. 1009-20.

106. Zhang, Z., Z. Zhang, U. Fauser, M. Artelt, M. Burnet, and H.J. Schluesener, *FTY720 attenuates accumulation of EMAP-II+ and MHC-II+ monocytes in early lesions of rat traumatic brain injury.* J Cell Mol Med, 2007. **11**(2): p. 307-14.

107. Czech, B., W. Pfeilschifter, N. Mazaheri-Omrani, M.A. Strobel, T. Kahles, T. Neumann-Haefelin, A. Rami, A. Huwiler, and J. Pfeilschifter, *The immunomodulatory sphingosine 1-phosphate analog FTY720 reduces lesion size and improves neurological outcome in a mouse model of cerebral ischemia.* Biochem Biophys Res Commun, 2009. **389**(2): p. 251-6.

108. Jackson, S.J., G. Giovannoni, and D. Baker, *Fingolimod modulates microglial activation to augment markers of remyelination.* J Neuroinflammation, 2011. **8**: p. 76.

109. Zozulya, A.L., B.D. Clarkson, S. Ortler, Z. Fabry, and H. Wiendl, *The role of dendritic cells in CNS autoimmunity.* J Mol Med (Berl), 2010. **88**(6): p. 535-44.

110. Correale, J. and A. Villa, *The blood-brain-barrier in multiple sclerosis: functional roles and therapeutic targeting.* Autoimmunity, 2007. **40**(2): p. 148-60.

111. Lee, M.J., S. Thangada, K.P. Claffey, N. Ancellin, C.H. Liu, M. Kluk, M. Volpi, R.I. Sha'afi, and T. Hla, *Vascular endothelial cell adherens junction assembly and morphogenesis induced by sphingosine-1-phosphate.* Cell, 1999. **99**(3): p. 301-12.

112. Zhu, D., Y. Wang, I. Singh, R.D. Bell, R. Deane, Z. Zhong, A. Sagare, E.A. Winkler, and B.V. Zlokovic, *Protein S controls hypoxic/ischemic blood-brain barrier disruption through the TAM receptor Tyro3 and sphingosine 1-phosphate receptor.* Blood, 2010. **115**(23): p. 4963-72.

113. Sanchez, T., T. Estrada-Hernandez, J.H. Paik, M.T. Wu, K. Venkataraman, V. Brinkmann, K. Claffey, and T. Hla, *Phosphorylation and action of the immunomodulator FTY720 inhibits vascular endothelial cell growth factor-induced vascular permeability.* J Biol Chem, 2003. **278**(47): p. 47281-90.

114. Peng, X., P.M. Hassoun, S. Sammani, B.J. McVerry, M.J. Burne, H. Rabb, D. Pearse, R.M. Tuder, and J.G. Garcia, *Protective effects of sphingosine 1-*

phosphate in murine endotoxin-induced inflammatory lung injury. Am J Respir Crit Care Med, 2004. **169**(11): p. 1245-51.

115. Dudek, S.M., S.M. Camp, E.T. Chiang, P.A. Singleton, P.V. Usatyuk, Y. Zhao, V. Natarajan, and J.G. Garcia, *Pulmonary endothelial cell barrier enhancement by FTY720 does not require the S1P1 receptor.* Cell Signal, 2007. **19**(8): p. 1754-64.

116. Correale, J. and A. Villa, *Cellular elements of the blood-brain barrier.* Neurochem Res, 2009. **34**(12): p. 2067-77.

117. Cuzner, M.L. and G. Opdenakker, *Plasminogen activators and matrix metalloproteases, mediators of extracellular proteolysis in inflammatory demyelination of the central nervous system.* J Neuroimmunol, 1999. **94**(1-2): p. 1-14.

118. Waubant, E., D.E. Goodkin, L. Gee, P. Bacchetti, R. Sloan, T. Stewart, P.B. Andersson, G. Stabler, and K. Miller, *Serum MMP-9 and TIMP-1 levels are related to MRI activity in relapsing multiple sclerosis.* Neurology, 1999. **53**(7): p. 1397-401.

119. Foster, C.A., D. Mechtcheriakova, M.K. Storch, B. Balatoni, L.M. Howard, F. Bornancin, A. Wlachos, J. Sobanov, A. Kinnunen, and T. Baumruker, *FTY720 rescue therapy in the dark agouti rat model of experimental autoimmune encephalomyelitis: expression of central nervous system genes and reversal of blood-brain-barrier damage.* Brain Pathol, 2009. **19**(2): p. 254-66.

120. Al-Izki, S., G. Pryce, S.J. Jackson, G. Giovannoni, and D. Baker, *Immunosuppression with FTY720 is insufficient to prevent secondary progressive neurodegeneration in experimental autoimmune encephalomyelitis.* Mult Scler, 2011. **17**(8): p. 939-48.

121. Kataoka, H., K. Sugahara, K. Shimano, K. Teshima, M. Koyama, A. Fukunari, and K. Chiba, *FTY720, sphingosine 1-phosphate receptor modulator, ameliorates experimental autoimmune encephalomyelitis by inhibition of T cell infiltration.* Cell Mol Immunol, 2005. **2**(6): p. 439-48.

122. Papadopoulos, D., J. Rundle, R. Patel, I. Marshall, J. Stretton, R. Eaton, J.C. Richardson, M.I. Gonzalez, K.L. Philpott, and R. Reynolds, *FTY720 ameliorates MOG-induced experimental autoimmune encephalomyelitis by suppressing both cellular and humoral immune responses.* J Neurosci Res, 2010. **88**(2): p. 346-59.

123. Hu, Y., X. Lee, B. Ji, K. Guckian, D. Apicco, R.B. Pepinsky, R.H. Miller, and S. Mi, *Sphingosine 1-phosphate receptor modulator fingolimod (FTY720) does not promote remyelination in vivo.* Mol Cell Neurosci, 2011. **48**(1): p. 72-81.

124. Kim, H.J., V.E. Miron, D. Dukala, R.L. Proia, S.K. Ludwin, M. Traka, J.P. Antel, and B. Soliven, *Neurobiological effects of sphingosine 1-phosphate receptor modulation in the cuprizone model.* FASEB J, 2011. **25**(5): p. 1509-18.

125. Anthony, D.C., N.R. Sibson, P.H. Losey, D. Piani Meier, and D. Leppert, *Fingolimod (FTY720) therapy for a focal pattern I model of multiple sclerosis prevents lesion formation and progression in both prophylactic and treatment regimens.* J Neuropathol Exp Neurol, 2012. **Submitted**.

126. Deogracias, R., M. Yazdani, M.P. Dekkers, J. Guy, M.C. Ionescu, K.E. Vogt, and Y.A. Barde, *Fingolimod, a sphingosine-1 phosphate receptor modulator, increases BDNF levels and improves symptoms of a mouse model of Rett syndrome.* Proc Natl Acad Sci U S A, 2012.

127. Sheridan, G.K. and K.K. Dev, *S1P1 receptor subtype inhibits demyelination and regulates chemokine release in cerebellar slice cultures.* Glia, 2012. **60**(3): p. 382-92.

128. Greenberg, M.E. and E.B. Ziff, *Stimulation of 3T3 cells induces transcription of the c-fos proto-oncogene.* Nature, 1984. **311**(5985): p. 433-8.

129. Muller, R., R. Bravo, J. Burckhardt, and T. Curran, *Induction of c-fos gene and protein by growth factors precedes activation of c-myc.* Nature, 1984. **312**(5996): p. 716-20.

130. Cochran, B.H., J. Zullo, I.M. Verma, and C.D. Stiles, *Expression of the c-fos gene and of an fos-related gene is stimulated by platelet-derived growth factor.* Science, 1984. **226**(4678): p. 1080-2.

131. Lau, L.F. and D. Nathans, *Expression of a set of growth-related immediate early genes in BALB/c 3T3 cells: coordinate regulation with c-fos or c-myc.* Proc Natl Acad Sci U S A, 1987. **84**(5): p. 1182-6.

132. Beckmann, A.M. and P.A. Wilce, *Egr transcription factors in the nervous system.* Neurochem Int, 1997. **31**(4): p. 477-510; discussion 517-6.

133. Tullai, J.W., M.E. Schaffer, S. Mullenbrock, G. Sholder, S. Kasif, and G.M. Cooper, *Immediate-early and delayed primary response genes are distinct in function and genomic architecture.* J Biol Chem, 2007. **282**(33): p. 23981-95.

134. Sagar, S.M., F.R. Sharp, and T. Curran, *Expression of c-fos protein in brain: metabolic mapping at the cellular level.* Science, 1988. **240**(4857): p. 1328-31.

135. Shaulian, E. and M. Karin, *AP-1 as a regulator of cell life and death.* Nat Cell Biol, 2002. **4**(5): p. E131-6.

136. Peterson, L.K. and R.S. Fujinami, *Inflammation, demyelination, neurodegeneration and neuroprotection in the pathogenesis of multiple sclerosis.* J Neuroimmunol, 2007. **184**(1-2): p. 37-44.

137. Oo, T.F., C. Henchcliffe, D. James, and R.E. Burke, *Expression of c-fos, c-jun, and c-jun N-terminal kinase (JNK) in a developmental model of induced apoptotic death in neurons of the substantia nigra.* J Neurochem, 1999. **72**(2): p. 557-64.

138. Zheng, W., L. Niu, C. Zhang, C. Zhu, F. Xie, C. Cao, and G. Li, *Brain edema and protein expression of c-Fos and c-Jun in the brain after diffused brain injury.* Int J Clin Exp Pathol, 2014. **7**(6): p. 2809-17.

139. Cohen, R.I., E. Molina-Holgado, and G. Almazan, *Carbachol stimulates c-fos expression and proliferation in oligodendrocyte progenitors.* Brain Res Mol Brain Res, 1996. **43**(1-2): p. 193-201.

140. Khorchid, A., J.N. Larocca, and G. Almazan, *Characterization of the signal transduction pathways mediating noradrenaline-stimulated MAPK activation and c-fos expression in oligodendrocyte progenitors.* J Neurosci Res, 1999. **58**(6): p. 765-78.

141. Bichenkov, E. and J.S. Ellingson, *Ethanol alters the expressions of c-Fos and myelin basic protein in differentiating oligodendrocytes.* Alcohol, 2009. **43**(8): p. 627-34.

142. Liu, H.N. and G. Almazan, *Glutamate induces c-fos proto-oncogene expression and inhibits proliferation in oligodendrocyte progenitors: receptor characterization.* Eur J Neurosci, 1995. **7**(12): p. 2355-63.

143. Radhakrishna, M. and G. Almazan, *Protein kinases mediate basic fibroblast growth factor's stimulation of proliferation and c-fos induction in oligodendrocyte progenitors.* Brain Res Mol Brain Res, 1994. **24**(1-4): p. 118-28.

144. Condorelli, D.F., L. Kaczmarek, F. Nicoletti, A. Arcidiacono, P. Dell'Albani, F. Ingrao, G. Magri, L. Malaguarnera, R. Avola, A. Messina, and et al., *Induction of protooncogene fos by extracellular signals in primary glial cell cultures.* J Neurosci Res, 1989. **23**(2): p. 234-9.

145. Hisanaga, K., S.M. Sagar, K.J. Hicks, R.A. Swanson, and F.R. Sharp, *c-fos proto-oncogene expression in astrocytes associated with differentiation or proliferation but not depolarization.* Brain Res Mol Brain Res, 1990. **8**(1): p. 69-75.

146. Butler, T.L. and K.R. Pennypacker, *Temporal and regional expression of Fos-related proteins in response to ischemic injury.* Brain Res Bull, 2004. **63**(1): p. 65-73.

147. Suzuki, S., A.J. Li, T. Akaike, and T. Imamura, *Intracerebroventricular infusion of fibroblast growth factor-1 increases Fos immunoreactivity in periventricular astrocytes in rat hypothalamus.* Neurosci Lett, 2001. **300**(1): p. 29-32.

148. Wu, B.Y. and A.C. Yu, *Quercetin inhibits c-fos, heat shock protein, and glial fibrillary acidic protein expression in injured astrocytes.* J Neurosci Res, 2000. **62**(5): p. 730-6.

149. Fernandez, A.M., J. Garcia-Estrada, L.M. Garcia-Segura, and I. Torres-Aleman, *Insulin-like growth factor I modulates c-Fos induction and astrocytosis in response to neurotoxic insult.* Neuroscience, 1997. **76**(1): p. 117-22.

150. Bodega, G., I. Suarez, L. Almonacid, S. Ciordia, A. Beloso, L.A. Lopez-Fernandez, A. Zaballos, and B. Fernandez, *Effect of ammonia on ciliary neurotrophic factor mRNA and protein expression and its upstream signalling pathway in cultured rat astroglial cells: possible implication of c-fos, Sp1 and p38MAPK.* Neuropathol Appl Neurobiol, 2007. **33**(4): p. 420-30.

151. Sorkin, L.S., K. Maruyama, D.L. Boyle, L. Yang, M. Marsala, and G.S. Firestein, *Spinal adenosine agonist reduces c-fos and astrocyte activation in dorsal horn of rats with adjuvant-induced arthritis.* Neurosci Lett, 2003. **340**(2): p. 119-22.

152. Fraczek, L.A., C.B. Martin, and B.K. Martin, *c-Jun and c-Fos regulate the complement factor H promoter in murine astrocytes.* Mol Immunol, 2011. **49**(1-2): p. 201-10.

153. Hiscock, J.J., L. Mackenzie, and J.O. Willoughby, *Pentobarbitone induces Fos in astrocytes: increased expression following picrotoxin and seizures.* Exp Neurol, 1996. **139**(1): p. 115-20.

154. Schinelli, S., P. Zanassi, M. Paolillo, H. Wang, A. Feliciello, and V. Gallo, *Stimulation of endothelin B receptors in astrocytes induces cAMP response element-binding protein phosphorylation and c-fos expression via multiple mitogen-activated protein kinase signaling pathways.* J Neurosci, 2001. **21**(22): p. 8842-53.

155. Hung, A.C., H.M. Huang, H.J. Tsay, T.N. Lin, J.S. Kuo, and S.H. Sun, *ATP-stimulated c-fos and zif268 mRNA expression is inhibited by chemical hypoxia in a rat brain-derived type 2 astrocyte cell line, RBA-2.* J Cell Biochem, 2000. **77**(2): p. 323-32.

156. Matsunaga, W., S. Osawa, S. Miyata, and T. Kiyohara, *Astrocytic Fos expression in the rat posterior pituitary following LPS administration.* Brain Res, 2001. **898**(2): p. 215-23.

157. Gabellini, N., L. Facci, D. Milani, A. Negro, L. Callegaro, S.D. Skaper, and A. Leon, *Differences in induction of c-fos transcription by cholera toxin-derived cyclic AMP and Ca2+ signals in astrocytes and 3T3 fibroblasts.* Exp Cell Res, 1991. **194**(2): p. 210-7.

158. Jenab, S. and V. Quinones-Jenab, *The effects of interleukin-6, leukemia inhibitory factor and interferon-gamma on STAT DNA binding and c-fos mRNA levels in cortical astrocytes and C6 glioma cells.* Neuro Endocrinol Lett, 2002. **23**(4): p. 325-8.

159. Suh, H.W., S.S. Choi, J.K. Lee, H.K. Lee, E.J. Han, and J. Lee, *Regulation of c-fos and c-jun gene expression by lipopolysaccharide and cytokines in primary cultured astrocytes: effect of PKA and PKC pathways.* Arch Pharm Res, 2004. **27**(4): p. 396-401.

160. Sagar, S.M., K.J. Price, N.W. Kasting, and F.R. Sharp, *Anatomic patterns of Fos immunostaining in rat brain following systemic endotoxin administration.* Brain Res Bull, 1995. **36**(4): p. 381-92.

161. Rubio, N. and B. Martin-Clemente, *Theiler's murine encephalomyelitis virus infection induces early expression of c-fos in astrocytes.* Virology, 1999. **258**(1): p. 21-9.

162. Rubio, N., *Interferon-gamma induces the expression of immediate early genes c-fos and c-jun in astrocytes.* Immunology, 1997. **91**(4): p. 560-4.

163. Sun, Y.N., J.Y. Luo, Z.R. Rao, L. Lan, and L. Duan, *GFAP and Fos immunoreactivity in lumbo-sacral spinal cord and medulla oblongata after chronic colonic inflammation in rats.* World J Gastroenterol, 2005. **11**(31): p. 4827-32.

164. Hsieh, H.L., H.H. Wang, C.Y. Wu, and C.M. Yang, *Reactive Oxygen Species-Dependent c-Fos/Activator Protein 1 Induction Upregulates Heme Oxygenase-1 Expression by Bradykinin in Brain Astrocytes.* Antioxid Redox Signal, 2010. **13**(12): p. 1829-44.

165. Yester, J.W., L. Bryan, M.R. Waters, B. Mierzenski, D.D. Biswas, A.S. Gupta, R. Bhardwaj, M.J. Surace, J.M. Eltit, S. Milstien, S. Spiegel, and T. Kordula, *Sphingosine-1-phosphate inhibits IL-1-induced expression of C-C motif ligand 5 via c-Fos-dependent suppression of IFN-beta amplification loop.* FASEB J, 2015.

166. Jain, J., E.A. Nalefski, P.G. McCaffrey, R.S. Johnson, B.M. Spiegelman, V. Papaioannou, and A. Rao, *Normal peripheral T-cell function in c-Fos-deficient mice.* Mol Cell Biol, 1994. **14**(3): p. 1566-74.

167. Eun, S.Y., Y.H. Hong, E.H. Kim, H. Jeon, Y.H. Suh, J.E. Lee, C. Jo, S.A. Jo, and J. Kim, *Glutamate receptor-mediated regulation of c-fos expression in cultured microglia.* Biochem Biophys Res Commun, 2004. **325**(1): p. 320-7.

168. Lin, H.Y., C.H. Tang, J.H. Chen, J.Y. Chuang, S.M. Huang, T.W. Tan, C.H. Lai, and D.Y. Lu, *Peptidoglycan induces interleukin-6 expression through the TLR2 receptor, JNK, c-Jun, and AP-1 pathways in microglia.* J Cell Physiol, 2011. **226**(6): p. 1573-82.

169. Kruijer, W., J.A. Cooper, T. Hunter, and I.M. Verma, *Platelet-derived growth factor induces rapid but transient expression of the c-fos gene and protein.* Nature, 1984. **312**(5996): p. 711-6.

170. Smeyne, R.J., K. Schilling, L. Robertson, D. Luk, J. Oberdick, T. Curran, and J.I. Morgan, *fos-lacZ transgenic mice: mapping sites of gene induction in the central nervous system.* Neuron, 1992. **8**(1): p. 13-23.

171. Reijmers, L.G., B.L. Perkins, N. Matsuo, and M. Mayford, *Localization of a stable neural correlate of associative memory.* Science, 2007. **317**(5842): p. 1230-3.

172. Foudi, A., K. Hochedlinger, D. Van Buren, J.W. Schindler, R. Jaenisch, V. Carey, and H. Hock, *Analysis of histone 2B-GFP retention reveals slowly cycling hematopoietic stem cells.* Nat Biotechnol, 2009. **27**(1): p. 84-90.

173. Kanda, T., K.F. Sullivan, and G.M. Wahl, *Histone-GFP fusion protein enables sensitive analysis of chromosome dynamics in living mammalian cells.* Curr Biol, 1998. **8**(7): p. 377-85.

174. Tayler, K.K., E. Lowry, K. Tanaka, B. Levy, L. Reijmers, M. Mayford, and B.J. Wiltgen, *Characterization of NMDAR-Independent Learning in the Hippocampus.* Front Behav Neurosci, 2011. **5**: p. 28.

175. Tumbar, T., G. Guasch, V. Greco, C. Blanpain, W.E. Lowry, M. Rendl, and E. Fuchs, *Defining the epithelial stem cell niche in skin.* Science, 2004. **303**(5656): p. 359-63.

176. Tayler, K.K., K.Z. Tanaka, L.G. Reijmers, and B.J. Wiltgen, *Reactivation of neural ensembles during the retrieval of recent and remote memory.* Curr Biol, 2013. **23**(2): p. 99-106.

Chapter 2:

Assessing the capabilities of c-Fos reporter mice to indicate EAE activity

2.A. Introduction

The use of IEGs as indicators of neuronal activity has been extensively used to track brain activation in response to external stimuli and, in learning and memory. The novel TetTag system extends the utility of IEG expression allowing active cells to be semi-permanently marked only during experimentally defined time periods. In this chapter, EAE will be induced in TetTag mice to determine if a c-Fos reporter can identify EAE-related activity within the spinal cord. Further, the time course of such c-Fos activity induction will be established. Finally, the cell-type(s) that are c-Fos activated by EAE will be identified in the spinal cord.

2.B. Materials and Methods

TetTag mice

The TetTag bi-transgenic mice expressing a c-Fos inducible tetracycline transactivator (tTA) protein and a histone 2B-GFP (H2B-GFP) fusion protein controlled by a tetO promoter were created and provided by Dr. Mark Mayford of The Scripps Research Institute [1]. Mice were maintained on DOX chow (40 mg/kg) throughout breeding, birth, and development to prevent GFP-H2B expression until experimental examination.

EAE induction

EAE was induced in 7- to 10-wk old TetTag mice. Equal parts of 3 mg/mL MOG_{35-55} (MEVGWYRSPFSRVVHLYRNGK, EZBiolab) in Dulbecco's phosphate

buffered saline without calcium and magnesium (Life Technologies) and complete Freund's adjuvant (CFA; made with 2 mg/mL M. Tuberculosis H37Ra (Difco) in incomplete Freund's adjuvant (Difco)) was emulsified. Mice were anesthetized with isoflurane and 0.1 mL of the CFA-MOG_{35-55} emulsion was injected subcutaneously on the lower back. Mice were weighed and monitored daily.

EAE scoring

Daily clinical scores corresponding to the most severe sign observed were given as follows:

0	no signs
0.5	mild tail tone loss
1.0	complete tail tone loss
1.5	abnormal gait
2.0	impaired righting reflex
2.5	hind-limb paresis
3.0	hind-limb paralysis
3.5	hind-body paresis
4.0	fore-limb paralysis
4.5	death or severity necessitating euthanasia

Experimental examination by doxycycline removal

To allow examination of c-Fos activity during distinct phases of EAE, DOX chow was removed and replaced with normal chow for the specified period. Pre-onset period is defined as a period in which no clinical signs were observed for the entire duration. The post-onset period begins when a mouse reaches a clinical score of 1.0 or greater, at

which point DOX chow is removed for the specified period of time. Mice were sacrificed at the end of the examination period.

Histological examination of lower spinal cords

Mice were deeply anesthetized with an overdose of isoflurane anesthesia then lower spinal cords (LSC) were rapidly dissected out, embedded in Tissue-Tek Optimal Cutting Temperature (OCT; Ted Pella Inc) in 3 sections to ensure complete examination throughout the LSC, and frozen on crushed dry ice. Cryostat sections (16 μm) were collected on Superfrost Plus microscope slides (Fisher Scientific) and fixed (10 min) with freshly prepared 4% paraformaldehyde (PFA) in PBS.

For the examination of the extent of activity, sections were counterstained with 4',6-diamidino-2-phenylindole (DAPI; 1:10,000), washed, and coverslipped with Vectashield Antifade Mounting Medium (Vector). Sections were visualized and images acquired on either a Zeiss Imager 1D microscope (Axiovision 4.8), a Zeiss ApoTome.2 (Zen 2 Blue Edition) or a Nikon $A1^+$ (NIS Elements 4.4). Image brightness and contrast were adjusted with Adobe Photoshop (CS6) for visual display. Quantification of the nuclear GFP-H2B as a percent of total nuclei was done using ImageJ (v 1.46r) and Dunnett's multiple comparison tests were used to compare extent of GFP-H2B.

Immunohistochemistry to determine active cell type(s)

EAE was induced in TetTag mice and DOX was removed upon EAE sign onset for 5 days (Acute EAE, 5d post-onset), and LSCs were collected. Fixed sections, prepared as described above, were washed (3x, 5 min) in 0.3M glycine in TBS, permeabilized (10 min) with 0.1% triton x-100 in TBS, blocked (1h) with species-appropriate serum, and immunolabeled (overnight at 4°C). Co-localization of GFP-H2B

and cell type specific markers was performed using antibodies specific for astrocytes with GFAP (Neuromics; 1:1000), neurons with NeuN (EMD Millipore, 1:400), T cells with CD3 (eBioscience, 1:500), oligodendrocytes lineage cells with Olig1,2,3 (Neuromics, 1:100), and microglia with Iba1 (Wako, 1:500). Antigen retrieval with Diva Decloaker (Biocare) was performed in place of permeabilization for Olig1,2,3 staining. Sections were washed in TBS, labeled with species-appropriate secondary antibodies, counterstained with DAPI (1:10,000), and coverslipped with Vectashield. Sections were visualized and images acquired on either a Zeiss Imager 1D microscope (Axiovision 4.8), a Zeiss ApoTome.2 (Zen 2 Blue Edition) or a Nikon A1$^+$ (NIS Elements 4.4). Image brightness and contrast were adjusted with Adobe Photoshop (CS6) for visual display.

Peripheral lymphocyte examination by histology and flow cytometry

Mice were deeply anesthetized with an overdose of isoflurane anesthesia and inguinal lymph nodes were dissected out. For histological examination, lymph nodes were embedded in OCT, frozen on crushed dry ice, and cryosectioned (16 μm thick). Sections were counterstained with DAPI and imaged on a Zeiss Imager 1D microscope (Axiovision 4.8). For flow cytometric analysis, lymph nodes were mechanically dissociated, filtered (40 μm), and immunolabelled with anti-mouse CD3e PE-Cyanine5 (eBioscience, 1:1000). Flow cytometry was performed on an LSR-II (BD Biosciences) and analyzed using FlowJo (10.0.8r1).

2.C. Results

EAE is inducible in TetTag mice

The TetTag mice were backcrossed into C57BL/6J for at least 7 generations. To ensure these TetTag mice were susceptible to EAE, mice were immunized and scores

were monitored daily (**Figure 2.1**). The EAE phenotype was typical, progressing from tail paralysis to hind limb impairment and paralysis, indicating that TetTag system and DOX chow had no apparent effect on the EAE clinical course.

EAE induces activation in the CNS within lesions

Most EAE studies focus on the spinal cord as they contain more pathological hallmarks that closely parallel those of MS including dense, inflammatory lesions with demyelination [2]. Spinal cords were examined in TetTag mice for their ability to produce EAE-activity dependent expression of GFP-H2B upon removal of DOX (**Figure 2.2**). First, the LSCs were examined in animals receiving DOX chow (ON DOX) in naïve mice. Naïve ON DOX mice effectively exhibited no GFP-H2B expression. After removal of DOX for 5 days (5d Naïve), naïve mice exhibited few, sparse GFP expressing cells. When DOX was removed during acute EAE (5d post-onset), GFP expressing cells were abundantly increased. Most of the expression was in distinctly apparent lesions and on the periphery of the LSCs.

Onset of EAE signs coincides with increases in GFP-H2B in the CNS

To determine when EAE stimulation initiates c-Fos activity, LSCs were observed at multiple time points until EAE sign onset. Three groups of EAE-immunized mice had DOX removed for 5-day periods (each ending on either 6-days post immunization (dpi), 8-dpi, or 10-dpi) then sacrificed to examine extent of GFP positivity (**Figure 2.3**). All examination periods prior to the onset of EAE signs had low levels of activation. Mice that developed EAE signs had a significantly higher level of activation with increases coinciding with both severity and EAE sign duration before sacrifice. These results

provide a rationale for the further characterization of CNS c-Fos activation during the acute phase of EAE by removing DOX at the onset of EAE signs.

Cell type(s) activated in c-Fos reporter mice during acute EAE:

Lymphocytes are c-Fos activated in the periphery but not in the CNS

The pathogenesis of EAE is initiated in lymph nodes whereby dendritic cells present myelin peptide components to activate myelin-specific T cells [3]. Lymph nodes were examined for activity dependent GFP expression for 5 days in CD3+ (present in all stages of T cell development) cells in naïve and 5d post-onset (**Figure 2.4.1**). Histological examination revealed GFP expression throughout the lymph nodes, which were labeled with a CD3 antibody and quantified by flow cytometry. T cell c-Fos activation in naïve lymph nodes was 21.30% ± 2.702, while in post-onset EAE lymph nodes was 29.15% ± 0.950. T cells were then interrogated for c-Fos dependent GFP expression in the acute EAE spinal cord. The presence of CD3 positive lymphocytes was confirmed in 5d post-onset EAE mice, however co-localization of CD3 with c-Fos activated GFP-H2B was not observed.

Microglia are not c-Fos activated during acute EAE

Microglia re-stimulate myelin-specific T cells as they first cross the BBB and release cytokines which help more pathogenic T cells to enter the CNS [4]. Ionized calcium-binding adaptor molecule 1 (Iba1) is a protein that is specifically expressed in microglia in the CNS [5]. An antibody against Iba1 revealed many microglia throughout the acute EAE LSC, however there appeared to be no c-Fos activated GFP in microglia during this 5d post-onset period (**Figure 2.4.2**).

Oligodendrocyte lineage cells are not c-Fos activated during acute EAE

Demyelination and oligodendrocyte damage are hallmarks of MS and EAE pathology, and processes of remyelination are important to the clinical course [6]. Localizing the nucleus of oligodendrocytes with a traditional oligodendrocyte markers may be difficult since oligodendrocyte projections are numerous and diffuse. An antibody against oligodendrocyte transcription factors 1, 2, and 3 (olig1,2,3) preferentially stains the nucleus of oligodendrocyte lineage cells at various stages of development [7-10]. Labeling olig1,2,3 revealed oligodendrocyte lineage cells which were not c-Fos activated as they did not co-localize with H2B-GFP during the 5d post-onset time period (**Figure 2.4.3**).

Neurons are activated sparsely and not in acute EAE lesions

Neuronal c-Fos activity was assessed in acute EAE (5d post-onset) LSCs. The neuronal nuclear (NeuN) protein was used to specifically label neurons [11] (**Figure 2.4.4**). Co-localization of NeuN and GFP-H2B was observed in 5d post-onset LSCs in 0.66% ± 0.14 of the c-Fos active cells. The vast majority of GFP positive cells were NeuN negative. Additionally, c-Fos activated neurons were also present to a similar degree during 5d naïve and 5d pre-onset examinations.

Astrocytes are the predominant c-Fos activated cell type in EAE

Astrocytes have many proposed roles in MS and EAE and astrocytic $S1P_1$ has been shown to be the primary target of fingolimod efficacy in EAE [12]. The c-Fos activity of astrocytes was assessed during 5d post-onset by labeling with astrocyte-specific glial fibrillary acidic protein (GFAP) antibody. The vast majority of GFP positive cells were GFAP labeled (% 95.09 ± 0.73) (**Figure 2.4.5**). In lesions containing high c-

Fos activation, astrocytes comprised nearly all of the GFP positive cells. There were also GFP-H2B positive astrocytes on the periphery of the LSCs. Many astrocytes were not c-Fos activated, especially outside of lesion areas.

2.D. Discussion

The TetTag c-Fos reporter mice have tremendous utility in the mouse model of MS, EAE, by permitting a comprehensive survey for activity in the CNS. Before the development of EAE signs, there is negligible “baseline” activation. At the onset of EAE signs, c-Fos dependent GFP expression is robustly increased. The acute phase of EAE (5 days post-onset of EAE signs) was further examined to identify which cell types were c-Fos activated. Some c-Fos activation is seen in neurons, however the vast majority of activation occurs in astrocyte populations. In the next chapter I will leverage the TetTag mice to expansively explore how astrocyte activity during EAE is altered by relevant S1P receptor modulation. In this context, I will characterize how astrocyte activity is related to disease severity and disease progression.

The near exclusive c-Fos activation of astrocytes in the spinal cord during acute EAE is consistent with some previous studies and does not indicate the absence of “activity” in other cell types. In neural cell types isolated from the cerebral cortex, expression levels of c-Fos in astrocytes may be over three times that of neurons and microglia and nearly thirty-times that of oligodendrocyte lineage cells [10]. EAE related stimuli, such as S1P, elicit even further c-Fos expression in astrocytes [13]. In neurons, “activity” is relatively easy to define as neurons have virtually one functional modality of firing action potentials that is reliably associated with c-Fos expression. In other cell types, “activity” is more difficult to define and often more diverse. The dependency on c-Fos in all these diverse activity states is not absolute and if one were to examine an

activity reporter mouse using an IEG such as the activity-regulated cytoskeletal-associated protein (Arc) [14], one would likely find different patterns of “activation”. Definitively T cells are active in acute EAE as they are producing damage to myelin and responding to and releasing cytokines [4]. However, while c-Fos may have been required during the development and initial activation of these myelin-specific T cells, their subsequent peripheral functioning may not require c-Fos [15]. In other cells involved in EAE, c-Fos dependent activity may not be occurring at all (or at negligible levels) or does not occur during the examined acute EAE period. For example, microglia may be c-Fos active during the first wave of T cell entry into the CNS, before clinical sign onset or that oligodendrocytes are c-Fos active during the chronic phase of EAE when S1P signaling may alter remyelination processes. The selective labeling of astrocytes in the TetTag activity reporter mice solely indicates that astrocytes, when in acute EAE conditions, respond to any number of EAE related stimuli with the expression of c-Fos. Examining the c-Fos activated astrocytes during EAE progression and with modulations of S1P receptors can deliver insights into the astrocyte’s role in EAE and MS.

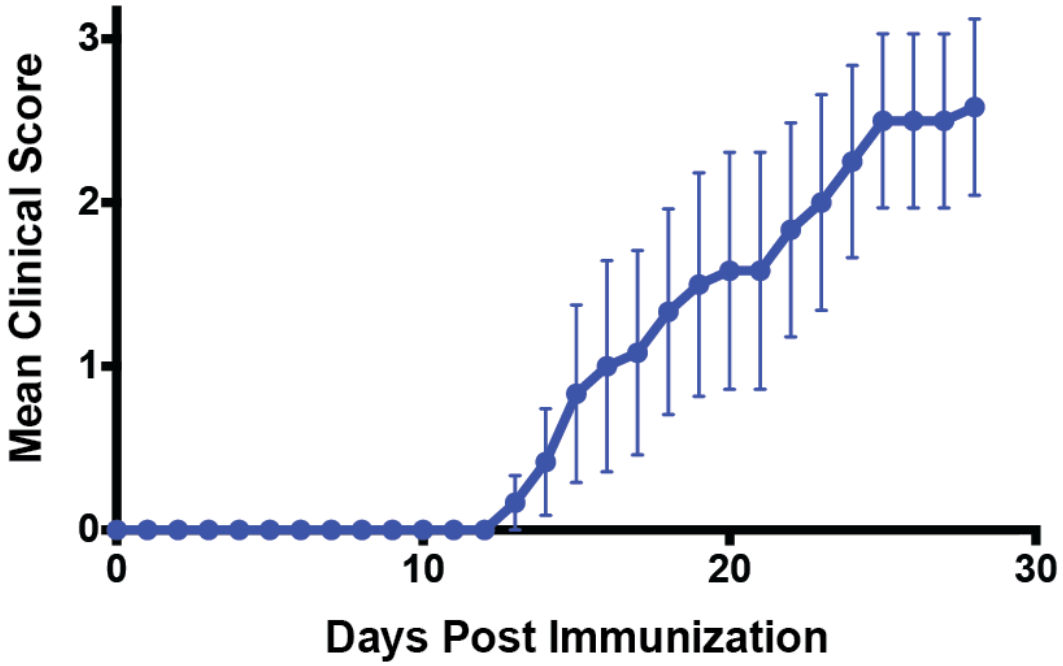

Figure 2.1. EAE is inducible in TetTag mice. Doxycycline chow and the transgenes did not affect the development of EAE. The typical phenotype of EAE, progressing from tail paralysis to hind limb paralysis, was observed in the TetTag mice (n = 6). Data represented is mean ± SEM.

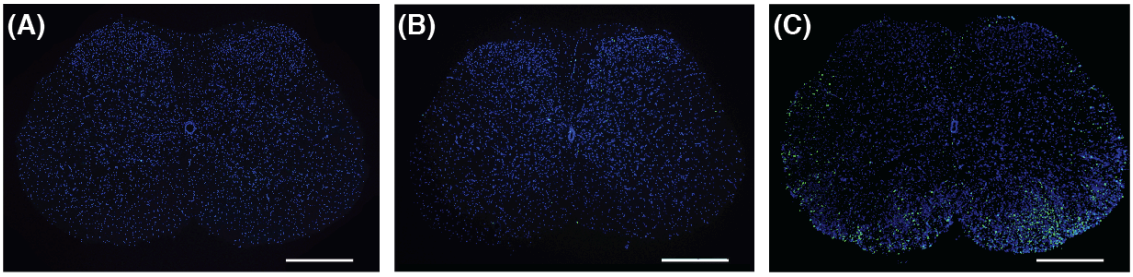

Figure 2.2. EAE induces robust c-Fos activity in the spinal cord. (A) In the naïve spinal cord DOX inhibits extra-experimental tagging of active cells. Virtually no GFP-H2B is observed. **(B)** Upon DOX removal there are few active cells in the naïve spinal cord over 5 days. GFP-H2B is sparse and dispersed. **(C)** EAE induces robust activity in the spinal cord over 5 days that is clustered in lesions (defined by cellular densities shown by DAPI) and along the periphery. Scale bar = 500 μm.

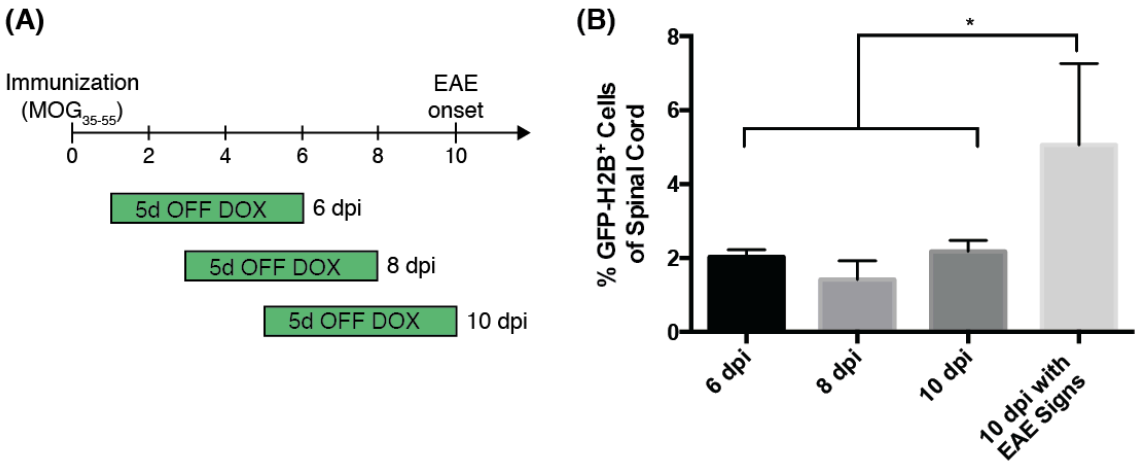

Figure 2.3. The onset of EAE clinical signs initiates increases in c-Fos activity. (A) EAE related activity was assessed in TetTag mice during three different, 5-day examination periods ending on 6 days post immunization (dpi), 8 dpi, and 10 dpi (n = 4 for each group). EAE onset was determined in control mice (n = 7) that were induced at the same time and had an average onset of 10.6 dpi ± 1.07 (SEM). **(B)** All 5-day examination periods that were pre-onset (6 dpi, 8 dpi, and 10 dpi) had similar activation to each other and to naïve mice (not shown). Mice sacrificed after onset (10 dpi with EAE signs) had significantly higher c-Fos activated cells. Data represented are mean ± SEM.

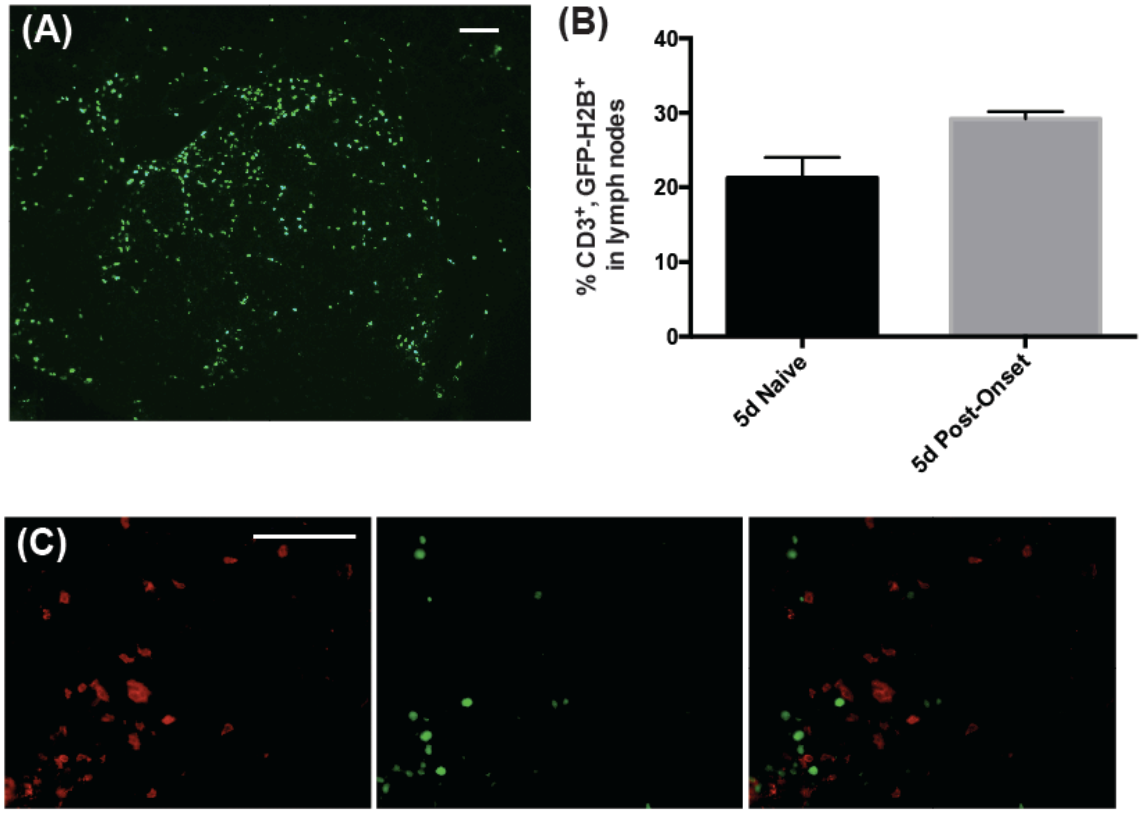

Figure 2.4.1. Lymphocytes are c-Fos active in lymph nodes, but not in the spinal cord during acute EAE. (A) Inguinal lymph nodes from naïve and 5d post-onset (shown) TetTag mice show abundant c-Fos dependent GFP-H2B expression (green). **(B)** The majority of c-Fos active cells from peripheral lymph nodes are $CD3^+$ T cells. c-Fos active T cells increase in lymph nodes during acute EAE. **(C)** Infiltrative $CD3^+$ cells (CD3 shown in red) are in lesions in the spinal cord during acute EAE, however they are not GFP-H2B positive. Scale bar = 100 μm. Data are represented as mean ± SEM.

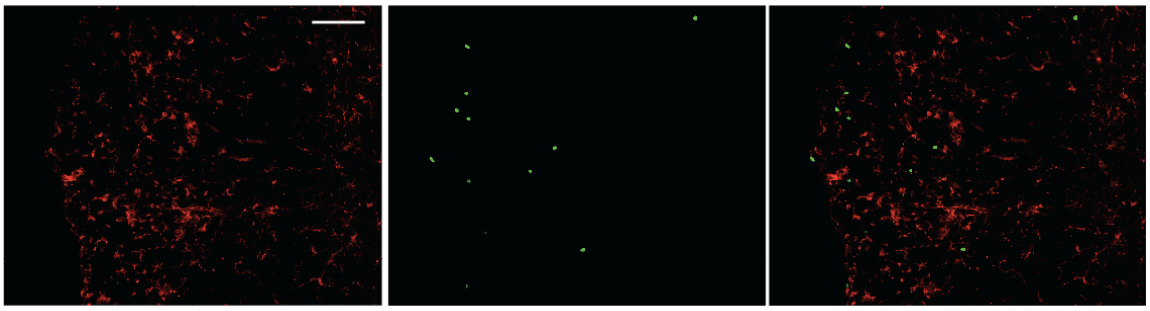

Figure 2.4.2. Microglia are not c-Fos active in the spinal cord during acute EAE. Microglia are identified with Iba1 (red) in lesions of the spinal cord during acute EAE, however these microglia do not show activity-dependent GFP-H2B expression during 5d post-onset. Scale bar = 100 μm.

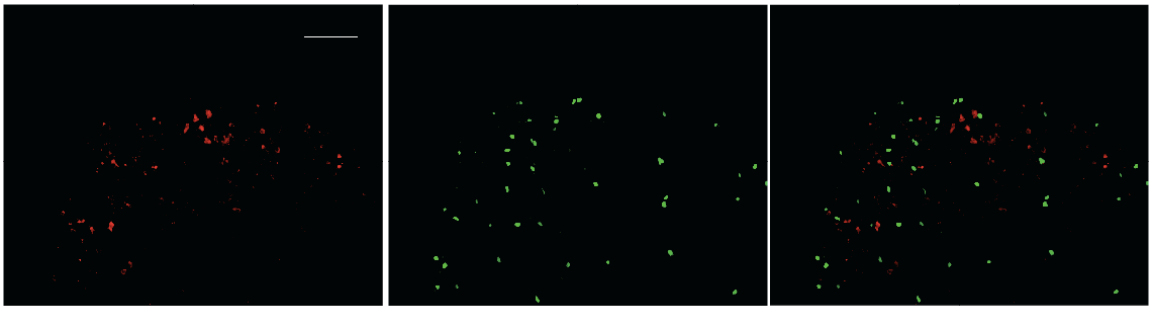

Figure 2.4.3. Oligodendrocytes and oligodendrocyte precursor cells are not c-Fos active during acute EAE in the spinal cord. Oligodendrocytes and/or oligodendrocyte precursor cells are identified by olig1,2,3 (red) and are in lesions of the acute EAE spinal cord. There is no co-localization between activity-dependent GFP-H2B and olig1,2,3. Scale bar = 100 μm.

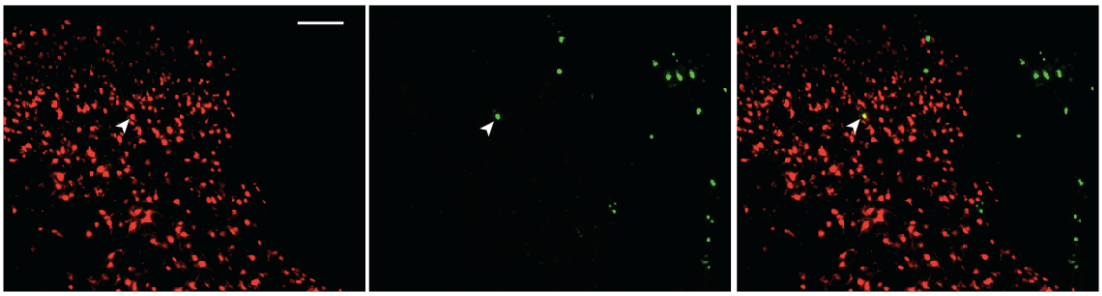

Figure 2.4.4. Few neurons are c-Fos activated during acute EAE. Neurons were identified with NeuN (red) and rarely co-localized with activity-dependent GFP-H2B (0.66% ± 0.14 of GFP-H2B positive cells, one shown with arrowhead). Most c-Fos active cells were NeuN negative. Scale bar = 100 μm.

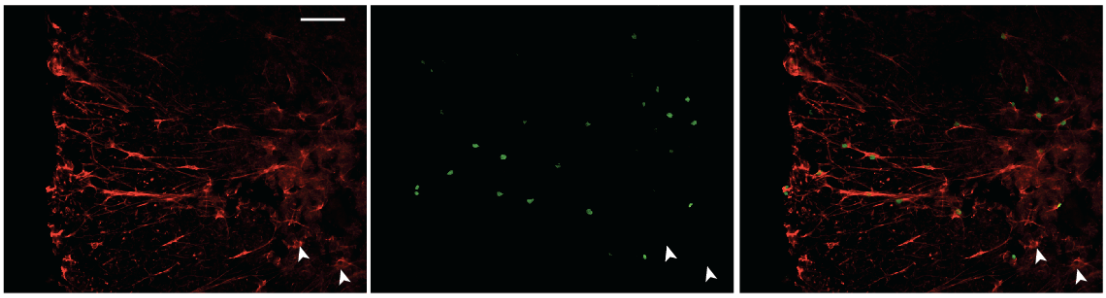

Figure 2.4.5. Astrocytes are the predominant c-Fos active cell-type in acute EAE. Astrocytes were identified with GFAP (red). Nearly all GFP-H2B positive cells are GFAP positive. Not all GFAP positive cells are c-Fos activated (arrowhead). Scale bar = 100 μm.

Chapter 2 References

1. Tayler, K.K., K.Z. Tanaka, L.G. Reijmers, and B.J. Wiltgen, *Reactivation of neural ensembles during the retrieval of recent and remote memory.* Curr Biol, 2013. **23**(2): p. 99-106.

2. Recks, M.S., K. Addicks, and S. Kuerten, *Spinal cord histopathology of MOG peptide 35-55-induced experimental autoimmune encephalomyelitis is time- and score-dependent.* Neurosci Lett, 2011. **494**(3): p. 227-31.

3. Mempel, T.R., S.E. Henrickson, and U.H. Von Andrian, *T-cell priming by dendritic cells in lymph nodes occurs in three distinct phases.* Nature, 2004. **427**(6970): p. 154-9.

4. Ransohoff, R.M. and B. Engelhardt, *The anatomical and cellular basis of immune surveillance in the central nervous system.* Nat Rev Immunol, 2012. **12**(9): p. 623-35.

5. Imai, Y., I. Ibata, D. Ito, K. Ohsawa, and S. Kohsaka, *A novel gene iba1 in the major histocompatibility complex class III region encoding an EF hand protein expressed in a monocytic lineage.* Biochem Biophys Res Commun, 1996. **224**(3): p. 855-62.

6. Miller, R.H. and S. Mi, *Dissecting demyelination.* Nat Neurosci, 2007. **10**(11): p. 1351-4.

7. Dai, J., K.K. Bercury, J.T. Ahrendsen, and W.B. Macklin, *Olig1 function is required for oligodendrocyte differentiation in the mouse brain.* J Neurosci, 2015. **35**(10): p. 4386-402.

8. Othman, A., D.M. Frim, P. Polak, S. Vujicic, B.G. Arnason, and A.I. Boullerne, *Olig1 is expressed in human oligodendrocytes during maturation and regeneration.* Glia, 2011. **59**(6): p. 914-26.

9. Kim, H.M., D.H. Hwang, J.Y. Choi, C.H. Park, H. Suh-Kim, S.U. Kim, and B.G. Kim, *Differential and cooperative actions of Olig1 and Olig2 transcription factors on immature proliferating cells after contusive spinal cord injury.* Glia, 2011. **59**(7): p. 1094-106.

10. Zhang, Y., K. Chen, S.A. Sloan, M.L. Bennett, A.R. Scholze, S. O'Keeffe, H.P. Phatnani, P. Guarnieri, C. Caneda, N. Ruderisch, S. Deng, S.A. Liddelow, C.

Zhang, R. Daneman, T. Maniatis, B.A. Barres, and J.Q. Wu, *An RNA-sequencing transcriptome and splicing database of glia, neurons, and vascular cells of the cerebral cortex.* J Neurosci, 2014. **34**(36): p. 11929-47.

11. Mullen, R.J., C.R. Buck, and A.M. Smith, *NeuN, a neuronal specific nuclear protein in vertebrates.* Development, 1992. **116**(1): p. 201-11.

12. Choi, J.W., S.E. Gardell, D.R. Herr, R. Rivera, C.W. Lee, K. Noguchi, S.T. Teo, Y.C. Yung, M. Lu, G. Kennedy, and J. Chun, *FTY720 (fingolimod) efficacy in an animal model of multiple sclerosis requires astrocyte sphingosine 1-phosphate receptor 1 (S1P1) modulation.* Proc Natl Acad Sci U S A, 2011. **108**(2): p. 751-6.

13. Yester, J.W., L. Bryan, M.R. Waters, B. Mierzenski, D.D. Biswas, A.S. Gupta, R. Bhardwaj, M.J. Surace, J.M. Eltit, S. Milstien, S. Spiegel, and T. Kordula, *Sphingosine-1-phosphate inhibits IL-1-induced expression of C-C motif ligand 5 via c-Fos-dependent suppression of IFN-beta amplification loop.* FASEB J, 2015.

14. Wang, K.H., A. Majewska, J. Schummers, B. Farley, C. Hu, M. Sur, and S. Tonegawa, *In vivo two-photon imaging reveals a role of arc in enhancing orientation specificity in visual cortex.* Cell, 2006. **126**(2): p. 389-402.

15. Jain, J., E.A. Nalefski, P.G. McCaffrey, R.S. Johnson, B.M. Spiegelman, V. Papaioannou, and A. Rao, *Normal peripheral T-cell function in c-Fos-deficient mice.* Mol Cell Biol, 1994. **14**(3): p. 1566-74.

Chapter 3:

Spatial and temporal properties of astrocyte activation in EAE and correlation to clinical severity with modulation of S1P receptors

3.A. Introduction

The TetTag c-Fos reporter mice identified two cell types that were activated during acute EAE, neurons and astrocytes. Activation of neurons was sparse and did not appear to be increased by EAE. Activation of astrocytes was robustly increased during acute EAE. The effects of EAE will be examined in the c-Fos reporter mice as it is altered by relevant S1P modulation via genetic removal of $S1P_1$ specifically on astrocytes or by fingolimod treatment [1]. Approaches allowing three-dimensional imaging of the intact LSC will be utilized to determine temporal and spatial properties of EAE-activated astrocytes. Further, the relationships amongst disease severity, S1P receptor modulations, and extent of astrocyte activation will be explored.

The indicator of c-Fos activity, GFP-H2B, lends itself well to new clearing methods and volume imaging that would allow three-dimensional visualization of temporal and spatial properties of astrocyte activation throughout intact LSCs during EAE. Immunolabeling-enabled three-dimensional imaging of solvent-cleared organs (iDISCO) [2] is implemented to visualize the progression of astrocyte activation in the LSC during acute EAE. The spatial distribution of activated astrocytes is characterized during acute EAE and compared when altering astrocytic $S1P_1$ signaling genetically or with fingolimod treatment.

Accurately quantifying the extent of c-Fos activation in the CNS presents unique challenges. This complex organ system is comprised of several heterogeneous neural cell types that are deeply intertwined. Flow cytometry and fluorescence-activated cell

sorting (FACS) are tremendously powerful tools that allow high-throughput analysis and isolation of specific cell types from heterogeneous populations, but can be problematic with CNS tissues. The entwined neurons, oligodendrocytes, and astrocytes that comprise most of the CNS have long and interconnected processes often making single cell isolations without significant damage and cell loss, prohibitive. Isolating nuclei from CNS tissue evades some of these challenges and has allowed high-throughput characterizations of neural cell subtypes [3-8]. The high specificity of GFP-H2B expression in astrocytes during EAE provides the opportunity to establish a relationship between astrocyte activation and disease severity during acute EAE, and as it is affected by S1P modulation, using nuclear isolation and flow cytometric analysis. Together, these approaches will identify and characterize a population of astrocytes that is integral to EAE development and fingolimod efficacy.

3.B. Materials and Methods

TetTag mice with astrocyte specific $S1P_1$ knockout

TetTag mice with astrocyte specific $S1P_1$ deletion ($S1P_1$-Ast-KO) were created by crossing astrocyte specific $S1P_1$ knockout mice (*S1pr1*$^{loxP/loxP}$ *; GFAP-cre*) [1] with TetTag mice for multiple generations. TetTag littermate controls ($S1P_1$-CTRL) were either without GFAP-Cre and/or $S1P_1^{+/+}$.

Fingolimod treatment during acute EAE

The acute EAE examination period begins at the onset of EAE clinical signs (clinical score ≥ 1.0), at which point DOX is removed. Fingolimod treatment (1.0 mg/kg, p.o., q.d.) was initiated upon DOX removal.

Three-dimensional imaging of LSC using iDISCO

Immunolabeling-enabled three-dimensional imaging of solvent-cleared organs (iDISCO) was employed to visualize GFP-H2B in intact LSCs [2]. First, mice were deeply anesthetized with an overdose of isoflurane anesthesia then fixed by intracardiac perfusion of PBS followed by 4% PFA in PBS. LSC were dissected out, postfixed overnight in 4% PFA in PBS, and further fixed with 4%PFA in PBS at RT (1h). LSC were washed in PBS (twice, 1h), 50% methanol in PBS (1h), 80% methanol in PBS (1h), methanol (twice, 1h), and bleached in 5% H_2O_2 in 20% dimethyl sulfoxide (DMSO)/methanol at 4°C (overnight). Samples were again washed in methanol (twice, 1h), 20% DMSO in methanol (twice, 1h), 80% methanol in PBS (1h), 50% methanol in PBS (1h), PBS (twice, 1h), PBS+0.2% Triton X-100 (twice, 1h), incubated at 37°C in PBS/0.2% triton X-100/20%DMSO/ 0.3 M glycine (overnight). Samples were blocked in PBS/0.2% Triton X-100/10% DMSO/6% Goat Serum at 37°C (4h), washed in PBS/0.2% Tween-20 with 10 µg/ml heparin (PTwH; twice, 1h), and incubated in a rabbit anti-GFP antibody (MBL, 1:1000) in PTwH at 37°C (2d). Samples were washed in PTwH (>10 times, >1h each) then incubated in anti-rabbit Alexa Fluor-488 (ThermoFisher Scientific, 1:1000). Samples were again washed in PTwH (>10 times, >1h each) before tissue clearing.

LSC samples were incubated in 50% v/v tetrahydrofuran/H_2O (THF, Sigma; overnight), 70% THF/H_2O (20m), 80% THF/H_2O (20m), 100% THF (thrice, 20m), dichloromethane (DCM, Sigma; 20m), and finally in dibenzyl ether (DBE; >20m). Cleared LSC were placed in a microscope chamber made with 2-3 stacked Fastwells (Research Products Int.), filled with DBE, and coverslipped. The intact LSCs were imaged on a Nikon $A1^+$ confocal microscope using z-steps of 10 µm, a 10x objective, and NIS-Elements (v4.3) to produce a three-dimensional reconstruction.

Quantifying spatial properties

The spatial properties of clustering and cluster volume were calculated in NIS-Elements by first expanding the GFP-H2B signals using intensity thresholding to merge signals in close proximity. A range of volumes for a single GFP-H2B was determined. Larger volumes than the single GFP-H2B range were classified as clusters. The number of nuclear GFP-H2B in clusters was determined by dividing the cluster volume by the mean volume of single GFP-H2B in each LSC.

LSC nuclear isolation, immunolabeling, and fluorescent-activated cell sorting

Precautions were taken to maintain an RNase-free environment, use RNase-free reagents, and mitigate RNA degradation by processing samples at 4ºC for subsequent RNA analysis. LSCs were rapidly dissected and frozen in liquid nitrogen. Samples were equilibrated to 4°C and dounce homogenized in a nuclei extraction buffer made with 0.32 M sucrose/5 mM $CaCl_2$/3 mM $Mg(CH_3COO)_2$/0.1 mM EDTA/20 mM Tris-HCl pH 8.0/0.1% Triton X-100 in DEPC-treated H_2O. Homogenized samples were filtered (50μm) and washed in DEPC-treated PBS/2 mM EDTA in DEPC-treated H_2O (PBSE-d). Nuclei were purified by centrifugation at 3250 x g for 12 min in an isosmotic iodixanol gradient made of a 35%, 10%, and 5% OptiPrep (Sigma) in 20 mM tricine-KOH (pH 7.8)/25 mM KCl/30 mM $MgCl_2$ in DEPC-treated H_2O [9]. Nuclei were recovered in the 35%-10% interface, washed in PBSE-d and immunolabeled with a rabbit anti-NeuN antibody (EMD Millipore, 1:400) in 1%BSA in PBSE-d for 20 min. Samples were washed in PBSE-d and labeled with a goat anti-rabbit APC conjugated secondary antibody (Life Technologies, 1:500) and DAPI (1:5000) in 1%BSA/PBSE-d for 10 min. Samples were washed in PBSE-d and suspended in PBSE-d.

Nuclear populations were analyzed and sorted on an Aria–II (BD) fluorescent-activated cell sorter (FACS). Gating was performed as follows: (i) DAPI positive (ii) size and granularity consistent with nuclei by forward-scatter area (FSC-A) and side-scatter area (SSC-A) (iii) single nuclei selected by both FSC-A and forward scatter height (FSC-H), and SSC-A and side-scatter height (SSC-H). Analysis was performed on FlowJo (10.0.8r1).

Statistical Analyses

Results are expressed as mean ± SEM. Data were statistically analyzed as appropriate by two-way analysis of variance (ANOVA) with Dunnett's multiple comparison, Kruskal-Wallis test and Dunn's multiple comparison test, and Spearman's rank-order correlation.

3.C. Results

TetTag mice with astrocytic deletion of $S1P_1$ or fingolimod treatment show reduced clinical scores

EAE was induced in TetTag mice with the genetic removal of $S1P_1$ on astrocytes and compared to littermate controls (**Figure 3.1-A**). The $S1P_1$-AstKO group showed a similar reduction of EAE severity when compared to $S1P_1$-CTRL group, as previously reported [1]. The TetTag transgenes and DOX diet had no apparent effects on the phenotype observed in astrocyte specific $S1P_1$ knockouts during EAE, supporting the suitability of TetTag mice for studying S1P receptor modulation during the disease.

The time until onset of EAE signs was nearly identical between $S1P_1$-CTRL (17.70 ± 0.32 days post immunization (dpi)) and $S1P_1$-AstKO groups (18.00 ± 0.45 dpi). The clinical scores of EAE-induced TetTag mice were thoroughly examined during the 5-

dpo period, as this examination window exhibited c-Fos activation that was specific to astrocytes as described in the last chapter. The clinical presentation at onset (0-dpo - when DOX was removed and fingolimod administration was initiated) was not significantly different amongst any groups (Figure 3.1-B). After 1-dpo, $S1P_1$-CTRL mice had significantly increased clinical severity compared to both $S1P_1$-AstKO and $S1P_1$-CTRL + fingolimod mice. This difference in clinical severity increased until 5-dpo. The mean clinical scores during 5-dpo was similarly reduced in both $S1P_1$-AstKO and $S1P_1$-CTRL + fingolimod mice as compared to $S1P_1$-CTRL mice. These phenotypical differences during EAE with S1P receptor modulation were next compared to properties of c-Fos activated astrocytes during EAE.

Astrocytes are the predominant c-Fos activated cell-type during acute EAE with S1P modulation

Specificity of c-Fos activation to astrocytes in $S1P_1$-CTRL mice during acute EAE was described in chapter 2. To see if this unique specificity is maintained upon S1P receptor modulation, co-localization of GFAP and GFP-H2B was determined (**Figure 3.2**). Nearly identical astrocyte specificity was seen during acute EAE in $S1P_1$-CTRL, $S1P_1$-AstKO, and $S1P_1$-CTRL + fingolimod groups. Neuron activation determined by GFP-H2B co-localization with NeuN was scarce in all groups (>1%). Thus, the c-Fos dependent expression of GFP-H2B can be used as a highly-specific marker of EAE-activated astrocytes in the LSC during the acute stage of disease.

Astrocyte activation occurs in expanding lesions along peripheral white matter tracts of the spinal cord

The progression of astrocyte activation during acute EAE was examined in intact LSCs using a tissue clearing technique and volume imaging (**Figure 3.3**). Several lesions indicated by densities of GFP-H2B can be visualized at 1-dpo that range in size and frequency. A single large lesion appears to span the entire lumbar enlargement region of the LSC. Numerous small lesions appear to be forming. Most lesions are on the periphery of the spinal cord along the lateral white matter tracts. At 3-dpo, lesions increase in frequency and size, with growth extending primarily in the rostral-caudal axis. Lesions also begin appearing in the dorsomedial and ventromedial white matter tracts of the LSC. By 5-dpo, lesions increased in size and number to occupy much of the white matter tracts of the LSC.

Astrocyte activation during acute EAE occurs in clusters that decrease in frequency with $S1P_1$ deletion on astrocytes and fingolimod treatment

Spatial properties of astrocyte activation during the 5-dpo period were compared in $S1P_1$-CTRL, $S1P_1$-AstKO, and $S1P_1$-CTRL + fingolimod groups using iDISCO and volume imaging (**Figure 3.4**). Astrocyte activation in $S1P_1$-CTRL, $S1P_1$-AstKO, and $S1P_1$-CTRL + fingolimod groups is similarly distributed in several lesions of various sizes that are distributed along regions of white matter tracts. Spatial properties of the lesions of astrocytes were calculated by determining a range of GFP-H2B signal volumes that were equivalent to single nuclei (B - *i*) and those that were above this range in clusters (B - *ii and iii*). The percent of GFP-H2B nuclei in clusters was similar during acute EAE in $S1P_1$-CTRL, $S1P_1$-AstKO, and $S1P_1$-CTRL + fingolimod groups. The frequency of activated astrocyte clusters was characterized in $S1P_1$-CTRL, $S1P_1$-AstKO, and $S1P_1$-CTRL + fingolimod 5-dpo groups. The $S1P_1$-CTRL group had a higher frequency of clusters than both $S1P_1$-AstKO, and $S1P_1$-CTRL + fingolimod groups. Contrastingly, in

pre-onset (or naïve) TetTag mice, there was no clustering (0.23 ± 0.09%, n = 3, data not shown).

Astrocyte activation is correlated with disease severity during acute EAE

Flow cytometric analysis was performed on LSC nuclei to determine the relationship between the extent of astrocyte c-Fos activation and disease severity **(Figure 3.5**). Single nuclei were identified by DAPI staining and size/granularity to exclude debris and doublets. Astrocytes activated by acute EAE (NeuN negative, GFP-H2B positive nuclei of the LSC) were quantified. The mean clinical score differences between the $S1P_1$-CTRL group and $S1P_1$-AstKO / $S1P_1$-CTRL + fingolimod (similar to those observed in **Figure 3.1**) are reflected in the amount of astrocyte activation in each group. There is a direct linear relationship between the clinical severity and extent of astrocyte activation during the 5-dpo acute EAE period in $S1P_1$-CTRL, $S1P_1$-AstKO, and $S1P_1$-CTRL + fingolimod groups. $S1P_1$-AstKO, and $S1P_1$-CTRL + fingolimod groups are left-shifted along the correlation line. Mice showing no EAE signs exhibit low astrocyte activation (1.368 ± 0.409%).

3.D. Discussion

During the acute EAE 5-dpo period, TetTag transgenic mice display phenotypic differences due to S1P receptor modulation in astrocytes and remarkably identify c-Fos activation specifically in astrocytes that is EAE-dependent. The distinct GFP-H2B activation marker was utilized to monitor when and where astrocytes are activated during acute EAE. Astrocytes are activated at onset in clusters within the white matter. These clusters appear to grow in the rostral-caudal axis and are first observed in the lateral white matter tracts followed by the formation in both dorsal and ventral, medial

white matter tracts. The genetic removal of $S1P_1$ on astrocytes or the functional antagonism of $S1P_1$ by fingolimod, retains the tendency of astrocytes to be activated in clusters, but reduces the frequency of clusters. The reduction of frequency of clusters is reflected in the flow cytometric analysis that shows a reduction in activated astrocytes in $S1P_1$-AstKO, and $S1P_1$-CTRL + fingolimod when compared to $S1P_1$-CTRL. This reduction in astrocyte activation by S1P modulation is directly correlated to EAE disease severity. Thus, the c-Fos reporter mice distinguish astrocyte activity during EAE that is largely confined to clusters in white matter tracts and directly correlated to disease severity.

A major limitation to studying astrocytes in health and disease is their remarkable heterogeneity. Astrocytes are the most numerous and the most functionally diverse cell type in the CNS. Routine astrocytic functions include local regulation of blood flow, maintenance of the BBB, removal/recycling of neurotransmitters, potassium homeostasis, and roles in neuronal plasticity and synapse formation [10-20]. The detection of astrocyte specific molecular markers is extensively used to study astrocytes and their roles in health and disease, though these markers are often limiting. For example, the prototypical astrocyte marker GFAP is variably expressed and can be absent in mature, resting astrocytes [18, 21]. In environments causing reactive astrocytosis and glial scaring, such as EAE and MS, GFAP is up regulated and expressed in all astrocytes [1, 22-24]. However, GFAP largely serves cyto-structural functions and is not necessarily related to any of an astrocyte's diverse functions [22]. The TetTag c-Fos reporter mice not only exhibit great astrocyte specificity in EAE, but also identify a subset of astrocytes that is related to EAE processes, as they localize to EAE lesions in clusters. Additionally, the extent of these c-Fos activated astrocytes is directly related to EAE clinical severity. As detection of c-Fos is able to distinguish

active neurons amongst vast neuronal circuits, it also has the ability to distinguish active astrocytes in a highly heterogeneous cell population during a complex disease of EAE. This powerful tool will next be leveraged to reveal the functional processes that are carried out by astrocytes in EAE and how these processes are altered by the direct CNS effects of fingolimod.

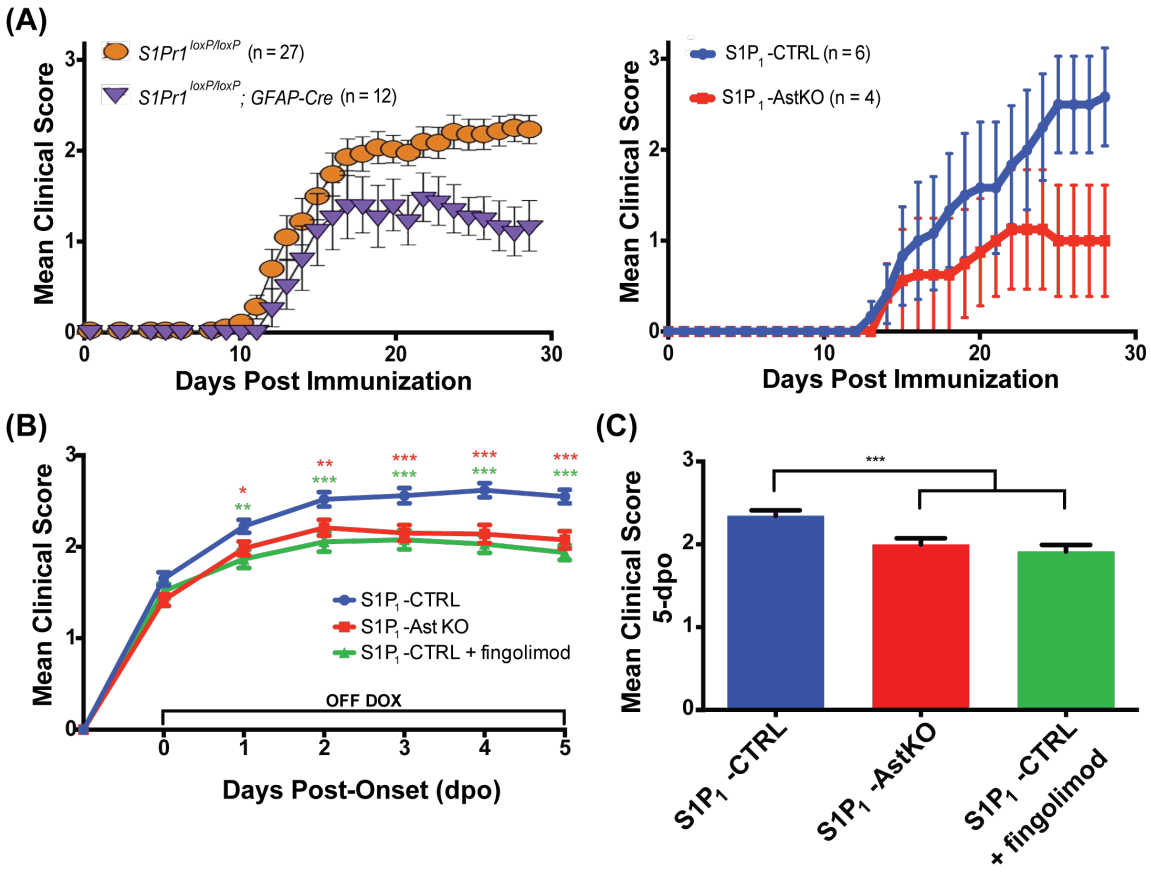

Figure 3.1. The TetTag c-Fos reporter mice have reduced EAE severity in astrocyte specific $S1P_1$ knockouts and with fingolimod treatment during 5-dpo. (A) Data from Choi et al. 2011 (left) displays the reduction of EAE severity in mice with genetic removal of $S1P_1$ specifically on astrocytes [1]. TetTag mice crossed into the same *S1Pr1*$^{loxP/loxP;}$ *GFAP-Cre* mouse line ($S1P_1$-AstKO; n = 4) have a similar reduced clinical score when compared to littermate controls ($S1P_1$-CTRL; n = 6) shown on the right. **(B)** At the time of onset (dpo = 0, clinical score ≥ 1.0) there are no differences in EAE clinical severity. DOX was removed and fingolimod (1.0 mg/kg, p.o., q.d.) was administered in the $S1P_1$-CTRL + fingolimod at 0 dpo. By 1 dpo., $S1P_1$-CTRL mice exhibit increased EAE severity when compared to both $S1P_1$-AstKO and $S1P_1$-CTRL + fingolimod. Mean clinical score differences between $S1P_1$-CTRL and both $S1P_1$-AstKO and $S1P_1$-CTRL + fingolimod increase and appear to plateau by 4-5 dpo (n = 50, 43, and 32, respectively). **(C)** The mean clinical score over the 5 dpo is significantly increased in $S1P_1$-CTRL and both $S1P_1$-AstKO and $S1P_1$-CTRL + fingolimod (n = 50, 43, and 32, respectively). Data are represented as mean ± SEM.

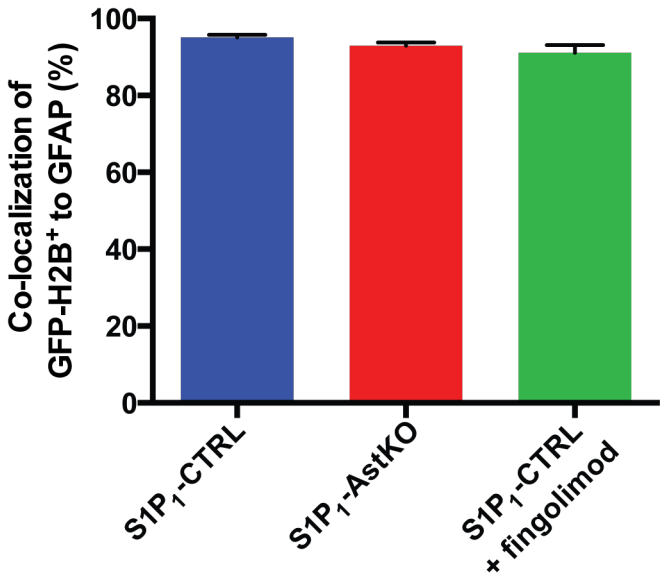

Figure 3.2. Genetic removal of $S1P_1$ on astrocytes or fingolimod treatment retains the prevalence of c-Fos activation in astrocytes during acute EAE. The percent of GFP-H2B that co-localizes with the astrocyte-specific marker GFAP during EAE does not change in $S1P_1$-AstKO and $S1P_1$-CTRL + fingolimod compared to $S1P_1$-CTRL groups (n = 3 for each group with a minimum quantification of 500 GFP-H2B per LSC). The vast majority of c-Fos activated cells are astrocytes (see Figure 2.4.5). The only other cell identified as GFP-H2B positive was neurons in all EAE groups (<1% of total GFP-H2B in all groups). Data are represented as mean ± SEM

Figure 3.3. TetTag mice show the temporal and spatial progression of astroctye c-Fos activation during acute EAE. At 1-dpo, astrocytes are robustly activated in clusters that extend along lateral white matter tracts (shown in 500 μm cross-section) on the rostral-caudal axis. Clusters range in size, with several small and a single large cluster spanning the length of the lumbar enlargement. At 3-dpo, there are increased clusters of larger sizes and some appear along the dorsomedial and ventromedial surfaces (dorsomedial clusters, along with lateral, shown in cross-section). At 5-dpo, larger clusters appear frequently and extend into all white matter tracts. Scale = 500 μm.

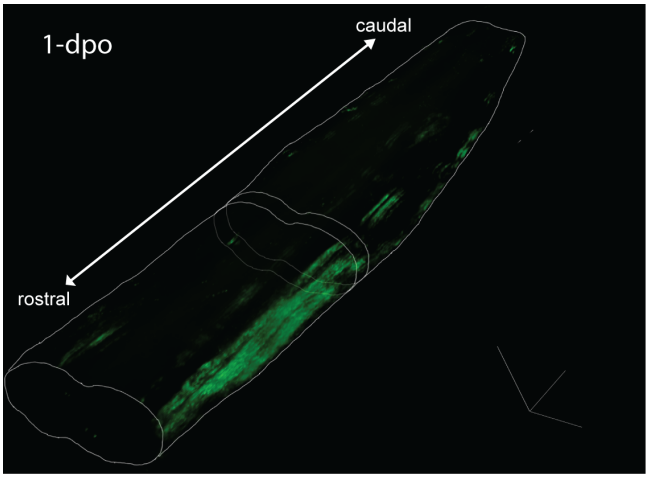
1-dpo
caudal
rostral

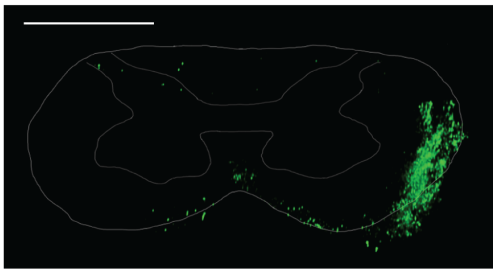

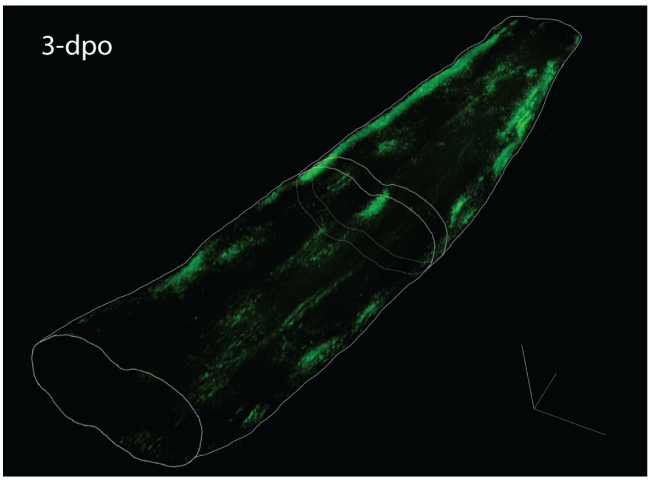
3-dpo

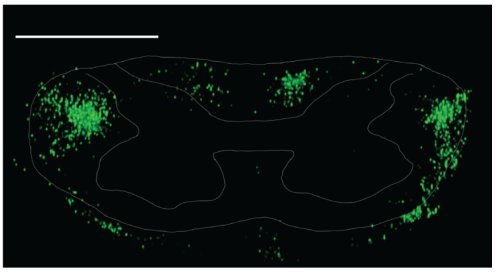

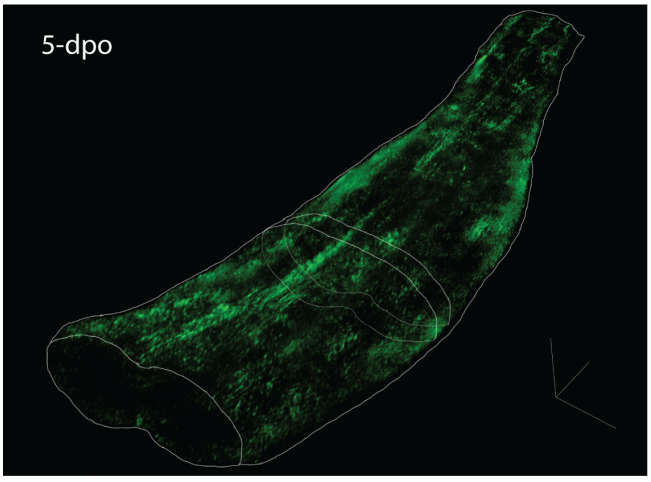
5-dpo

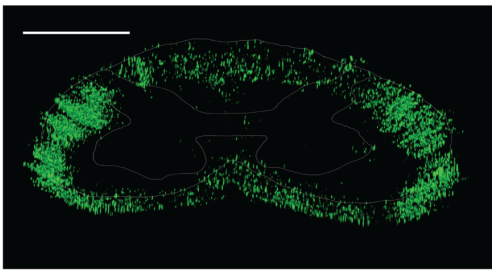

Figure 3.4. Astrocyte activation during 5-dpo occurs in similarly structured clusters, but at different frequencies in $S1P_1$-CTRL, $S1P_1$-AstKO, and $S1P_1$-CTRL + fingolimod groups. (**A)** Representative three-dimensional reconstructions of astrocyte activation during acute EAE in $S1P_1$-CTRL, $S1P_1$-AstKO, and $S1P_1$-CTRL + fingolimod LSCs show widespread activation and clusters on all surfaces of the white matter tracts that vary in size and frequency. **(B)** To measure properties of clustering, the GFP-H2B signals were expanded by intensity thresholding in order to merge those in close proximity. Isolated GFP-H2B signals (*i*) and clusters, ranging from two merged GFP-H2B (*ii*) to several thousand GFP-H2B (*iii*), were identified. The mean volume of single, isolated GFP-H2B positive nuclei was determined and used to calculate the number of nuclei in clusters. **(C)** Most of the GFP-H2B positive nuclei during 5-dpo in $S1P_1$-CTRL, $S1P_1$-AstKO, and $S1P_1$-CTRL + fingolimod groups are in clusters (n = 3, 4, and 5, respectively). **(D)** The clustering frequency, calculated as the percent of GFP-H2B signals that were clustered, is higher in $S1P_1$-CTRL mice compared to $S1P_1$-AstKO, and $S1P_1$-CTRL + fingolimod groups. Scale = 500 μm. Data are represented as mean ± SEM.

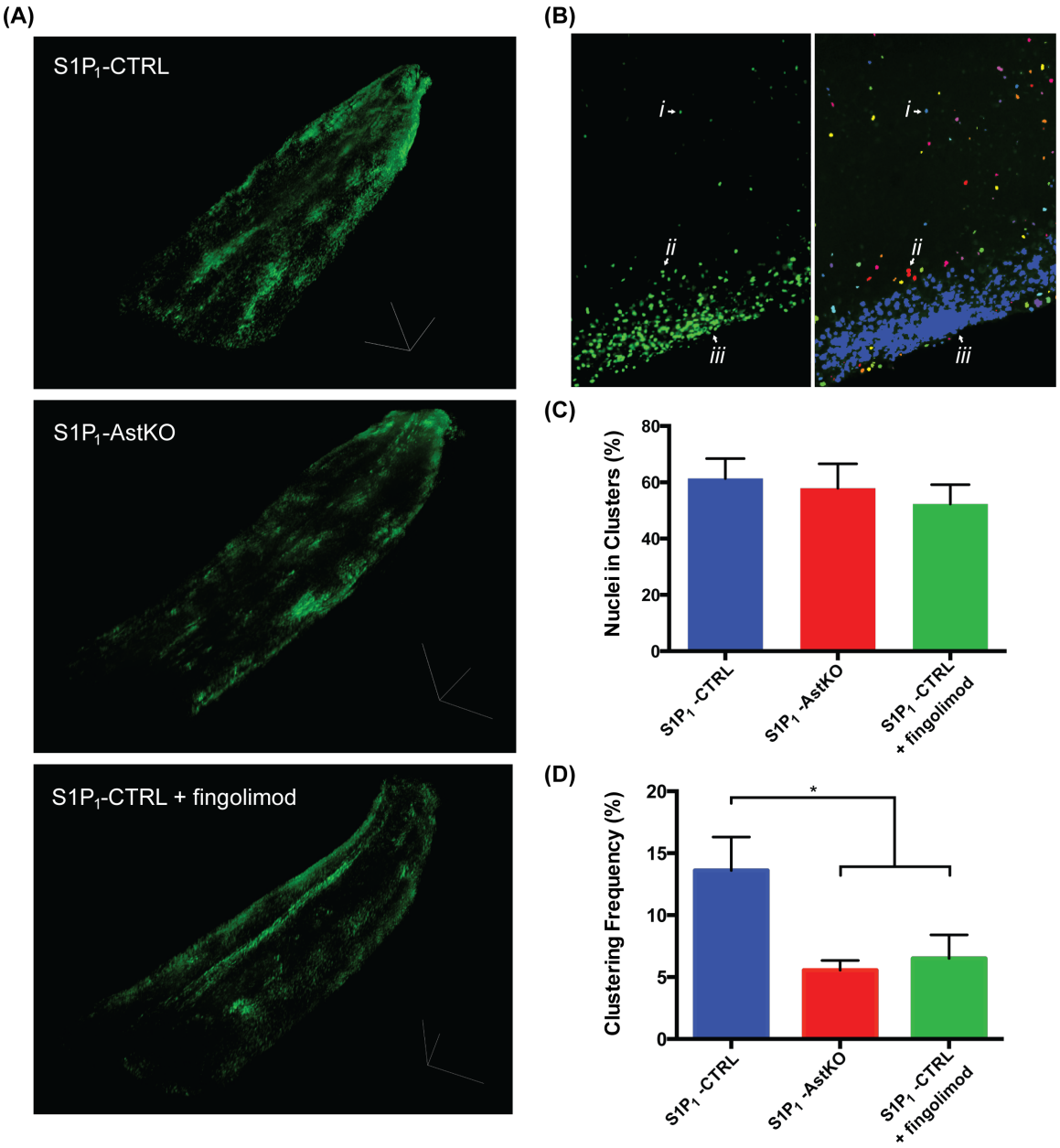
(A)
S1P1-CTRL
S1P1-AstKO
S1P1-CTRL + fingolimod
(B)
i
ii
iii
(C)
Nuclei in Clusters (%)
0
20
40
60
80
S1P1 -CTRL
S1P1 -AstKO
S1P1 -CTRL + fingolimod
(D)
Clustering Frequency (%)
0
5
10
15
20
*
S1P1 -CTRL
S1P1 -AstKO
S1P1 -CTRL + fingolimod

Figure 3.5 - Astrocyte activation is correlated with disease severity during 5-dpo acute EAE. (A) Nuclear isolates from the LSC were analyzed by flow cytometry and shown by a representative sample. Nuclei are identified by DAPI positivity. The level of GFP-H2B positive, NeuN negative nuclei (activated astrocytes) in the LSC were determined in $S1P_1$-CTRL, $S1P_1$-AstKO, and $S1P_1$-CTRL + fingolimod, and related to clinical score. **(B)** The mean clinical scores of the analyzed LSCs are higher in $S1P_1$-CTRL mice than $S1P_1$-AstKO and $S1P_1$-CTRL + fingolimod, and similar to the score trends in all 5 dpo groups shown in **Figure 3.1**. **(C)** Astrocyte activation is higher in $S1P_1$-CTRL mice than $S1P_1$-AstKO and $S1P_1$-CTRL + fingolimod (n = 10, 9, and 10, respectively). **(D)** Astrocyte activation is correlated to the 5 dpo mean clinical score. Pre-onset TetTag mice were used to determine the extent of astrocyte activation with a mean clinical score = 0. Increases in disease severity are correlated to increases in astrocyte activation. The phenotype of decreased disease severity in $S1P_1$-AstKO and $S1P_1$-CTRL + fingolimod groups corresponds to a left-shift along the correlation line to astrocyte activation. Data are represented as mean ± SEM

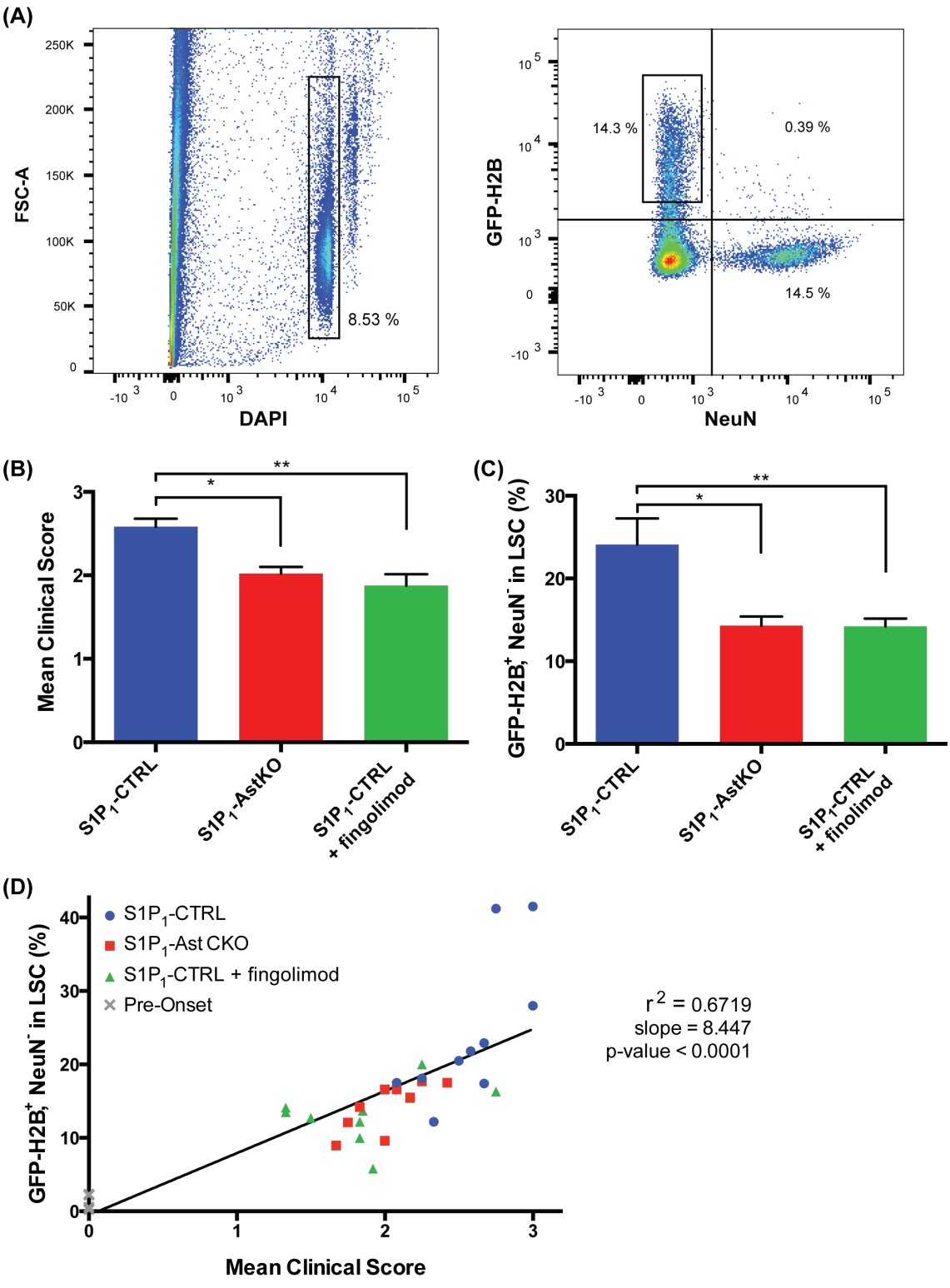
(A)
FSC-A
DAPI
8.53 %
GFP-H2B
NeuN
14.3 %
0.39 %
14.5 %
(B)
Mean Clinical Score
S1P1-CTRL
S1P1-AstKO
S1P1-CTRL + fingolimod
(C)
GFP-H2B+ NeuN- in LSC (%)
S1P1-CTRL
S1P1-AstKO
S1P1-CTRL + finolimod
(D)
S1P1-CTRL
S1P1-Ast CKO
S1P1-CTRL + fingolimod
Pre-Onset
r2 = 0.6719
slope = 8.447
p-value < 0.0001
GFP-H2B+ NeuN- in LSC (%)
Mean Clinical Score

Chapter 3 References

1. Choi, J.W., S.E. Gardell, D.R. Herr, R. Rivera, C.W. Lee, K. Noguchi, S.T. Teo, Y.C. Yung, M. Lu, G. Kennedy, and J. Chun, *FTY720 (fingolimod) efficacy in an animal model of multiple sclerosis requires astrocyte sphingosine 1-phosphate receptor 1 (S1P1) modulation.* Proc Natl Acad Sci U S A, 2011. **108**(2): p. 751-6.

2. Renier, N., Z. Wu, D.J. Simon, J. Yang, P. Ariel, and M. Tessier-Lavigne, *iDISCO: a simple, rapid method to immunolabel large tissue samples for volume imaging.* Cell, 2014. **159**(4): p. 896-910.

3. Okada, S., H. Saiwai, H. Kumamaru, K. Kubota, A. Harada, M. Yamaguchi, Y. Iwamoto, and Y. Ohkawa, *Flow cytometric sorting of neuronal and glial nuclei from central nervous system tissue.* J Cell Physiol, 2011. **226**(2): p. 552-8.

4. Westra, J.W., S.E. Peterson, Y.C. Yung, T. Mutoh, S. Barral, and J. Chun, *Aneuploid mosaicism in the developing and adult cerebellar cortex.* J Comp Neurol, 2008. **507**(6): p. 1944-51.

5. Bushman, D.M., G.E. Kaeser, B. Siddoway, J.W. Westra, R.R. Rivera, S.K. Rehen, Y.C. Yung, and J. Chun, *Genomic mosaicism with increased amyloid precursor protein (APP) gene copy number in single neurons from sporadic Alzheimer's disease brains.* Elife, 2015. **4**.

6. Peterson, S.E., A.H. Yang, D.M. Bushman, J.W. Westra, Y.C. Yung, S. Barral, T. Mutoh, S.K. Rehen, and J. Chun, *Aneuploid cells are differentially susceptible to caspase-mediated death during embryonic cerebral cortical development.* J Neurosci, 2012. **32**(46): p. 16213-22.

7. Westra, J.W., R.R. Rivera, D.M. Bushman, Y.C. Yung, S.E. Peterson, S. Barral, and J. Chun, *Neuronal DNA content variation (DCV) with regional and individual differences in the human brain.* J Comp Neurol, 2010. **518**(19): p. 3981-4000.

8. Westra, J.W., S. Barral, and J. Chun, *A reevaluation of tetraploidy in the Alzheimer's disease brain.* Neurodegener Dis, 2009. **6**(5-6): p. 221-9.

9. Graham, J.M., *Isolation of nuclei and nuclear membranes from animal tissues.* Curr Protoc Cell Biol, 2001. **Chapter 3**: p. Unit 3 10.

10. Allaman, I., M. Belanger, and P.J. Magistretti, *Astrocyte-neuron metabolic relationships: for better and for worse.* Trends Neurosci, 2011. **34**(2): p. 76-87.

11. Allen, N.J. and B.A. Barres, *Neuroscience: Glia - more than just brain glue.* Nature, 2009. **457**(7230): p. 675-7.

12. Barnabe-Heider, F., J.A. Wasylnka, K.J. Fernandes, C. Porsche, M. Sendtner, D.R. Kaplan, and F.D. Miller, *Evidence that embryonic neurons regulate the onset of cortical gliogenesis via cardiotrophin-1.* Neuron, 2005. **48**(2): p. 253-65.

13. Bonni, A., Y. Sun, M. Nadal-Vicens, A. Bhatt, D.A. Frank, I. Rozovsky, N. Stahl, G.D. Yancopoulos, and M.E. Greenberg, *Regulation of gliogenesis in the central nervous system by the JAK-STAT signaling pathway.* Science, 1997. **278**(5337): p. 477-83.

14. Clarke, L.E. and B.A. Barres, *Emerging roles of astrocytes in neural circuit development.* Nat Rev Neurosci, 2013. **14**(5): p. 311-21.

15. Molofsky, A.V., R. Krencik, E.M. Ullian, H.H. Tsai, B. Deneen, W.D. Richardson, B.A. Barres, and D.H. Rowitch, *Astrocytes and disease: a neurodevelopmental perspective.* Genes Dev, 2012. **26**(9): p. 891-907.

16. Murphy, M., R. Dutton, S. Koblar, S. Cheema, and P. Bartlett, *Cytokines which signal through the LIF receptor and their actions in the nervous system.* Prog Neurobiol, 1997. **52**(5): p. 355-78.

17. Pfrieger, F.W., *Roles of glial cells in synapse development.* Cell Mol Life Sci, 2009. **66**(13): p. 2037-47.

18. Sofroniew, M.V. and H.V. Vinters, *Astrocytes: biology and pathology.* Acta Neuropathol, 2010. **119**(1): p. 7-35.

19. Stahl, N. and G.D. Yancopoulos, *The tripartite CNTF receptor complex: activation and signaling involves components shared with other cytokines.* J Neurobiol, 1994. **25**(11): p. 1454-66.

20. Wang, D.D. and A. Bordey, *The astrocyte odyssey.* Prog Neurobiol, 2008. **86**(4): p. 342-67.

21. Sofroniew, M.V., *Molecular dissection of reactive astrogliosis and glial scar formation.* Trends Neurosci, 2009. **32**(12): p. 638-47.

22. Pekny, M. and M. Pekna, *Astrocyte intermediate filaments in CNS pathologies and regeneration.* J Pathol, 2004. **204**(4): p. 428-37.

23. Herrmann, J.E., T. Imura, B. Song, J. Qi, Y. Ao, T.K. Nguyen, R.A. Korsak, K. Takeda, S. Akira, and M.V. Sofroniew, *STAT3 is a critical regulator of astrogliosis and scar formation after spinal cord injury.* J Neurosci, 2008. **28**(28): p. 7231-43.

24. Pekny, M., P. Leveen, M. Pekna, C. Eliasson, C.H. Berthold, B. Westermark, and C. Betsholtz, *Mice lacking glial fibrillary acidic protein display astrocytes devoid of intermediate filaments but develop and reproduce normally.* EMBO J, 1995. **14**(8): p. 1590-8.

Chapter 4:

Functional properties of astrocyte activity during acute EAE with modulation of S1P receptors

4.A. Introduction

The TetTag mice have revealed that EAE-related stimuli during acute EAE cause c-Fos activation in expanding astrocyte clusters throughout the white matter tracts of the LSC. The extent of this astrocyte activation is correlated with EAE severity and reduced by fingolimod treatment or by the genetic removal of $S1P_1$ on astrocytes. Thus, the subset of astrocytes identified by this activity reporter is directly involved with EAE processes and affected by fingolimod treatment. Together, these data further support evidence for the direct effects of fingolimod acting through S1P receptors on astrocytes as an important and novel efficacious target in EAE and possibly MS. To advance the understanding of the astrocyte's function in EAE and elucidate a mechanism of direct CNS action of fingolimod, transcriptome studies will be performed on EAE-activated astrocytes and compared across $S1P_1$-CTRL, $S1P_1$-AstKO, and $S1P_1$-CTRL + fingolimod groups.

RNA sequencing (RNA-seq) will be used to characterize the functions of the EAE-activated astrocytes and determine how fingolimod and $S1P_1$ signaling alters these functions. RNA-seq is a transcriptome profiling method that can provide a snapshot of the presence and abundance of global gene transcripts in any isolated RNA. The abundances of these transcripts reflect the functionality of the cell. In RNA-seq, the amount of a gene product is directly proportional to the sequencing reads to a given transcript, thus providing great linear range of expression detection and lower false-positive and false-negative discovery rates [1-9]. Additionally, with the progress of

single-cell sequencing technologies and whole transcriptome amplification (WTA), transcriptome analysis is achievable in situations with limited total RNA.

As previously discussed, the CNS has several cell types that are highly interconnected making isolation of intact cells for transcriptome analysis difficult. The most common method of proteolytic dissociation to isolate intact CNS cells likely perturbs transcriptional activity [10, 11]. However, mRNA is recoverable from bulk nuclei and can be sequenced [11-15]. This nascent nuclear RNA (nucRNA) is comparable to whole cell RNA by measures of presence and relative expression of transcripts as measured by RNA-seq [16]. The GFP-H2B in EAE-activated astrocytes allows relatively simple isolation by FACS. RNA-seq on activated astrocytes from $S1P_1$-CTRL, $S1P_1$-AstKO, and $S1P_1$-CTRL + fingolimod groups will be compared. This comparison will aid in identifying the roles of astrocytes in EAE and help delineate the effects of S1P signaling during EAE in the CNS.

4.B. Materials and Methods

RNA isolation from nuclei sorted by FACS

Populations of 15,000 c-Fos activated astrocytes (GFP-H2B$^+$, NeuN$^-$ nuclei) from single animals were sorted with an Aria II into a cell lysis buffer as described in chapter 3. RNA was isolated and deoxyribonuclease I (DNase I) treated to remove the relatively abundant genomic DNA (gDNA) that is contained in nuclei. RNA concentration and quality was assessed using a 2100 Bioanalyzer (Agilent Technologies).

Library production

Between 1-3 ng of the nucRNA was used in the SMART-seq v4 Ultra Low Input RNA Kit for Sequencing (Clontech) according to the manufacturers protocols. Briefly,

first-strand synthesis by poly(A)-priming is followed by template switching and extension by reverse transcription, allowing high fidelity amplification of full length cDNA transcripts by long distance PCR. A sequencing library was produced using 0.75 ng of the amplified cDNA in the Nextera XT Library Preparation Kit (Illumina). A Bioanalyzer assessed libraries concentration and quality. Each group of $S1P_1$-CTRL, $S1P_1$-AstKO, and $S1P_1$-CTRL + fingolimod had replicates samples of 4, 3, and 3, respectively.

Sequencing, alignment, and expression

Libraries were sequenced using the Illumina NextSeq 500 sequencer with 100 base pair single-end reads. The Genome Analyzer Pipeline (v1.5) and Casava (v1.8.2) software perform the early data analysis of the sequencing run, including image analysis, base calling, and demultiplexing. Cutadapt trims adaptors on the sequence and low base pair called scores. Spliced Transcrips Alignment to a Reference (STAR) was used to align to the *Mus musculus* genome (mm10). All reads that map to exons and introns were used in this analysis, as nuclear RNA has previously been noted to contain higher levels of intronic mapping (~27%) and intron expression is highly correlated with transcriptional activity [16, 17]. Partek software (v6.6) is used for transcript annotations.

The data were filtered to exclude transcripts for which the maximum number of reads for all samples was <40 reads. This eliminates noise and calculated infinite fold-changes. The R Bioconductor package, edgeR, provided statistical routines and methods for determining differential expression [18, 19]. EdgeR accounts for the total size (read number) in each library for all calculations of fold-changes, concentrations, and statistical significances. Normalization is performed by the trimmed mean of M-values (TMM) method where the sample whose 75^{th} percentile (of libraries scaled to total counts) is closest to the mean 75^{th} percentile is used as the reference. The Cox-

Reid approximate conditional maximum likelihood was used for estimating data dispersion parameters. The Bayes moderated dispersion parameter estimation was used to estimate the biological or sample-to-sample variability. The generalized linear model (GLM) uses a likelihood ratio test as the statistical test for significant differences. EdgeR identifies differentially expressed transcripts that are significantly changed and with a false discovery rate (FDR) >0.15.

The log2 counts-per-million (log2 CPM) in the results can be used to avoid undefined values and poorly defined log-fold-changes for low counts shrunk towards zero. The logCPM values can optionally be converted to RPKM or FPKM by subtracting log2 or gene length. The avg(log_2(X)) is used to calculate the fold-change (FC) because the log scale is the relevant scale for RNA-seq analysis starting with log transformed data. This is due to the distribution of noise in the intensity measurements as well as the transformation of a normal distribution. The log(FC) for variables X and Y is calculated as avg(log X) – avg(log Y).

To identify transcripts that were commonly altered in $S1P_1$-AstKO and $S1P_1$-CTRL + fingolimod groups, and the $S1P_1$-CTRL group, the CPM values for each group were averaged. Transcripts that commonly had a two-fold difference between $S1P_1$-AstKO and $S1P_1$-CTRL + fingolimod groups, and the $S1P_1$-CTRL group were identified.

4.C. Results

RNA isolated from EAE-activated astrocyte nuclei produces sequencing libraries

The nucRNA isolated from EAE-activated astrocytes isolated by FACS was examined by electrophoretic measurements on the bioanalayzer (**Figure 4.1**). The RNA integrity number (RIN), measured using the 28S to 18S ribosomal RNA (rRNA) ratio and often used to evaluate RNA degradation, was 2.30, a value often associated with

strongly degraded RNA [20]. However, RNA of considerable length and consistent with full-length mouse cDNA is present [21]. Additionally, rRNA does not accumulate in the nucleus and therefore an RIN is not suitable for RNA integrity evaluation of the nucRNA [22]. Sequencing libraries, made from the nuclear RNA from SMART-seq cDNA amplification and library preparation with Nextera XT, show typical size distribution as measured by a bioanalyzer. Typical lengths are 200-1000 bp.

Sequencing of cDNA libraries made with nucRNA from EAE-activated astrocytes shows characteristic alignment and mapping properties

The cDNA libraries made with nucRNA isolated from EAE-activated astrocytes were sequenced on a NextSeq sequencer (**Table 4.2**). Biological replicates from each acute EAE group, $S1P_1$-CTRL, $S1P_1$-AstKO, and $S1P_1$-CTRL + fingolimod (n = 4, 3, and 3, respectively), generated an average of 14,335,387 clusters with high quality metrics for the fidelity of base pair calls.

Alignment and mapping from the nucRNA-seq libraries was performed onto the mouse genome (**Figure 4.3**). The samples had an average sequencing depth of 7,530,622 reads, which is twice the amount typically needed to identify the majority of transcripts [23]. The percent of reads that mapped to exons and introns were uniquely characteristic of nucRNA, with an increased representation of intronic reads [16, 24-26]. The percent of reads mapping to exons from the EAE-activated astrocyte sequencing libraries was 15.88. The intronic reads likely represent pre-mRNA and their expressions will be further explored [15].

Reads mapping to introns correspond to reads mapping to exons

The relatively low level of exonic reads and high level of intronic reads seen during the mapping of the nucRNA from EAE-activated astrocytes was analyzed to determine if these intronic reads, which likely represent pre-mRNA, can be incorporated into the assessment of transcriptional activity (**Figure 4.4**). The expression values (in log[CPM]) of all reads mapping to exons were compared to the combined reads of exons and introns for 10,852 genes. In $S1P_1$-CTRL, $S1P_1$-AstKO, and $S1P_1$-CTRL + fingolimod groups all exon + intron expressions were significantly correlated with exon expression ($p < 0.001$).

Internal validation indicates the sequenced transcriptomes come from astrocytes and c-Fos activity is reduced $S1P_1$-AstKO, and $S1P_1$-CTRL + fingolimod by 5 dpo

$S1P_1$ is produced in virtually all cell types relevant to EAE. In the $S1P_1$-AstKO, most of the gene is removed by a GFAP-driven cre-recombinase (**Figure 4.5**) [27]. The expression of the *S1pr1* gene is greatly reduced in the sorted population of GFP-H2B$^+$, NeuN$^-$ from the $S1P_1$-AstKO group, indicating this population is GFAP positive and has therefore had the *S1pr1* gene removed. Some expression remains likely due to the exon coverage outside of the open-reading frame (ORF), which would map to the *S1pr1* gene.

EAE-activated astrocytes via the c-Fos dependent expression of GFP-H2B were identified using the TetTag mice. The temporal properties of this c-Fos reporter mouse are such that any activity within the 5-day acute EAE examination window would result in GFP-H2B expression. Activity of these EAE-activated astrocytes just prior to termination was determined by the examination of c-Fos expression (**Figure 4.5c**). As noted in chapter 3, there is less c-Fos activation of astrocytes in $S1P_1$-AstKO and $S1P_1$-CTRL + fingolimod groups. Further, EAE-activated astrocytes from $S1P_1$-AstKO and $S1P_1$-CTRL

+ fingolimod groups become less c-Fos active by the end of the examination window, while the $S1P_1$-CTRL group remains highly c-Fos active.

EAE-activated astrocytes from $S1P_1$-CTRL, $S1P_1$-AstKO, and $S1P_1$-CTRL + fingolimod groups show numerous differentially expressed transcripts

There are 339 transcripts that are significantly changed between $S1P_1$-CTRL and $S1P_1$-AstKO groups (**Table 4.6**). There are 175 significantly changed transcripts between $S1P_1$-CTRL and $S1P_1$-CTRL + fingolimod groups (**Table 4.7**).

$S1P_1$-AstKO and $S1P_1$-CTRL + fingolimod groups show commonly upregulated and downregulated transcripts compared to $S1P_1$-CTRL

A heatmap was generated using the expression values for commonly altered transcripts of $S1P_1$-CTRL, $S1P_1$-AstKO, and $S1P_1$-CTRL + fingolimod groups **(Figure 4.8**). There were 83 genes that were up regulated or down regulated in both $S1P_1$-AstKO and $S1P_1$-CTRL + fingolimod, compared to $S1P_1$-CTRL. Not all genes were up regulated in $S1P_1$-AstKO and $S1P_1$-CTRL + fingolimod groups or down regulated in $S1P_1$-AstKO and $S1P_1$-CTRL + fingolimod groups. The transcript cluster starting at *Slc26a1* to *Med12* was commonly down regulated when compared to $S1P_1$-CTRL. The transcript cluster starting at *Fam120aos* to *Hars2* were commonly up regulated.

4.D. Discussion

The approach to use nucRNA isolated from FAC-sorted samples to describe transcriptome and functional differences among cohorts was novel and achieved. The many challenges of dealing with nucRNA, including relatively small abundances and differences in the available quality assessments, make this approach uniquely

challenging. However, this approach circumvents the difficulties of single cell isolations and more importantly the alterations to the transcriptome by enzymatic and elevated temperature digestion [10, 11]. Sequencing libraries made from these nucRNAs show characteristic increases in intron coverage with concurrent decreases in exon coverage [16, 24-26], however using combined exon and intron expression data was confirmed as correlated with exon expression and transcriptional activity [17]. Using these data, the astrocyte specificity of the sorted populations was confirmed by the selective reduction of *S1pr1* expression in the $S1P_1$-AstKO group. Additionally, EAE-activated astrocytes, which already were shown to less numerous in $S1P_1$-AstKO and $S1P_1$-CTRL + fingolimod groups, are also less c-Fos active by measure of Fos expression at 5-dpo. The large lists of significantly altered transcripts give functional insights into the effects of altering S1P signaling in astrocytes.

Several transcripts significantly altered by S1P modulation were identified by RNA-seq of the EAE-activated astrocytes that could explain the decrease in EAE severity with the functional antagonism of $S1P_1$ by fingolimod or by the specific removal of $S1P_1$ on astrocytes. For example, transcripts from the complement system (both *C4b* and *C3*) were found to increase in $S1P_1$-CTRL mice when compared to $S1P_1$-AstKO. The complement system is a component of the innate immune system that has roles in inflammation, opsonization, and cytolysis. The primary site of complement production is in the liver, though astrocytes and other glia produce it locally in the CNS [28-31]. In EAE, demyelinated lesions are colocalized with complement depositions and contribute to demyelination [32, 33], and inhibition of complement pathways attenuates disease [34, 35]. Additionally, astrocytic production of complement proteins disrupts synapse morphology and neuron function [36]. However, a reduction in complement transcripts was not observed in the $S1P_1$-CTRL + fingolimod group.

Perhaps the best evidence for fingolimod having direct CNS effects comes from the observation that EAE severity is reduced in mice with astrocytic deletion of $S1P_1$ and fingolimod shows no efficacy in these mice, despite exhibiting normal lymphocyte trafficking [27]. Thus, it is expected that the mechanism responsible for the reduction in clinical score by fingolimod and the reduction in clinical score in astrocytic $S1P_1$ nulls would be the same. Therefore, examining commonly altered transcripts in $S1P_1$-AstKO and $S1P_1$-CTRL + fingolimod groups, when compared to the $S1P_1$-CTRL group, could give us a shared mechanism to further explore as the MOA for fingolimod in the CNS. Several transcripts were commonly up regulated or down regulated in both $S1P_1$-AstKO and $S1P_1$-CTRL + fingolimod groups and will be evaluated in future studies.

A promising transcript that is similarly changed on EAE-activated astrocytes in both $S1P_1$-AstKO and $S1P_1$-CTRL + fingolimod groups is *Cd320*, a transcobalamin receptor (TCblR). Cobalamin (Cbl, vitamin B12) is a vital nutrient required by all cells. It is distributed throughout the body by transporting proteins, including transcobalamin (TC). The TCblR is the only receptor capable of Cbl uptake in the CNS, as a TCblR knockout mouse exhibits severe deficiencies of Cbl in the CNS [37]. Remarkably, Cbl deficiencies appear phenotypically and pathologically similar to MS [38]. Patients with a Cbl deficiency often display parasthesia, sensory loss, and ataxia, with a consistent pathology of demyelination in the spinal cord, brain, and optic nerve [39, 40]. Cbl deficiencies have been speculated to play a role in MS pathogenesis as they lead to defective formation of myelin basic protein and the myelin sheath, which may generate an autoimmune response [41-43]. MS patients also may have reduced Cbl in serum and in the CNS [44, 45] and TCblR gene expression is reduced in MS lesions of various stages [46]. In addition to the demyelinating effects of Cbl deficiencies, Cbl stimulates neurotrophic and oligotrophic actions through the stimulation of epidermal growth factor

(EGF), which promotes the survival, development, and functions of neurons and oligodendrocytes [47, 48]. These properties of Cbl functions in the CNS may consolidate the observations of phenotypic changes with S1P modulations and TCblR expression changes with S1P modulations.

In EAE-activated astrocytes from $S1P_1$-CTRL mice, TCblR is reduced, as it is reduced in MS lesions [46]. This could cause a CNS deficiency of Cbl and concurrent demyelination, and increased disease severity. Cbl would additionally have less oligotrophic and neurotrophic effects. In both $S1P_1$-AstKO and $S1P_1$-CTRL + fingolimod groups, EAE-activated astrocytes had increased TCblR expression, allowing free entry of Cbl into the CNS and providing amelioration to EAE severity through the neurotrophic and oligotrophic effects of Cbl. There has been much debate over similarities of Cbl deficiency and MS and whether MS patients could successfully be treated with Cbl. Cbl therapy has been used with some success in EAE [49]. If astrocytes in EAE and MS are prohibiting Cbl from entering the CNS, Cbl therapy will continue to fall short. However, if fingolimod, which already shows great efficacy in treating MS and EAE, increases the transport of Cbl into the CNS, then a combination therapy may have great clinical potential.

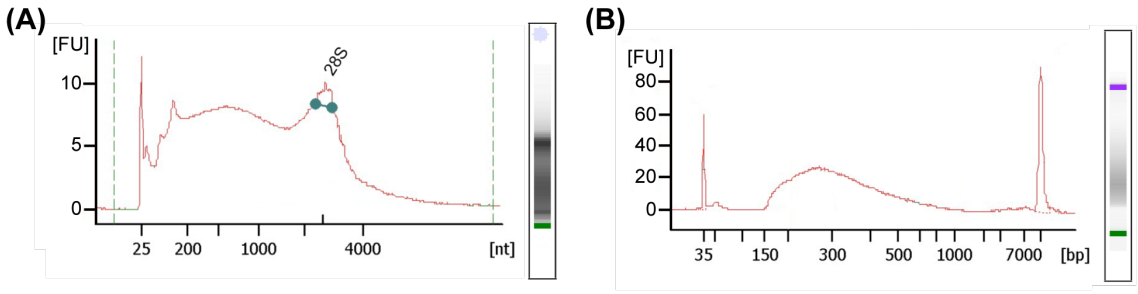

Figure 4.1. Total RNA isolated from EAE-activated astrocytes is full-length and yields normal cDNA library profiles. (A) Total RNA from EAE-activated astrocytes isolated by FACS is of typical transcriptome length as measured by electrophoretic RNA measurement on a bioanalyzer. The RNA integrity number (RIN), calculated using the 28S to 18S ribosomal RNA (rRNA) ratio, is low (RIN = 2.30 shown) due to the relative depletion of rRNA in the nucleus. **(B)** Sequencing libraries made from cDNA amplification using SMART-seq and Nextera XT DNA Library Prep Kit are of typical length distribution from 200 to 1000 bp.

Table 4.2. Fidelity of sequencing data from EAE-activated astrocytes from $S1P_1$-CTRL, $S1P_1$-AstKO, and $S1P_1$-CTRL + fingolimod groups. There were an average of 14,335,387 clusters from each sample with indexes identified perfectly 97.44% of the time. Single mismatches accounted for the remainder and are still identifiable. The % >= Q30 represents the percentage of base pair calls that had a 0.1% or less chance of being called incorrect. The mean quality scores were all above 30, representing a less than 1 of 1000 chance that any base pair is called incorrectly.

Sample ID	Clusters	% Perfect	% One mismatch	% >= Q30	Mean Quality
$S1P_1$-CTRL_1	19,078,068	98.29	1.71	91.62	33.85
$S1P_1$-CTRL_2	18,333,087	97.89	2.11	92.5	34.04
$S1P_1$-CTRL_3	15,938,931	97.82	2.18	92.38	34.01
$S1P_1$-CTRL_4	12,371,226	96.75	3.25	94.02	34.37
$S1P_1$-AstKO_1	7,844,920	97.6	2.4	90.5	33.6
$S1P_1$-AstKO_2	7,782,500	97.28	2.72	87.09	32.85
$S1P_1$-AstKO_3	17,562,740	98.07	1.93	93.48	34.26
$S1P_1$-CTRL + fingolimod_1	15,797,659	97.09	2.91	92.93	34.13
$S1P_1$-CTRL + fingolimod_2	16,705,338	96.8	3.2	93.35	34.22
$S1P_1$-CTRL + fingolimod_3	11,939,403	96.79	3.21	91.98	33.92

Table 4.3. Sequencing libraries derived from nucRNA from EAE-activated astrocytes show characteristic mapping properties. The reads that overlap exons are lower in RNA-seq libraries made with nucRNA. There are an average of 15.88% of reads that overlap exons. The intronic reads may represent pre-spliced RNA products.

Sample ID	Number of Alignments	Total Number of Reads	Reads that overlap exon (%)	Reads within an intron (%)
$S1P_1$-CTRL_1	7,786,531	6,525,914	4.86	39.16
$S1P_1$-CTRL_2	8,794,329	7,420,795	11.55	37.9
$S1P_1$-CTRL_3	12,041,198	10,739,833	40.04	39.67
$S1P_1$-CTRL_4	7,684,449	6,744,080	13.05	44.32
$S1P_1$-AstKO_1	5,182,931	4,304,839	6.58	38.2
$S1P_1$-AstKO_2	3,627,801	3,017,472	8.4	38.93
$S1P_1$-AstKO_3	10,599,859	8,849,287	7.04	38.62
$S1P_1$-CTRL + fingolimod_1	11,958,203	10,391,457	32.19	39.02
$S1P_1$-CTRL + fingolimod_2	11,836,935	9,939,610	15.12	38.7
$S1P_1$-CTRL + fingolimod_3	8,792,934	7,372,929	19.94	38.66

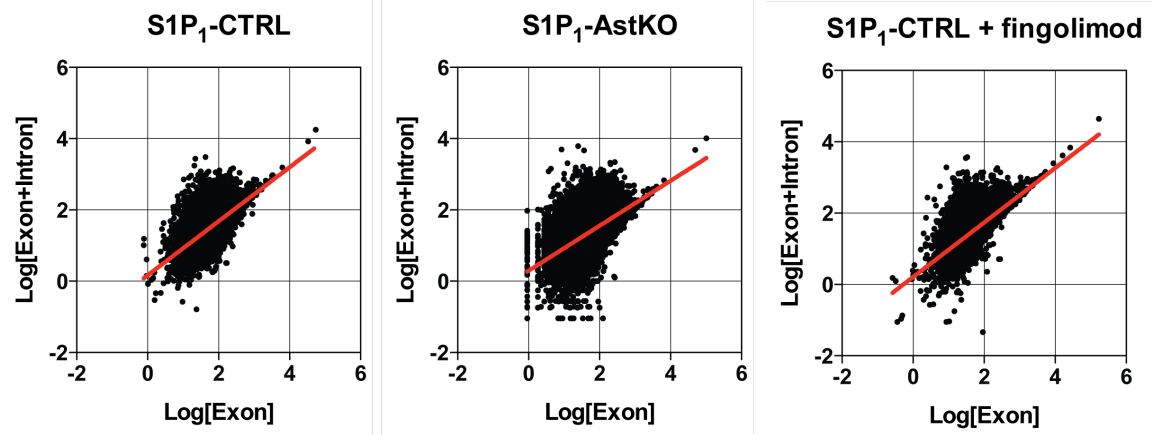

Figure 4.4. Inclusion of introns from nucRNA does not affect the evaluation of transcriptional activity by RNA-seq. Expression values from reads within exons were compared to expression values with exons + introns in 10,852 genes. In all groups exon and exon + intron expression was similarly correlated ($p < 0.001$), supporting the inclusion of intron reads for the determination of transcriptional activity.

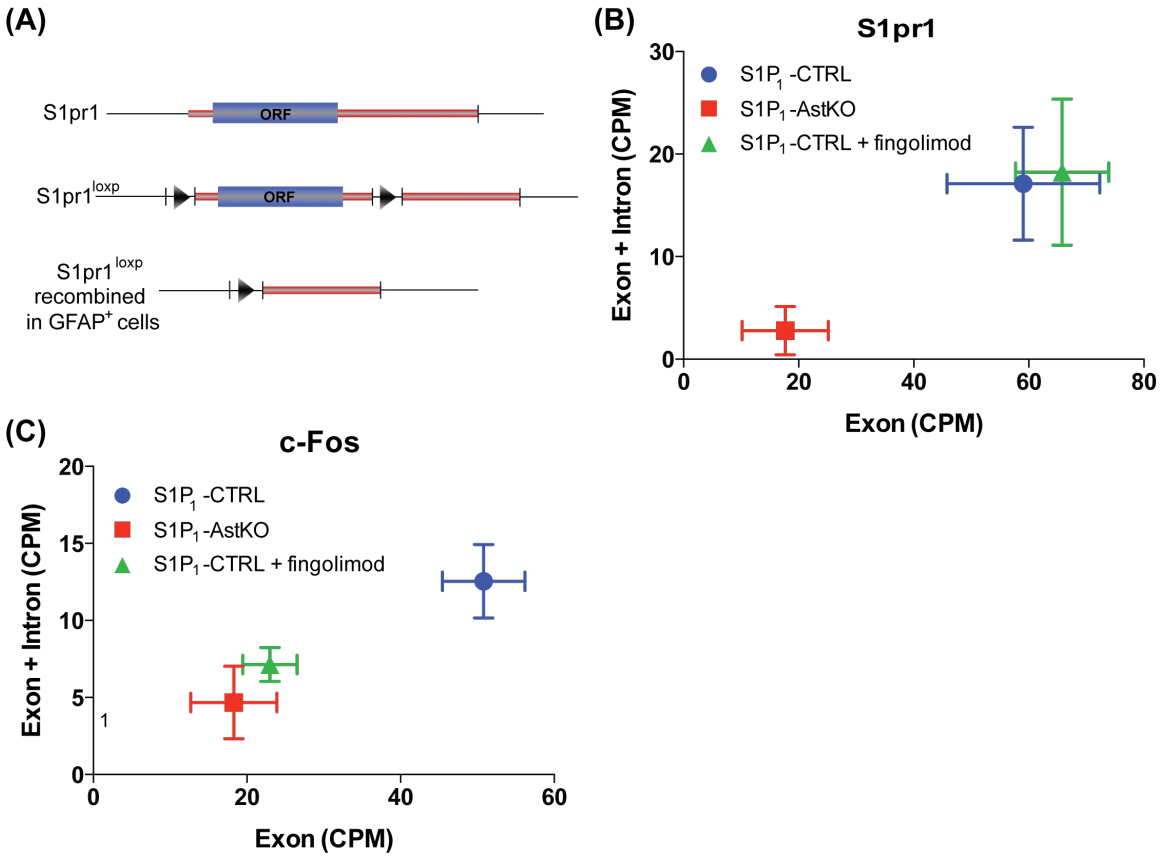

Figure 4.5. The reduction of *S1pr1* in S1P$_1$-AstKO group indicates efficient astrocyte isolation and EAE-activated astrocytes show reduced c-Fos activity after 5-dpo. (A) The loxp sites flank and remove the ORF in GFAP expressing cells. **(B)** S1pr1 is greatly reduced in the S1P$_1$-AstKO group indicating that c-Fos activated cells examined are GFAP-expressing and therefore astrocytes. **(C)** The level of c-Fos is reduced in EAE-activated cells from both S1P$_1$-AstKO and S1P$_1$-CTRL + fingolimod groups. In the S1P$_1$-CTRL group, c-Fos activity remains high in these EAE-activated astrocytes.

Table 4.6. Differentially expressed transcripts identified by RNA-seq that are significantly changed between $S1P_1$-CTRL and $S1P_1$-AstKO groups. The results are filtered with a FDR <1.5. A subsequent filter using *log Counts per Million* (log2(CPM)) > 4.0 is used to avoid poorly defined log-fold-changes when counts are shrunk towards zero.

Gene Symbol	FC	P-Value	FDR	Gene Symbol	FC	P-Value	FDR
Lair1	1843.9210	8.43E-14	1.99E-10	**Ccl12**	12.0568	1.89E-05	0.00135
Sh3pxd2a	1602.7051	2.55E-13	4.69E-10	**Adamts10**	11.9196	4.31E-05	0.00257
Asic2	1481.4940	4.73E-13	6.81E-10	**Fgd2**	11.5347	1.37E-05	0.00106
Hdac8	1468.8987	5.02E-13	6.81E-10	**Gorasp2**	11.0205	2.94E-05	0.00189
Afap1l2	1049.6048	6.83E-12	8.09E-09	**Nhlrc2**	10.4133	3.08E-05	0.00196
Srcin1	982.6837	1.13E-11	1.25E-08	**Cnp**	10.2794	2.46E-05	0.00164
Lgi1	670.4482	2.01E-10	1.23E-07	**Phka2**	9.7781	9.43E-05	0.00475
Cacng4	613.1956	3.94E-10	2.04E-07	**Rab11b**	9.6437	6.58E-05	0.00359
Iqsec2	174.1675	1.49E-10	9.85E-08	**MARCH5**	9.1238	9.81E-05	0.00492
Tmbim1	155.3471	3.57E-10	2.02E-07	**Mbd5**	9.0000	5.02E-05	0.00291
6430706D22Rik	60.8720	5.51E-09	1.76E-06	**Msn**	8.8686	4.25E-05	0.00254
Cd274	48.4944	3.00E-08	7.42E-06	**Slc43a2**	8.7958	5.80E-05	0.00322
Inpp5k	45.5619	4.76E-08	1.01E-05	**Il33**	8.6252	0.00016	0.00703
Gm35612	45.2059	2.00E-07	3.28E-05	**Atrnl1**	8.6034	7.13E-05	0.00379
Fmnl1	42.0387	3.42E-08	8.10E-06	**Coro1b**	8.4439	0.00014	0.00615
Tbl1x	41.0767	1.23E-08	3.34E-06	**Plxnb3**	8.4410	9.86E-05	0.00492
Elf4	25.7114	5.80E-08	1.16E-05	**Flna**	8.3730	0.00011	0.00533
Tmem104	22.7479	3.19E-07	4.93E-05	**Zfp91Cntf**	8.2065	0.00013	0.00601
Hprt	22.6826	7.55E-07	9.38E-05	**Abcc3**	8.0600	0.00016	0.00703
Stard3	20.5478	3.07E-06	0.00032	**Pik3ap1**	8.0190	9.10E-05	0.00463
Abi3	19.9976	5.44E-07	7.64E-05	**Plxdc1**	8.0110	0.00018	0.00788
Arhgap23	17.2714	4.61E-06	0.00044	**Nxn**	7.9899	0.00013	0.00600
Wbp1l	16.2222	1.36E-06	0.00016	**Lgals9**	7.8437	0.00018	0.00769
Ttyh2	13.9550	6.23E-06	0.00056	**Oaz1**	7.5223	0.00017	0.00742
Myo18a	13.6898	4.62E-06	0.00044	**H2-T23**	7.4262	0.00019	0.00795
Cdc37l1	12.3277	5.79E-06	0.00053	**Grb14**	7.3681	0.00020	0.00832
Smarce1	12.0802	2.05E-05	0.00143	**C230004F18Rik**	7.3501	0.00021	0.00877

Table 4.6. Differentially expressed transcripts identified by RNA-seq that are significantly changed between $S1P_1$-CTRL and $S1P_1$-AstKO groups, continued.

Gene Symbol	FC	PValue	FDR	Gene Symbol	FC	PValue	FDR
Stub1	7.2361	0.00022	0.00899	**Gm6548**	5.7749	0.00134	0.03956
Gm11149	7.2199	0.00048	0.01726	**Slfn2**	5.7414	0.00123	0.03676
Ube2e3	7.2151	0.00040	0.01488	**Rps3**	5.7182	0.00098	0.03085
Olfml3	7.1343	0.00036	0.01376	**Lasp1**	5.6934	0.00097	0.03069
Ubtd1	7.0684	0.00040	0.01507	**Jak3**	5.6911	0.00115	0.03502
Wdr81	6.8985	0.00044	0.01607	**Sdccag3**	5.6326	0.00122	0.03659
Htra2	6.7938	0.00054	0.01898	**E4f1**	5.5385	0.00141	0.04130
Cwc22	6.6561	0.00039	0.01466	**Med12**	5.5348	0.00104	0.03211
Ldb1	6.5359	0.00055	0.01940	**Stat3**	5.5217	0.00096	0.03046
Cyb5r1	6.4785	0.00055	0.01928	**Tlr1**	5.4699	0.00146	0.04196
Csf2ra	6.4399	0.00050	0.01792	**Rnf167**	5.4523	0.00169	0.04674
Scd2	6.3999	0.00036	0.01376	**Gdi1**	5.4304	0.00118	0.03553
Stambpl1	6.3885	0.00061	0.02102	**Fads1**	5.4138	0.00150	0.04277
Id3	6.3403	0.00065	0.02208	**Ifit3**	5.4065	0.00216	0.05553
Stk11	6.3188	0.00064	0.02164	**Rps29**	5.3937	0.00142	0.04132
Plce1	6.3015	0.00044	0.01616	**Evi2a**	5.3861	0.00160	0.04487
Arhgef6	6.2936	0.00055	0.01928	**AF251705**	5.3735	0.00143	0.04132
Bax	6.2700	0.00068	0.02283	**Sh3kbp1**	5.3458	0.00109	0.03328
Ndufv1	6.2484	0.00082	0.02680	**Vamp8**	5.3010	0.00159	0.04465
Csf3r	6.2103	0.00045	0.01650	**Saa3**	5.2863	0.00143	0.04132
H2-Q9	6.1904	0.00060	0.02059	**Pdcd11**	5.2745	0.00242	0.05946
Ifit1	6.1815	0.00081	0.02667	**Lipa**	5.2407	0.00166	0.04608
Dalrd3	6.1261	0.00093	0.02989	**Iffo1**	5.2370	0.00157	0.04426
Blnk	6.0404	0.00055	0.01940	**Sh2b1**	5.1977	0.00232	0.05802
SEPT4	5.9973	0.00091	0.02941	**Txnip**	5.1872	0.00259	0.06262
Xist	5.9795	0.00047	0.01702	**Psmb8**	5.1806	0.00181	0.04916
H2-Q7	5.9661	0.00080	0.02647	**Serf2**	5.1793	0.00177	0.04811

Table 4.6. Differentially expressed transcripts identified by RNA-seq that are significantly changed between $S1P_1$-CTRL and $S1P_1$-AstKO groups, continued.

Gene Symbol	FC	PValue	FDR	Gene Symbol	FC	PValue	FDR
Dtx3	5.1742	0.00177	0.04811	**C4b**	4.6380	0.00235	0.05857
Gk	5.1579	0.00171	0.04702	**Rps5**	4.6370	0.00361	0.07977
Slc11a1	5.1428	0.00188	0.05026	**Aup1**	4.6265	0.00338	0.07612
Irgm1	5.1032	0.00186	0.04980	**Tsc22d3**	4.6186	0.00300	0.06924
Mir5128	5.0573	0.00186	0.04980	**Maged1**	4.5988	0.00361	0.07977
Gfap	5.0468	0.00163	0.04560	**Ulk1**	4.5841	0.00357	0.07924
Fbrs	5.0394	0.00215	0.05553	**Sla**	4.5754	0.00291	0.06774
Adap2	5.0055	0.00166	0.04608	**Ahsa2**	4.5635	0.00317	0.07261
Slfn8	4.9928	0.00299	0.06907	**Zfp692**	4.5614	0.00428	0.08859
Sox10	4.9515	0.00266	0.06404	**Ndufs2**	4.5441	0.00382	0.08291
Gprasp2	4.9341	0.00312	0.07188	**Ncf4**	4.5333	0.00410	0.08634
Pfn1	4.9329	0.00252	0.06154	**Tmem255a**	4.5325	0.00456	0.09269
Sap25	4.9151	0.00226	0.05695	**Stat5b**	4.5041	0.00414	0.08709
Sorcs3	4.8997	0.00242	0.05946	**Cst7**	4.4867	0.00383	0.08292
Jak2	4.8652	0.00263	0.06327	**Fes**	4.4698	0.00338	0.07612
Tyrobp	4.8400	0.00209	0.05431	**Stam2**	4.4608	0.00474	0.09533
Tmem86a	4.8289	0.00398	0.08450	**Mrpl24**	4.4592	0.00420	0.08771
Xlr3b	4.8140	0.00224	0.05670	**Leng8**	4.4559	0.00356	0.07921
Gbp6	4.8086	0.00229	0.05772	**Stk19**	4.4495	0.00443	0.09073
Irf7	4.8065	0.00423	0.08789	**Rpl23**	4.4488	0.00397	0.08450
Rab24	4.7892	0.00260	0.06279	**Tm9sf3**	4.4375	0.00341	0.07637
H2-Aa	4.7864	0.00196	0.05144	**Igfbp5**	4.4318	0.00389	0.08338
Ftl1	4.7566	0.00202	0.05277	**Ppia**	4.4041	0.00370	0.08134
Colgalt1	4.7525	0.00252	0.06155	**Prnp**	4.3989	0.00502	0.09961
Cd14	4.7363	0.00421	0.08786	**H2-Eb1**	4.3861	0.00342	0.07648
Pkp4	4.6718	0.00237	0.05883	**Nrbp2**	4.3751	0.00527	0.10319
Xiap	4.6625	0.00260	0.06279	**Mx2**	4.3705	0.00509	0.10079

Table 4.6. Differentially expressed transcripts identified by RNA-seq that are significantly changed between $S1P_1$-CTRL and $S1P_1$-AstKO groups, continued.

Gene Symbol	FC	PValue	FDR	Gene Symbol	FC	PValue	FDR
Tlr2	4.3670	0.00448	0.09143	**Camk1**	4.1350	0.00552	0.10600
Dhx58	4.3600	0.00627	0.11501	**Tubb4a**	4.1301	0.00542	0.10482
Cuedc2	4.3594	0.00458	0.09311	**Calr**	4.1157	0.00615	0.11393
Iigp1	4.3543	0.00378	0.08229	**Irak1**	4.1128	0.00738	0.12638
Dbi	4.3502	0.00384	0.08292	**Olig1**	4.1111	0.00624	0.11489
Slc16a6	4.3326	0.00524	0.10294	**Klc4**	4.0610	0.00755	0.12812
Mt2	4.3254	0.00422	0.08787	**Bcan**	4.0450	0.00586	0.11009
Stab1	4.3025	0.00384	0.08292	**Taldo1**	4.0425	0.00651	0.11750
Ogfr	4.2936	0.00589	0.11050	**Fcer1g**	4.0368	0.00553	0.10600
Gns	4.2918	0.00372	0.08149	**Myof**	4.0362	0.00620	0.11428
Lgals3bp	4.2838	0.00400	0.08457	**Fgfr3**	4.0318	0.00756	0.12812
Slk	4.2642	0.00460	0.09330	**Ypel3**	4.0238	0.00682	0.12062
Pcyt2	4.2508	0.00475	0.09533	**Zfp36l1**	4.0212	0.00719	0.12445
Gmip	4.2431	0.00522	0.10264	**Atp1b2**	4.0210	0.00631	0.11537
C3	4.2427	0.00425	0.08811	**Tmbim6**	4.0184	0.00599	0.11187
Ppp1r9b	4.2265	0.00536	0.10402	**Zfx**	4.0093	0.00649	0.11743
Gpr155	4.2265	0.00657	0.11807	**2610035D17Rik**	3.9981	0.00617	0.11399
Gm20605	4.2233	0.00578	0.10925	**Sh3bgrl3**	3.9873	0.00824	0.13648
Ciz1	4.1801	0.00583	0.10993	**Fbxl20**	3.9845	0.00649	0.11743
Ncf1	4.1754	0.00662	0.11862	**Igsf10**	3.9832	0.00668	0.11921
Ensa	4.1580	0.00648	0.11733	**Helz2**	3.9514	0.00795	0.13268
Becn1	4.1507	0.00716	0.12428	**Ucp2**	3.9370	0.00764	0.12892
Timp3	4.1461	0.00582	0.10992	**Icam1**	3.9349	0.00851	0.13930
Ms4a7	4.1434	0.00574	0.10914	**Loxl2**	3.9242	0.00797	0.13286
Gm3435	4.1413	0.00575	0.10916	**Stat1**	3.9242	0.00628	0.11513
Vamp2	4.1398	0.00711	0.12381	**S100a6**	3.9199	0.00837	0.13818
Rps27	4.1360	0.00673	0.11967	**Rpl18**	3.9146	0.00851	0.13930

Table 4.6. Differentially expressed transcripts identified by RNA-seq that are significantly changed between $S1P_1$-CTRL and $S1P_1$-AstKO groups, continued.

Gene Symbol	FC	PValue	FDR	Gene Symbol	FC	PValue	FDR
S100a16	3.9146	0.00815	0.13536	**Snhg20**	3.7482	0.00858	0.14019
Atp6v0c	3.9028	0.00785	0.13153	**Napa**	3.7315	0.00963	0.14979
Psme1	3.8907	0.00834	0.13782	**Myo1f**	3.7264	0.00838	0.13829
Ctnnb1	3.8902	0.00677	0.12002	**Atp1a2**	3.6828	0.00888	0.14231
Ube2q1	3.8876	0.00895	0.14277	**Unc93b1**	3.6219	0.00958	0.14931
Abca7	3.8811	0.00863	0.14059	**Rfx3**	0.2932	0.00890	0.14231
Creld2	3.8793	0.00943	0.14765	**4933427G17Rik**	0.2930	0.00929	0.14622
Slc22a17	3.8759	0.00847	0.13910	**1700061I17Rik**	0.2906	0.00917	0.14514
Gpr34	3.8698	0.00879	0.14197	**Macc1**	0.2901	0.00915	0.14496
Ubb	3.8687	0.00845	0.13896	**Sult2a1**	0.2891	0.00883	0.14223
Cd300lf	3.8664	0.00763	0.12892	**Ms4a1**	0.2882	0.00888	0.14231
Aplp1	3.8580	0.00877	0.14171	**Rfc3**	0.2861	0.00867	0.14079
AI607873	3.8564	0.00751	0.12765	**Vmn2r51**	0.2852	0.00817	0.13556
Eef1a1	3.8561	0.00670	0.11927	**4930544M13Rik**	0.2837	0.00734	0.12583
Degs2	3.8509	0.00901	0.14314	**Cul2**	0.2836	0.00717	0.12428
Tspan4	3.8482	0.00928	0.14622	**Ube2j2**	0.2802	0.00693	0.12206
Kdm6a	3.8430	0.00851	0.13930	**Vmn2r50**	0.2775	0.00704	0.12329
Dock8	3.8280	0.00719	0.12445	**Cnksr2**	0.2769	0.00716	0.12428
Grina	3.8189	0.00775	0.13045	**Ei24**	0.2755	0.00636	0.11568
Myo1g	3.8145	0.00890	0.14231	**D7Ertd443e**	0.2752	0.00584	0.10998
Plekho1	3.8124	0.00822	0.13634	**Olfr1033**	0.2750	0.00680	0.12040
A2m	3.8090	0.00740	0.12661	**1700063A18Rik**	0.2734	0.00615	0.11393
Rtn4rl1	3.8036	0.00890	0.14231	**Gm13363**	0.2728	0.00643	0.11679
Hk3	3.7995	0.00842	0.13855	**Gm1976**	0.2716	0.00560	0.10701
Ppard	3.7923	0.00796	0.13268	**Platr21**	0.2715	0.00626	0.11501
Gpr137b-ps	3.7566	0.00855	0.13976	**Filip1l**	0.2696	0.00528	0.10319
Rbck1	3.7542	0.00925	0.14607	**Spty2d1**	0.2681	0.00512	0.10103

Table 4.6. Differentially expressed transcripts identified by RNA-seq that are significantly changed between $S1P_1$-CTRL and $S1P_1$-AstKO groups, continued.

Gene Symbol	FC	PValue	FDR	Gene Symbol	FC	PValue	FDR
Galnt3	0.2666	0.00527	0.10319	**Kcnj16**	0.2070	0.00107	0.03296
Crispld1	0.2643	0.00486	0.09677	**Zfp758**	0.2062	0.00095	0.03032
Klf8	0.2616	0.00475	0.09533	**4930412C18Rik**	0.2056	0.00087	0.02832
Trim9	0.2601	0.00399	0.08451	**Ar**	0.2046	0.00087	0.02812
Usp29	0.2598	0.00392	0.08381	**Dynlrb2**	0.2013	0.00080	0.02646
Lyplal1	0.2571	0.00432	0.08915	**Slc18a1**	0.1996	0.00068	0.02294
Gm5797	0.2555	0.00431	0.08910	**Tub**	0.1976	0.00068	0.02295
Rnls	0.2536	0.00403	0.08503	**Itgb6**	0.1943	0.00065	0.02209
Atp5g2	0.2507	0.00340	0.07635	**Zfp534**	0.1908	0.00060	0.02059
Pdlim1	0.2474	0.00345	0.07704	**Sult2a2**	0.1873	0.00052	0.01845
Trim12c	0.2455	0.00312	0.07188	**Syt9**	0.1837	0.00042	0.01569
Vmn2r78	0.2424	0.00293	0.06799	**Otc**	0.1830	0.00037	0.01407
Neto2	0.2399	0.00255	0.06195	**Gm13483**	0.1805	0.00039	0.01475
Hiatl1	0.2391	0.00238	0.05886	**Klrb1c**	0.1691	0.00025	0.01008
Pgr	0.2388	0.00238	0.05886	**Gm2087**	0.1686	0.00027	0.01068
Il1rapl2	0.2363	0.00219	0.05588	**Epc2**	0.1569	0.00011	0.00527
Alas2	0.2332	0.00230	0.05772	**Tcaf3**	0.1452	8.01E-05	0.00415
Pde11a	0.2274	0.00192	0.05089	**Dct**	0.1425	5.33E-05	0.00301
Morc4	0.2273	0.00194	0.05118	**Bccip**	0.1420	5.38E-05	0.00303
9530091C08Rik	0.2269	0.00173	0.04739	**Zfp617**	0.1400	5.12E-05	0.00294
2410141K09Rik	0.2243	0.00194	0.05118	**4930474H20Rik**	0.1393	4.23E-05	0.00254
Acad8	0.2223	0.00153	0.04338	**Zfp474**	0.1379	4.35E-05	0.00258
Gm15127	0.2198	0.00146	0.04194	**E030044B06Rik**	0.1356	4.17E-05	0.00253
Vmn2r40	0.2183	0.00151	0.04293	**Zfp12**	0.1339	3.42E-05	0.00215
Ugt2b38	0.2166	0.00141	0.04132	**Cldn16**	0.1251	1.84E-05	0.00132
Spata22	0.2165	0.00144	0.04160	**C4bp-ps1**	0.1189	1.28E-05	0.00099
Ythdf1	0.2119	0.00106	0.03263	**Tyms**	0.1151	1.02E-05	0.00083

Table 4.6. Differentially expressed transcripts identified by RNA-seq that are significantly changed between $S1P_1$-CTRL and $S1P_1$-AstKO groups, continued.

Gene Symbol	FC	PValue	FDR
2500002B13Rik	0.1080	6.08E-06	0.00055
Fam63a	0.1062	4.37E-06	0.00042
Jtb	0.1047	3.74E-06	0.00037
Wfdc3	0.0885	1.24E-06	0.00015
Mboat4	0.0823	7.00E-07	8.98E-05
Acsm4	0.0725	1.55E-07	2.64E-05
Vmn2r45	0.0673	1.29E-07	2.30E-05
4921531P14Rik	0.0466	2.57E-09	8.68E-07
Bsph1	0.0462	3.25E-09	1.08E-06
Chrnb1	0.0356	1.91E-10	1.22E-07
Acyp1	0.0317	6.20E-11	5.14E-08
Nkapl	0.0161	1.06E-13	2.19E-10
Olfr1089	0.0143	6.53E-14	1.80E-10
Lrfn1	0.0099	2.55E-15	1.06E-11
Zfp600	0.0050	8.64E-18	7.15E-14

Table 4.7. Differentially expressed transcripts significantly changed between $S1P_1$-CTRL and $S1P_1$-CTRL + fingolimod groups. The results are filtered with a FDR <0.15.

Gene Symbol	FC	P-Value	FDR	Gene Symbol	FC	P-Value	FDR
Gm2799	494.4524	1.39E-12	2.31E-08	**Armcx5**	123.3173	5.14E-08	2.50E-05
Slit1	419.3031	5.10E-12	4.22E-08	**Olfr111**	114.1675	8.95E-08	4.24E-05
Reps2	331.3363	2.97E-11	1.23E-07	**Zfp385b**	110.1783	7.18E-11	1.32E-07
Sdk2	311.6384	5.12E-11	1.32E-07	**Cnga2**	108.8902	1.25E-07	0.0001
Nhsl2	308.7158	5.41E-11	1.32E-07	**Gm14812**	106.4653	1.45E-07	0.0001
Wnt3	303.5573	6.27E-11	1.32E-07	**Tas2r118**	104.0865	1.69E-07	0.0001
Fndc3c1	299.9559	6.90E-11	1.32E-07	**Itga3**	103.8087	1.66E-07	0.0001
Pax2	227.0076	5.94E-10	9.54E-07	**A730008H23Rik**	103.5713	1.76E-07	0.0001
Lgsn	224.5957	6.33E-10	9.54E-07	**Tmprss3**	101.5784	1.99E-07	0.0001
Crtac1	218.0866	7.86E-10	1.08E-06	**Hectd2**	101.5784	1.99E-07	0.0001
Kcnrg	209.8727	1.12E-09	1.42E-06	**Gm17727**	100.3948	2.20E-07	0.0001
Dmrt1	192.4290	2.01E-09	2.38E-06	**Gm11529**	97.6244	2.62E-07	0.0001
Tll2	190.4552	2.17E-09	2.40E-06	**4930428E07Rik**	97.6244	2.62E-07	0.0001
Slc39a11	188.6985	9.68E-12	5.35E-08	**Phex**	91.6924	4.01E-07	0.0001
Umodl1	188.0992	2.48E-09	2.56E-06	**Ppp3r2**	85.7590	6.29E-07	0.0002
Sytl4	178.0712	3.53E-09	3.44E-06	**Cfap43**	83.8308	6.13E-07	0.0002
Awat2	174.5135	4.47E-09	4.12E-06	**4930417O22Rik**	81.8025	8.62E-07	0.0002
BC023829	160.4757	7.33E-09	6.07E-06	**DXBay18**	81.8025	8.62E-07	0.0002
2610027K06Rik	158.8684	8.28E-09	6.53E-06	**Gm20759**	79.8240	1.01E-06	0.0003
Pof1b	150.3812	1.27E-08	9.15E-06	**Mir467c**	63.3910	4.15E-08	0.0000
4930552P12Rik	145.4980	1.55E-08	1.07E-05	**Pcdhgc3**	62.7764	5.95E-09	5.19E-06
Gm12669	134.6450	3.14E-08	1.95E-05	**Jade3**	62.4896	4.01E-06	0.0009
Kif4	131.2194	3.30E-08	1.95E-05	**C77370**	54.5462	9.18E-06	0.0018
Far1os	129.6653	3.89E-08	2.15E-05	**Tex11**	51.1225	1.35E-05	0.0025
Angptl2	129.2440	3.68E-08	2.10E-05	**Gldc**	50.1806	3.20E-08	1.95E-05
4930486I03Rik	125.2929	4.59E-08	2.38E-05	**Smgc**	49.5735	2.17E-05	0.0037
Gm16291	124.2809	4.88E-08	2.45E-05	**Mycbpap**	48.4685	2.86E-07	0.0001

Table 4.7. Differentially expressed transcripts significantly changed between $S1P_1$-CTRL and $S1P_1$-CTRL + fingolimod groups, continued.

Gene Symbol	FC	P-Value	FDR	Gene Symbol	FC	P-Value	FDR
Ifi27	44.4449	5.05E-07	0.0001	**Cpb2**	18.3394	1.36E-05	0.0025
Slc4a1	42.2955	7.76E-07	0.0002	**Fgd1**	18.2210	1.45E-05	0.0026
Olfr1084	40.6973	1.16E-06	0.0003	**Plac1**	18.0835	3.40E-06	0.0007
Cacna1g	38.2935	1.55E-06	0.0004	**1110028F11Rik**	17.8225	1.69E-05	0.0029
Hnf1b	38.2608	2.46E-07	0.0001	**Gabre**	17.1620	7.23E-06	0.0015
C730002L08Rik	37.1723	2.02E-06	0.0005	**Mdga1**	15.7897	6.69E-06	0.0014
Defb33	35.8837	3.79E-07	0.0001	**Angptl7**	15.4431	2.34E-05	0.0039
Akap14	35.3735	2.59E-06	0.0006	**D030025P21Rik**	14.9217	1.29E-05	0.0024
Efnb1	34.7926	4.48E-07	0.0001	**4933417O13Rik**	14.7594	5.82E-05	0.0088
Teddm1b	31.0738	1.03E-06	0.0003	**Mir7649**	13.7648	1.67E-05	0.0029
Gm5934	30.7148	0.0003	0.0345	**4930596I21Rik**	12.6597	0.0001	0.0187
Olfr242	29.8768	8.05E-06	0.0016	**Ecsit**	12.2125	4.81E-05	0.0075
Il1f9	28.3016	6.97E-07	0.0002	**Cldn34b2**	11.9587	0.0004	0.0486
Gm9079	27.9574	1.27E-05	0.0024	**Adgrg2**	11.3173	2.79E-05	0.0045
Cited1	26.2772	3.35E-06	0.0007	**Cox16**	11.2174	1.10E-05	0.0021
AU040972	26.2278	3.32E-06	0.0007	**Olfr1507**	10.9942	0.0001	0.0082
4933424G05Rik	25.9307	2.41E-07	0.0001	**Vmn2r13**	10.9651	0.0001	0.0187
Cnnm1	25.5828	7.04E-07	0.0002	**Xlr5b**	10.9218	0.0002	0.0279
Vmn1r175	25.1087	0.0007	0.0793	**Pramel3**	10.6417	0.0001	0.0099
Acsf2	23.2449	7.34E-06	0.0015	**Armcx4**	10.4477	0.0001	0.0122
Gm14405	22.0173	4.08E-06	0.0009	**1700019B03Rik**	10.3361	0.0001	0.0102
Hspa12a	20.8751	6.79E-07	0.0002	**Cbln3**	10.2363	0.0001	0.0126
Entpd7	19.8566	1.03E-06	0.0003	**Wfdc15b**	10.0640	0.0001	0.0159
Lhfpl1	19.6041	1.11E-06	0.0003	**Ifit1bl2**	9.4932	0.0002	0.0294
Rph3al	19.4918	1.50E-06	0.0004	**9030204H09Rik**	9.4336	0.0005	0.0594
Gm13032	19.1002	2.73E-05	0.0045	**4930533B01Rik**	8.5607	0.0001	0.0181
Olfr702	18.5914	3.35E-05	0.0053	**Gm11186**	8.5312	0.0002	0.0212

Table 4.7. Differentially expressed transcripts significantly changed between $S1P_1$-CTRL and $S1P_1$-CTRL + fingolimod groups, continued.

Gene Symbol	FC	P-Value	FDR	Gene Symbol	FC	P-Value	FDR
E030044B06Rik	8.5111	0.0001	0.0151	**Ssx9**	5.9405	0.0010	0.1037
Slc26a1	8.4236	0.0004	0.0481	**Capn10**	5.9238	0.0012	0.1133
Actl7a	8.2697	0.0005	0.0522	**Hs6st2**	5.8425	0.0008	0.0847
Wdr20rt	8.1062	0.0004	0.0433	**Tmco5**	5.8010	0.0010	0.0969
Gm13178	7.7899	0.0004	0.0496	**Sufu**	5.5035	0.0010	0.1008
Tymp	7.7851	0.0003	0.0414	**2900092D14Rik**	0.2049	0.0015	0.1422
E330011O21Rik	7.7624	0.0009	0.0888	**Ly6c2**	0.1963	0.0006	0.0702
Lrrc19	7.7415	0.0004	0.0514	**Klhl4**	0.1936	0.0008	0.0821
Kcnv1	7.7085	0.0006	0.0660	**Klrd1**	0.1922	0.0007	0.0785
Hoga1	7.5785	0.0007	0.0796	**Taf7l**	0.1904	0.0009	0.0899
Ugt1a7c	7.4266	0.0001	0.0193	**Ms4a4b**	0.1889	0.0005	0.0528
Casp7	7.3668	0.0002	0.0281	**Gm21975**	0.1844	0.0016	0.1483
Gm13102	7.2257	0.0003	0.0378	**Fgl2**	0.1782	0.0004	0.0454
Vmn2r79	7.1540	0.0006	0.0630	**Omg**	0.1720	0.0003	0.0335
Ripply3	6.9276	0.0008	0.0804	**Gm6710**	0.1698	0.0004	0.0499
4930511A08Rik	6.8793	0.0003	0.0401	**Dhrs13**	0.1673	0.0009	0.0905
Ttc39aos1	6.7108	0.0009	0.0955	**Sst**	0.1584	0.0002	0.0280
Gpr143	6.6362	0.0007	0.0785	**A330032B11Rik**	0.1556	0.0003	0.0404
2010001E11Rik	6.5755	0.0012	0.1130	**Gm14625**	0.1549	0.0003	0.0345
Pkdrej	6.5025	0.0011	0.1092	**Ltb**	0.1534	0.0001	0.0185
Olfr1124	6.3473	0.0009	0.0888	**Tktl1**	0.1341	0.0001	0.0156
Glp1r	6.2828	0.0011	0.1059	**Hist1h2bf**	0.1318	0.0002	0.0307
2310002L09Rik	6.2315	0.0016	0.1483	**Hsf2bp**	0.1250	0.0006	0.0669
Grin3b	6.1643	0.0008	0.0839	**Klre1**	0.1203	3.33E-05	0.0053
Cstf2	6.1397	0.0012	0.1185	**Pydc4**	0.1186	1.35E-05	0.0025
Pcdhga11	6.1251	0.0006	0.0705	**Rpp30**	0.1184	2.58E-05	0.0043
Nr4a2	5.9532	0.0012	0.1144	**Klra21**	0.1182	5.64E-05	0.0087

Table 4.7. Differentially expressed transcripts significantly changed between $S1P_1$-CTRL and $S1P_1$-CTRL + fingolimod groups, continued.

Gene Symbol	FC	P-Value	FDR
Prl3c1	0.1140	4.06E-05	0.0064
1700111N16Rik	0.1044	1.83E-05	0.0032
4930440I19Rik	0.0984	1.68E-05	0.0029
Olfr1206	0.0921	2.18E-05	0.0037
Nxt2	0.0858	0.0001	0.0181
Cd7	0.0832	2.99E-06	0.0007
Pglyrp2	0.0607	6.03E-06	0.0012
Vmn2r38	0.0553	3.96E-07	0.0001
Nkg7	0.0504	1.22E-08	9.15E-06
Zcchc16	0.0486	1.83E-08	1.22E-05
Zfp955b	0.0471	1.00E-07	4.61E-05
Smyd4	0.0435	3.39E-07	0.0001
Calcoco2	0.0117	1.26E-07	0.0001

Figure 4.8. Commonly altered transcripts between $S1P_1$-AstKO and $S1P_1$-CTRL + fingolimod, and $S1P_1$-CTRL groups. A heatmap of commonly altered transcripts (>two-fold difference of averaged CPM in both exon + intron expression (EI) and exon expression (E)) between $S1P_1$-AstKO and $S1P_1$-CTRL + fingolimod, and $S1P_1$-CTRL identifies commonly down regulated transcripts (*Slc26a1* to *Med12*) and commonly up regulated transcripts (*Fam120aos* to *Hars2*).

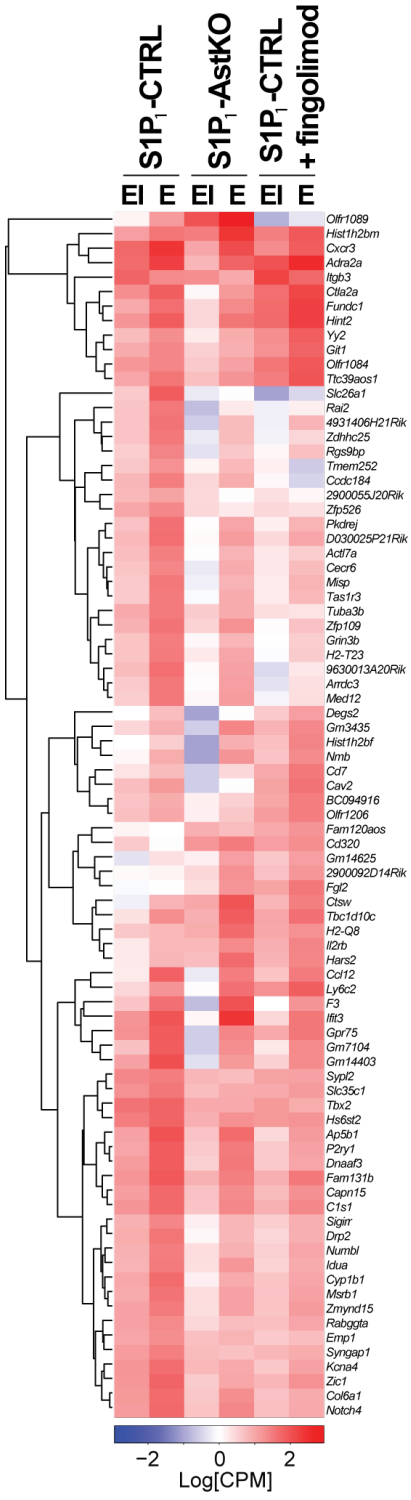
S1P1-CTRL
S1P1-AstKO
S1P1-CTRL + fingolimod
EI
E
EI
E
EI
E
Olfr1089
Hist1h2bm
Cxcr3
Adra2a
Itgb3
Ctla2a
Fundc1
Hint2
Yy2
Git1
Olfr1084
Tlc39aos1
Slc26a1
Rai2
4931406H21Rik
Zdhhc25
Rgs9bp
Tmem252
Ccdc184
2900055J20Rik
Zfp526
Pkdrej
D030025P21Rik
Actl7a
Cecr6
Misp
Tas1r3
Tuba3b
Zfp109
Grin3b
H2-T23
9630013A20Rik
Arrdc3
Med12
Degs2
Gm3435
Hist1h2bf
Nmb
Cd7
Cav2
BC094916
Olfr1206
Fam120aos
Cd320
Gm14625
2900092D14Rik
Fgl2
Ctsw
Tbc1d10c
H2-Q8
Il2rb
Hars2
Ccl12
Ly6c2
F3
Ifit3
Gpr75
Gm7104
Gm14403
Sypl2
Slc35c1
Tbx2
Hs6st2
Ap5b1
P2ry1
Dnaaf3
Fam131b
Capn15
C1s1
Sigirr
Drp2
Numbl
Idua
Cyp1b1
Msrb1
Zmynd15
Rabggta
Emp1
Syngap1
Kcna4
Zic1
Col6a1
Notch4
−2
0
2
Log[CPM]

Chapter 4 References

1. Marioni, J.C., C.E. Mason, S.M. Mane, M. Stephens, and Y. Gilad, *RNA-seq: an assessment of technical reproducibility and comparison with gene expression arrays.* Genome Res, 2008. **18**(9): p. 1509-17.

2. Mortazavi, A., B.A. Williams, K. McCue, L. Schaeffer, and B. Wold, *Mapping and quantifying mammalian transcriptomes by RNA-Seq.* Nat Methods, 2008. **5**(7): p. 621-8.

3. Nagalakshmi, U., Z. Wang, K. Waern, C. Shou, D. Raha, M. Gerstein, and M. Snyder, *The transcriptional landscape of the yeast genome defined by RNA sequencing.* Science, 2008. **320**(5881): p. 1344-9.

4. Sultan, M., M.H. Schulz, H. Richard, A. Magen, A. Klingenhoff, M. Scherf, M. Seifert, T. Borodina, A. Soldatov, D. Parkhomchuk, D. Schmidt, S. O'Keeffe, S. Haas, M. Vingron, H. Lehrach, and M.L. Yaspo, *A global view of gene activity and alternative splicing by deep sequencing of the human transcriptome.* Science, 2008. **321**(5891): p. 956-60.

5. Trapnell, C., B.A. Williams, G. Pertea, A. Mortazavi, G. Kwan, M.J. van Baren, S.L. Salzberg, B.J. Wold, and L. Pachter, *Transcript assembly and quantification by RNA-Seq reveals unannotated transcripts and isoform switching during cell differentiation.* Nat Biotechnol, 2010. **28**(5): p. 511-5.

6. Wilhelm, B.T., S. Marguerat, S. Watt, F. Schubert, V. Wood, I. Goodhead, C.J. Penkett, J. Rogers, and J. Bahler, *Dynamic repertoire of a eukaryotic transcriptome surveyed at single-nucleotide resolution.* Nature, 2008. **453**(7199): p. 1239-43.

7. Wu, J.Q., L. Habegger, P. Noisa, A. Szekely, C. Qiu, S. Hutchison, D. Raha, M. Egholm, H. Lin, S. Weissman, W. Cui, M. Gerstein, and M. Snyder, *Dynamic transcriptomes during neural differentiation of human embryonic stem cells revealed by short, long, and paired-end sequencing.* Proc Natl Acad Sci U S A, 2010. **107**(11): p. 5254-9.

8. Cloonan, N., A.R. Forrest, G. Kolle, B.B. Gardiner, G.J. Faulkner, M.K. Brown, D.F. Taylor, A.L. Steptoe, S. Wani, G. Bethel, A.J. Robertson, A.C. Perkins, S.J. Bruce, C.C. Lee, S.S. Ranade, H.E. Peckham, J.M. Manning, K.J. McKernan, and S.M. Grimmond, *Stem cell transcriptome profiling via massive-scale mRNA sequencing.* Nat Methods, 2008. **5**(7): p. 613-9.

9. Bainbridge, M.N., R.L. Warren, M. Hirst, T. Romanuik, T. Zeng, A. Go, A. Delaney, M. Griffith, M. Hickenbotham, V. Magrini, E.R. Mardis, M.D. Sadar, A.S. Siddiqui, M.A. Marra, and S.J. Jones, *Analysis of the prostate cancer cell line LNCaP transcriptome using a sequencing-by-synthesis approach.* BMC Genomics, 2006. **7**: p. 246.

10. Chaudhry, A., *Induction of gene expression alterations by culture medium from trypsinized cells.* J Biol Sci, 2008. **8**(1): p. 81-87.

11. Zeng, J., A. Mohammadreza, W. Gao, S. Merza, D. Smith, L. Kelbauskas, and D.R. Meldrum, *A minimally invasive method for retrieving single adherent cells of different types from cultures.* Sci Rep, 2014. **4**: p. 5424.

12. Barthelson, R.A., G.M. Lambert, C. Vanier, R.M. Lynch, and D.W. Galbraith, *Comparison of the contributions of the nuclear and cytoplasmic compartments to global gene expression in human cells.* BMC Genomics, 2007. **8**: p. 340.

13. Schwanekamp, J.A., M.A. Sartor, S. Karyala, D. Halbleib, M. Medvedovic, and C.R. Tomlinson, *Genome-wide analyses show that nuclear and cytoplasmic RNA levels are differentially affected by dioxin.* Biochim Biophys Acta, 2006. **1759**(8-9): p. 388-402.

14. Deal, R.B. and S. Henikoff, *The INTACT method for cell type-specific gene expression and chromatin profiling in Arabidopsis thaliana.* Nat Protoc, 2011. **6**(1): p. 56-68.

15. Tilgner, H., D.G. Knowles, R. Johnson, C.A. Davis, S. Chakraborty, S. Djebali, J. Curado, M. Snyder, T.R. Gingeras, and R. Guigo, *Deep sequencing of subcellular RNA fractions shows splicing to be predominantly co-transcriptional in the human genome but inefficient for lncRNAs.* Genome Res, 2012. **22**(9): p. 1616-25.

16. Grindberg, R.V., J.L. Yee-Greenbaum, M.J. McConnell, M. Novotny, A.L. O'Shaughnessy, G.M. Lambert, M.J. Arauzo-Bravo, J. Lee, M. Fishman, G.E. Robbins, X. Lin, P. Venepally, J.H. Badger, D.W. Galbraith, F.H. Gage, and R.S. Lasken, *RNA-sequencing from single nuclei.* Proc Natl Acad Sci U S A, 2013. **110**(49): p. 19802-7.

17. Gaidatzis, D., L. Burger, M. Florescu, and M.B. Stadler, *Analysis of intronic and exonic reads in RNA-seq data characterizes transcriptional and post-transcriptional regulation.* Nat Biotechnol, 2015. **33**(7): p. 722-9.

18. Robinson, M.D. and G.K. Smyth, *Moderated statistical tests for assessing differences in tag abundance.* Bioinformatics, 2007. **23**(21): p. 2881-7.

19. Robinson, M.D. and A. Oshlack, *A scaling normalization method for differential expression analysis of RNA-seq data.* Genome Biol, 2010. **11**(3): p. R25.

20. Schroeder, A., O. Mueller, S. Stocker, R. Salowsky, M. Leiber, M. Gassmann, S. Lightfoot, W. Menzel, M. Granzow, and T. Ragg, *The RIN: an RNA integrity number for assigning integrity values to RNA measurements.* BMC Mol Biol, 2006. **7**: p. 3.

21. Kawai, J., A. Shinagawa, K. Shibata, M. Yoshino, M. Itoh, Y. Ishii, T. Arakawa, A. Hara, Y. Fukunishi, H. Konno, J. Adachi, S. Fukuda, K. Aizawa, M. Izawa, K. Nishi, H. Kiyosawa, S. Kondo, I. Yamanaka, T. Saito, Y. Okazaki, T. Gojobori, H. Bono, T. Kasukawa, R. Saito, K. Kadota, H. Matsuda, M. Ashburner, S. Batalov, T. Casavant, W. Fleischmann, T. Gaasterland, C. Gissi, B. King, H. Kochiwa, P. Kuehl, S. Lewis, Y. Matsuo, I. Nikaido, G. Pesole, J. Quackenbush, L.M. Schriml, F. Staubli, R. Suzuki, M. Tomita, L. Wagner, T. Washio, K. Sakai, T. Okido, M. Furuno, H. Aono, R. Baldarelli, G. Barsh, J. Blake, D. Boffelli, N. Bojunga, P. Carninci, M.F. de Bonaldo, M.J. Brownstein, C. Bult, C. Fletcher, M. Fujita, M. Gariboldi, S. Gustincich, D. Hill, M. Hofmann, D.A. Hume, M. Kamiya, N.H. Lee, P. Lyons, L. Marchionni, J. Mashima, J. Mazzarelli, P. Mombaerts, P. Nordone, B. Ring, M. Ringwald, I. Rodriguez, N. Sakamoto, H. Sasaki, K. Sato, C. Schonbach, T. Seya, Y. Shibata, K.F. Storch, H. Suzuki, K. Toyo-oka, K.H. Wang, C. Weitz, C. Whittaker, L. Wilming, A. Wynshaw-Boris, K. Yoshida, Y. Hasegawa, H. Kawaji, S. Kohtsuki, Y. Hayashizaki, R.G.E.R.G.P.I. Team, and F.C. the, *Functional annotation of a full-length mouse cDNA collection.* Nature, 2001. **409**(6821): p. 685-90.

22. Thomson, E., S. Ferreira-Cerca, and E. Hurt, *Eukaryotic ribosome biogenesis at a glance.* J Cell Sci, 2013. **126**(Pt 21): p. 4815-21.

23. Ramskold, D., E.T. Wang, C.B. Burge, and R. Sandberg, *An abundance of ubiquitously expressed genes revealed by tissue transcriptome sequence data.* PLoS Comput Biol, 2009. **5**(12): p. e1000598.

24. van Heesch, S., M. van Iterson, J. Jacobi, S. Boymans, P.B. Essers, E. de Bruijn, W. Hao, A.W. MacInnes, E. Cuppen, and M. Simonis, *Extensive localization of long noncoding RNAs to the cytosol and mono- and polyribosomal complexes.* Genome Biol, 2014. **15**(1): p. R6.

25. Mitchell, J.A., I. Clay, D. Umlauf, C.Y. Chen, C.A. Moir, C.H. Eskiw, S. Schoenfelder, L. Chakalova, T. Nagano, and P. Fraser, *Nuclear RNA sequencing of the mouse erythroid cell transcriptome.* PLoS One, 2012. **7**(11): p. e49274.

26. Zaghlool, A., A. Ameur, L. Nyberg, J. Halvardson, M. Grabherr, L. Cavelier, and L. Feuk, *Efficient cellular fractionation improves RNA sequencing analysis of mature and nascent transcripts from human tissues.* BMC Biotechnol, 2013. **13**: p. 99.

27. Choi, J.W., S.E. Gardell, D.R. Herr, R. Rivera, C.W. Lee, K. Noguchi, S.T. Teo, Y.C. Yung, M. Lu, G. Kennedy, and J. Chun, *FTY720 (fingolimod) efficacy in an animal model of multiple sclerosis requires astrocyte sphingosine 1-phosphate receptor 1 (S1P1) modulation.* Proc Natl Acad Sci U S A, 2011. **108**(2): p. 751-6.

28. Gasque, P., A. Ischenko, J. Legoedec, C. Mauger, M.T. Schouft, and M. Fontaine, *Expression of the complement classical pathway by human glioma in culture. A model for complement expression by nerve cells.* J Biol Chem, 1993. **268**(33): p. 25068-74.

29. Gasque, P., M. Fontaine, and B.P. Morgan, *Complement expression in human brain. Biosynthesis of terminal pathway components and regulators in human glial cells and cell lines.* J Immunol, 1995. **154**(9): p. 4726-33.

30. Thomas, A., P. Gasque, D. Vaudry, B. Gonzalez, and M. Fontaine, *Expression of a complete and functional complement system by human neuronal cells in vitro.* Int Immunol, 2000. **12**(7): p. 1015-23.

31. Gasque, P., N. Julen, A.M. Ischenko, C. Picot, C. Mauger, C. Chauzy, J. Ripoche, and M. Fontaine, *Expression of complement components of the alternative pathway by glioma cell lines.* J Immunol, 1992. **149**(4): p. 1381-7.

32. Hundgeburth, L.C., M. Wunsch, D. Rovituso, M.S. Recks, K. Addicks, P.V. Lehmann, and S. Kuerten, *The complement system contributes to the pathology of experimental autoimmune encephalomyelitis by triggering demyelination and modifying the antigen-specific T and B cell response.* Clin Immunol, 2013. **146**(3): p. 155-64.

33. Ramaglia, V., S.J. Jackson, T.R. Hughes, J.W. Neal, D. Baker, and B.P. Morgan, *Complement activation and expression during chronic relapsing experimental autoimmune encephalomyelitis in the Biozzi ABH mouse.* Clin Exp Immunol, 2015. **180**(3): p. 432-41.

34. Hu, X., V.M. Holers, J.M. Thurman, T.R. Schoeb, T.N. Ramos, and S.R. Barnum, *Therapeutic inhibition of the alternative complement pathway attenuates chronic EAE.* Mol Immunol, 2013. **54**(3-4): p. 302-8.

35. Hu, X., S. Tomlinson, and S.R. Barnum, *Targeted inhibition of complement using complement receptor 2-conjugated inhibitors attenuates EAE.* Neurosci Lett, 2012. **531**(1): p. 35-9.

36. Lian, H., L. Yang, A. Cole, L. Sun, A.C. Chiang, S.W. Fowler, D.J. Shim, J. Rodriguez-Rivera, G. Taglialatela, J.L. Jankowsky, H.C. Lu, and H. Zheng, *NFkappaB-activated astroglial release of complement C3 compromises neuronal morphology and function associated with Alzheimer's disease.* Neuron, 2015. **85**(1): p. 101-15.

37. Lai, S.C., Y. Nakayama, J.M. Sequeira, B.J. Wlodarczyk, R.M. Cabrera, R.H. Finnell, T. Bottiglieri, and E.V. Quadros, *The transcobalamin receptor knockout mouse: a model for vitamin B12 deficiency in the central nervous system.* FASEB J, 2013. **27**(6): p. 2468-75.

38. Ghezzi, A. and M. Zaffaroni, *Neurological manifestations of gastrointestinal disorders, with particular reference to the differential diagnosis of multiple sclerosis.* Neurol Sci, 2001. **22 Suppl 2**: p. S117-22.

39. Lindenbaum, J., E.B. Healton, D.G. Savage, J.C. Brust, T.J. Garrett, E.R. Podell, P.D. Marcell, S.P. Stabler, and R.H. Allen, *Neuropsychiatric disorders caused by cobalamin deficiency in the absence of anemia or macrocytosis.* N Engl J Med, 1988. **318**(26): p. 1720-8.

40. Misra, U.K., J. Kalita, and A. Das, *Vitamin B12 deficiency neurological syndromes: a clinical, MRI and electrodiagnostic study.* Electromyogr Clin Neurophysiol, 2003. **43**(1): p. 57-64.

41. Ropper, A.H., R.D. Adams, M. Victor, R.H. Brown, and M. Victor, *Adams and Victor's principles of neurology*. 8th ed. 2005, New York: McGraw-Hill Medical Pub. Division. ix, 1382 pages.

42. Shevell, M.I. and D.S. Rosenblatt, *The neurology of cobalamin.* Can J Neurol Sci, 1992. **19**(4): p. 472-86.

43. Allen, R.H., S.P. Stabler, D.G. Savage, and J. Lindenbaum, *Metabolic abnormalities in cobalamin (vitamin B12) and folate deficiency.* FASEB J, 1993. **7**(14): p. 1344-53.

44. Reynolds, E.H., T. Bottiglieri, M. Laundy, R.F. Crellin, and S.G. Kirker, *Vitamin B12 metabolism in multiple sclerosis.* Arch Neurol, 1992. **49**(6): p. 649-52.

45. Nijst, T.Q., R.A. Wevers, H.C. Schoonderwaldt, O.R. Hommes, and A.F. de Haan, *Vitamin B12 and folate concentrations in serum and cerebrospinal fluid of neurological patients with special reference to multiple sclerosis and dementia.* J Neurol Neurosurg Psychiatry, 1990. **53**(11): p. 951-4.

46. Han, M.H., D.H. Lundgren, S. Jaiswal, M. Chao, K.L. Graham, C.S. Garris, R.C. Axtell, P.P. Ho, C.B. Lock, J.I. Woodard, S.E. Brownell, M. Zoudilova, J.F. Hunt, S.E. Baranzini, E.C. Butcher, C.S. Raine, R.A. Sobel, D.K. Han, I. Weissman, and L. Steinman, *Janus-like opposing roles of CD47 in autoimmune brain inflammation in humans and mice.* J Exp Med, 2012. **209**(7): p. 1325-34.

47. Scalabrino, G., F.R. Buccellato, D. Veber, and E. Mutti, *New basis of the neurotrophic action of vitamin B12.* Clin Chem Lab Med, 2003. **41**(11): p. 1435-7.

48. Scalabrino, G., *The multi-faceted basis of vitamin B12 (cobalamin) neurotrophism in adult central nervous system: Lessons learned from its deficiency.* Prog Neurobiol, 2009. **88**(3): p. 203-20.

49. Mastronardi, F.G., W. Min, H. Wang, S. Winer, M. Dosch, J.M. Boggs, and M.A. Moscarello, *Attenuation of experimental autoimmune encephalomyelitis and nonimmune demyelination by IFN-beta plus vitamin B12: treatment to modify notch-1/sonic hedgehog balance.* J Immunol, 2004. **172**(10): p. 6418-26.

Chapter 5:

Concluding remarks and future directions

The approaches of studying S1P signaling in EAE using c-Fos reporter mice, characterizing the spatial and temporal properties of astrocyte activation using volume imaging, and using the novel technique of nucRNA-seq to compare S1P modulated groups has yielded great insights into astrocyte's role in EAE and with fingolimod treatment. First, utilizing the TetTag c-Fos reporter mice, a specific population of astrocytes that are directly related to EAE processes in the spinal cord were identified. These EAE-activated astrocytes are predominant in lesions and expand along white matter tracts. The extent of their expanse is directly correlated with EAE severity, which is modulated by S1P signaling. Rather than studying an immensely heterogeneous population of astrocytes using traditional cell specific markers of astrocytes and reactive astrocytes such as GFAP, the use of c-Fos identified only those astrocytes that were involved in the disease. Comparing the transcriptomes of these EAE-activated astrocytes has identified several potential pathways that S1P modulation, acting directly through astrocytes, may alter the disease course in EAE and possibly MS.

The use of a c-Fos reporter system to indicate the activity of cells other than neurons and during a disease state is unique and may prove practical in other complex biological processes. In the TetTag mice, during the acute EAE time period, astrocytes were specifically activated. Examining activity during the chronic phase of EAE may identify other cells types. Likewise, using a different IEG reporter system might detect activity of other cell types. T cells were examined for activity both in the CNS and in lymph nodes. Interestingly, T cell c-Fos activity was different in these regions during acute EAE. Examining lymph nodes and other regions outside the CNS for activity may

bring to light important information on cellular activity during these disease processes. It is likely that diseases or insults involving reactive astrocytes, such as injury, ischemia, and neuromyelitis optica to name a few, might preferentially or specifically identify astrocytes in a c-Fos reporter system, and could be comprehensively studied in a similar manner.

The approach of examining and comparing the transcriptomes of cell population(s) by nucRNA used in this study, may provide a framework for studying human MS tissues. Researchers generally have access to fresh frozen or fixed tissues making single cell isolation prohibitive as enzymatic digestion requires fresh tissues to disentangle the complexly interwoven CNS neural cells. Isolating nuclei, if an appropriate specific nuclear marker is available, could allow the comparison of transcriptomes using RNA-seq across different disease states, treatment groups, etc. In MS tissue, using antibodies against c-Fos may preferentially identify astrocytes in which to characterize and validate the same processes shown here.

Finally, using the comparison of transcriptomes to study the mechanism of fingolimod and S1P signaling in astrocytes has yielded many interesting pathways that will need to be explored and validated. Some of these pathways, if validated, have the potential to dramatically change the way we think about the treatment of MS and could imply the use of a combination therapy that would be readily available to impact MS patients immediately.